



室蘭工業大学

学術資源アーカイブ

Muroran Institute of Technology Academic Resources Archive



高炉スラグ微粉末を用いたセメント系材料の強度改善および寒冷地での耐久性に関する研究

メタデータ	言語: English 出版者: 公開日: 2018-05-24 キーワード (Ja): キーワード (En): blast furnace slag (BFS), High early strength Portland Cement (HPC), XRD/Rietveld, TG-DTA, pore structure, C-S-H type high early strength agent, limestone powder (LSP), gypsum (CS), combine deterioration, freeze-thaw resistance, carbonation resistance, maturity, compressive strength 作成者: 金, 準鎬 メールアドレス: 所属:
URL	https://doi.org/10.15118/00009625

**STUDY ON STRENGTH IMPROVEMENT AND
DURABILITY IN COLD REGIONS OF CEMENTITIOUS
COMPOSITE USING BLAST FURNACE SLAG**

高炉スラグ微粉末を用いたセメント系材料の強度改善および
寒冷地での耐久性に関する研究

Junho Kim

Doctor of Philosophy

**Division of Engineering, Course of Advanced Sustainable and
Environmental Engineering
MURORAN INSTITUTE OF TECHNOLOGY**

ABSTRACT

Blast furnace slag (BFS) has been widely used as a mineral admixture in cement and concrete in the concrete industry in order to reduce CO₂ emissions. In Japan, the replacement levels of BFS are categorized into type A (5~30 wt%), type B (30~60 wt%), and type C (60~70 wt%) according to Japanese Industrial Standard (JIS). However, only type B BFS blended cement is actually used in the construction industry, and is mainly used in foundations or underground structures, and not in main structural elements due to the low compressive strength at early age. In order to broaden the practical application of BFS blended cement in the construction industry, the mechanical property and hydration process need to be further discussed.

Therefore, the purpose of this research is to investigate the BFS blended cement in cementitious composites affected by various replacement ratios, such as in compressive strength development methods, with combined deterioration of carbonation and frost damage. Moreover, the compressive strength development of BFS blended cement and the combined deterioration effects of accelerated carbonation and freeze–thaw resistance were investigated in this thesis.

In Chapter 2, a calcium silicate hydrate (C-S-H) type accelerator that was developed to serve the purpose of increased production efficiency and streamlining of manufacturing secondary products of concrete shows an effect in all temperature ranges. Therefore, it is the purpose of this research to establish if a C-S-H type accelerator is able to be used as a BFS blended concrete strength development method. The C-S-H type accelerator was compared with the quality standard of the accelerator, and proved possible to be positioned not merely as a hardening accelerator. Moreover, the addition of C-S-H type accelerator to BFS cement type B did not see a close relationship between additive amounts of C-S-H type accelerator and strength development; thus, we tested the heat of hydration by conduction calorimeter and analyzed it by X-ray diffraction (XRD). This indicates the cement hydration of the promotion mechanism of the C-S-H type accelerator.

In chapter 3, it was investigated the compressive strength development of blast furnace slag (BFS) blended mortar mixtures incorporating various mineral admixtures, namely BFS, limestone powder (LSP), and gypsum (CS). BFS replacement ratios of 15, 20, and 25 wt.%; LSP replacement ratios of 2, 3, 4, and 5 wt.%; and a CS

replacement ratio of 2 wt.% are employed to improve the strength of BFS blended mortar mixtures. The hydration reaction and products resulting from the use of cement, BFS, and mineral admixtures are quantitatively examined with respect to the XRD/Rietveld method in order to investigate the relationship between the produced hydrates and the strength. In addition, the strength is found to be decreased as the BFS replacement ratio increases. At a BFS replacement ratio above 20 wt.%, LSP affects the strength improvement of BFS cement and CS affects the initial strength improvement of BFS cement. The effect of high early strength Portland cement (HPC). The investigation of each concrete sample includes two curing cases, which are cured in air 5°C or 20°C at 30, 90, 210, 840 and 2730 Maturity. The result of experiments shows that, in the case of BFS A type, it has the same performance as the OPC. In the case of BFS B type, considering the advantage that largely reduced from the amount of CO₂, the mixture BFS35% + LSP 3% + CS2% is judged appropriate.

In chapter 4, the durability performance of cementitious material is traditionally based on assessing the effect of a single degradation process. However, this study investigates the mechanical and coupled deterioration properties of mortar incorporating industrial solid waste - ground granulated blast furnace slag (BFS) and different mineral admixtures, such as calcium sulfate (CS) and limestone powder (LSP). The combined deterioration properties caused by carbonation and frost damage in the mortar sample were experimentally investigated with respect to accelerated carbonation and freeze-thaw tests. Different degrees of deterioration, i.e., after subjected to 12, 30 and 60 freeze-thaw cycles were induced in the freeze-thaw tests. Mercury intrusion porosimetry (MIP) was used to measure the pore structure distribution in the mortar samples to quantify the influence of the mineral admixtures and the replacement ratio on the change in pore structure volume, providing reasonable guidance to assess the durability. The experimental investigation revealed that the compressive strength, frost resistance and carbonation resistance decrease as the BFS replacement ratio increases by weight from 0 to 45%. Moreover, to achieve the same strength as ordinary Portland cement, 2 wt. % CS and 4 wt. % LSP in the BFS mortar are required. However, the data shows that incorporating LSP into the BFS mortar produces a lower frost carbonation resistance. The combined damage tests revealed that different deterioration degrees resulting from 12, 30 and 60 freeze-thaw cycles slightly decreased the

carbonation resistance, which is related to the decrease in the inkbottle pore volume due to its water retention characteristics. Simultaneously, the pre-carbonation deterioration could effectively decrease the surface mass scaling of the freeze–thaw, indicating

In Chapter 5, the frost damage resistance of BFS cement has an effect on the carbonation. Hence, this study investigates the carbonation properties of pastes incorporating BFS and different replacement ratios, at 15%, 45%, and 65% of replacement ratio on weight percentage. The replacement ratio properties caused by the Ca/Si ratio of C-S-H in the paste samples were experimentally investigated with respect to mercury intrusion porosimetry (MIP), X-ray diffraction (XRD), and thermal analysis tests. Different degrees of curing age (2 week, 4weeks) were subjected to water curing. The experimental investigation of the pore structure indicated that the total porosity decreases after carbonation. Calcium carbonation (CC) is denser than calcium hydroxide (CH) due to the carbonation. We found vaterite through chemical composition analysis by XRD, which has a high expansion rate, and which influences the carbonation characteristic of BFS blended cement paste.

Keywords: blast furnace slag (BFS), High early strength Portland Cement (HPC), XRD/Rietveld, TG-DTA, pore structure, C-S-H type high early strength agent, limestone powder (LSP), gypsum (CS), combine deterioration, freeze-thaw resistance, carbonation resistance, maturity, compressive strength.

TABLE OF CONTENTS

ABSTRACT.....	i
TABLE OF CONTENTS.....	I
CHAPTER 1 INTRODUCTION	
1.1 Background.....	1
1.2 Previous research.....	2
1.2.1 Advantages and disadvantages of using blast furnace slag.....	2
1.2.2 Strength increase method of incorporating blast furnace slag cement at early curing age.....	2
1.2.3 Influence of C-S-H type accelerator on strength.....	6
1.2.4 Influence of Ca/Si ratio of C-S-H.....	9
1.2.5 Influence of affect Carbonation deterioration on concrete.....	10
1.3 Problem definition.....	14
1.4 Research aims and thesis organization.....	15
REFERENCES:.....	18
CHAPTER 2 EFFECT OF C-S-H TYPE ACCELERATOR ON THE COMPRESSIVE STRENGTH AT EARLY CURING AGE AS BLAST FURNACE SLAG BLENDED CONCRETE	
2.1 Overview.....	25
2.2 Experimental program and method.....	26
2.2.1 Materials and experimental design.....	26
2.2.2 Fresh property, setting time and compressive strength.....	26
2.2.3 Heat of hydration.....	27
2.2.4 X-ray diffraction.....	27
2.3 Experimental result and discussion.....	28
2.3.1 Relationship among the C-S-H type accelerator and compressive strength at low temperature.....	28
2.3.2 Effect of C-S-H type accelerator on the setting time and cement composition.....	30

2.3.3 Optimization of C3S ratio as C-S-H type accelerator reaction for compressive strength development	32
2.3.4 Characteristics of the C-S-H type accelerator on X-ray diffraction and heat production	34
2.4 Conclusion	38
REFERENCES:.....	39
CHAPTER 3 EFFECT OF LIMESTONE POWDER AND GYPSUM ON THE COMPRESSIVE STRENGTH MIXTURE DESIGN OF BLAST FURNACE SLAG BLENDED CEMENT MORTAR	
3.1 Overview	43
3.2 Experimental	44
3.2.1 Experimental program	44
3.2.2 Measurement Methods.....	47
3.3 Results and discussion	49
3.3.1 Characteristics of compressive strength development	49
3.3.2 Compressive Strength of BFS Blended Paste Samples Incorporating Various Mineral Admixtures	54
3.3.3 Hydration Reaction Analysis of Paste Samples	55
3.3.4 Relationship between Porosity and Compressive Strength.....	59
3.4 Mixture design of blast furnace slag concrete based on high early strength cement using the limestone powder and CaSO ₄	64
3.4.1 Experimental results and discussion	66
3.5 Conclusion	68
REFERENCES:	70
CHAPTER 4 EVALUATION OF THE COMBINED DETERIORATION BY FREEZE-THAW AND CARBONATION OF MORTAR INCORPORATING BFS	
4.1 Overview	77
4.2 Experimental program.....	79
4.2.1 Materials and mixture proportions	79
4.2.2 Experimental program for the combined deterioration	80

4.2.3 Testing method.....	81
4.3 Experiment result and discussion.....	83
4.3.1 Compressive strength.....	83
4.3.2 Frost resistance.....	84
4.3.3 Carbonation result.....	86
4.4 Combined deterioration.....	88
4.4.1 Effects of the degree of frost damage and the pore structure on carbonation resistance	88
4.4.2 Effects of the pre-carbonation deterioration and the pore structure on frost resistance	91
4.5 Conclusion	94
REFERENCES:.....	96
 CHAPTER 5 CURING AGE AND CARBONATION CHARACTERISTICS INCORPORATING BFS	
5.1 Overview.....	103
5.2 Experimental program.....	104
5.2.1 Experimental materials and sample preparation	104
5.2.2 Experimental methods	104
5.3 Experiment result and discussion.....	106
5.3.1 Characteristics of pore structure after carbonation	106
5.3.2 Characteristics of amount of calcium hydroxide and calcium carbonate after carbonation.....	113
5.3.3 Characteristics of chemical properties according to carbonation.....	120
5.4 Conclusion	125
REFERENCES:.....	126
 CHAPTER 6 CONCLUSIONS	
6.1 Introduction.....	131
6.2 Effect of C-S-H type accelerator on the compressive strength at early curing age as blended BFS (Chapter 2)	131
6.3 Effect of limestone powder and gypsum on the compressive strength mixture design of blended BFS (Chapter 3)	132

6.4 Evaluation of the combined deterioration by freeze-thaw and carbonation of mortar incorporating BFS (Chapter 4)	133
6.5 Curing age and carbonation characteristics incorporating BFS (Chapter 5).....	134
6.6 Summary and future work.....	136
ACKNOWLEDGEMENTS	137
LIST OF PAPERS.....	139

CHAPTER 1
INTRODUCTION

1.1 Background

Cementitious composites are widely used in the construction industry because of their relatively low cost and free surface implementation. However, CO₂ emissions from cement manufacturing pose environmental issues. Recently, research is underway in the construction industry to reduce CO₂ emissions. One way to reduce CO₂ emissions is to reduce the amount of cement used. In this case, blast furnace slag (BFS) is used as a replacement for cement. Replacing cement with BFS can reduce heat of hydration, increase strength at long-term curing age, and has increased chemical resistance. However, the decreasing of carbonation resistance and decreasing the compressive strength at early curing age has also been a disadvantage. This disadvantage is the biggest problem when using BFS.

When concrete mixture includes BFS, it affects the chemical compound ratios. The main compound in cement is C-S-H, and cement shows different characteristics depending on the Ca/Si ratio. Hence, replacement by BFS reveals a low Ca/Si ratio. The different characteristics compare to ordinary Portland cement (OPC). In addition, the pore structure will affect the various properties of the concrete. However, pore structure is also changed by the environment, whose characteristics also vary.

Therefore, research to increase the early curing compressive strength of concrete using BFS has been ongoing. Among the research, there are normally two methods. First, there is a method which involves adding a liquid type chemical accelerator for enhancing the compressive strength of BFS concrete. The second method involves increasing the compressive strength by the addition of mineral admixture. Each method has advantages and disadvantages, and liquid accelerators are highly effective, but quality control is difficult. However, powder type mineral admixture has a convenience in quality control. This is a method for improving the initial strength of BFS concrete.

On the other hand, in the case of concrete constructed in cold areas, it is influenced by the combination of frost damage in winter and the damage caused by carbonation in summer. Therefore, it is necessary to consider the combined deterioration effects due to freeze damage and carbonation. In particular, BFS concrete with low carbonation resistance will exhibit different characteristics as compared to using ordinary Portland cement concrete.

To increase the usage amount of BFS concrete, an improvement in compressive strength in early curing age is needed, and the impact of combined deterioration due to both carbonation and freeze damage needs to be determined. Therefore, a basic study to increase the usage amount of BFS by improving compressive strength in early curing age and understanding the problems in cold areas is needed.

1.2 Previous research

1.2.1 Advantage and disadvantages of using blast furnace slag

Blast furnace slag (BFS) has been widely used as a mineral admixture in cement and concrete in the concrete industry in order to reduce CO₂ emissions (Miyazawa et al., 2010; Chen et al., 2012; Kumar et al., 2008). However, only type B BFS blended cement is actually used in the construction industry, and is mainly used in foundations or underground structures and not in main structural elements due to the low compressive strength at early age (Nippon Slag Association, 2015). In order to increase the practical application of BFS blended cement, type A BFS blended cement is expected to be used in the construction industry, and the mechanical property and hydration process need to be further discussed.

In the literature (Gu et al., 2015; Cetin et al., 2016; Rakhimova et al., 2014; Rakhimova et al., 2015; Gu et al., 2014), BFS blended cement has the advantages of reducing hydration heat, enhancing the long-term strength, and providing some resistance to chloride-induced damage and sulfates. At present, to utilize these advantages of BFS blended cement effectively, studies to resolve the disadvantages of BFS blended cement are actively being pursued. Various studies are being conducted to resolve the issue of the initial strength degradation, and the temperature-dependency of BFS was also investigated (Castellano et al., 2016).

1.2.2 Strength increase method of incorporating blast furnace slag cement at early curing age

Haha et al. (2011) experimented with adding MgO for alkali-activated BFS blended samples. They used various analysis methods. In particular, they looked at microstructures from SEM images for understanding the

differences. Sajedi et al. (2010) investigated using a chemical activator on slag mortars. They used sodium hydroxide, potassium hydroxide, and sodium silicate. Sodium silicate had the greatest effect. The strength of the specimens cured in air showed the highest strength. The strength reduction in alkali-activated mortar depended on the blended slag. Gu et al. (2015) investigated using alkali-activated slag cement. Their conclusions were as follows: 1) The effect of the alkali activator had more impact on the curing temperature. 2) The low temperature reduced the early curing age strength. 3) Alkali-activated slag (AAS) at low-temperature curing reduced micro cracks.

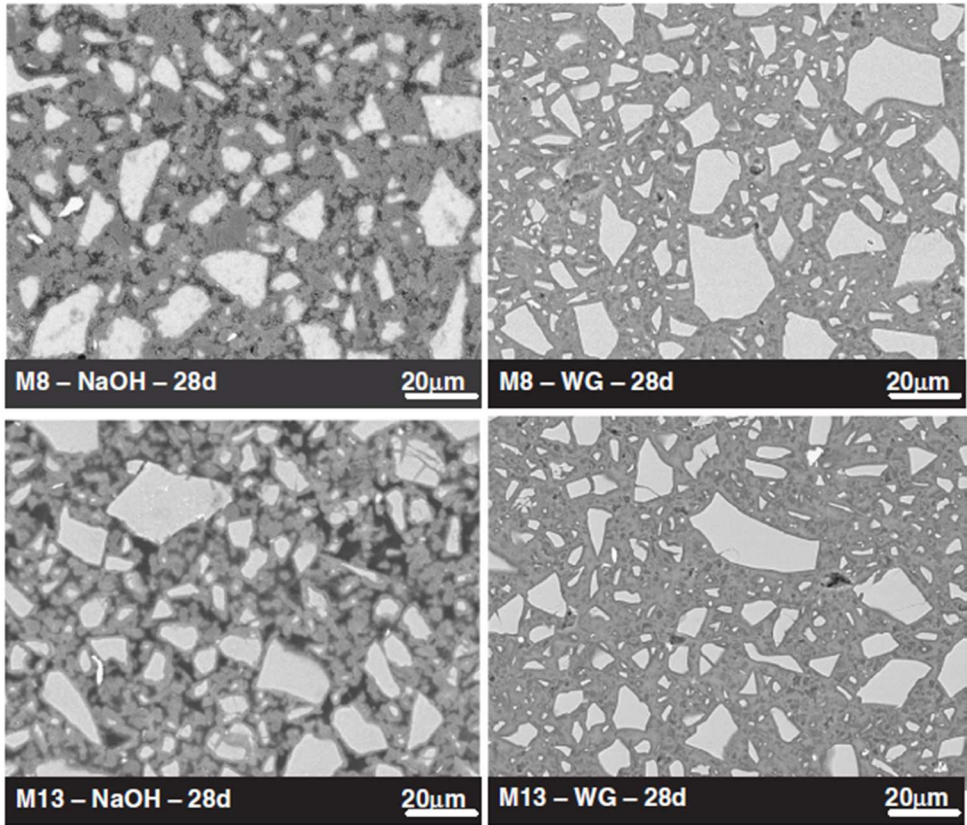


Fig. 1.1 SEM micrograph of specimen (Haha et al. 2011)

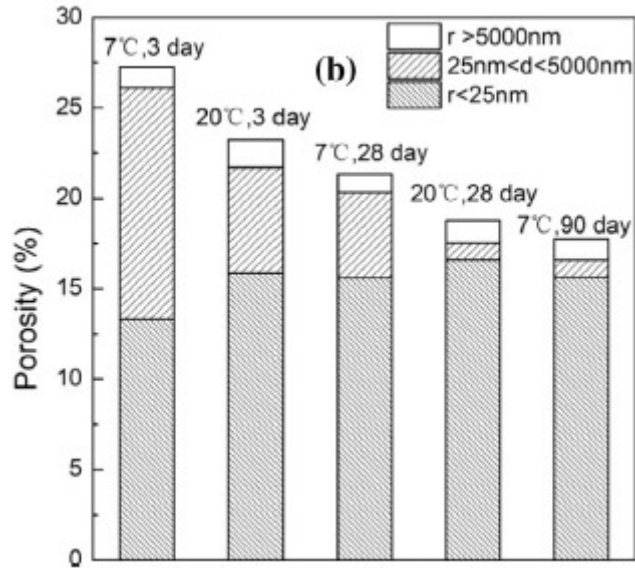


Fig. 1.2 Pore distribution of AAS paste (Gu et al. 2015)

Hoshino et al. (2006) investigated incorporating Lime stone powder (LSP) in the BFS blended cement. The analysis of the cement composite was attempted by quantification; the relationship between porosity and strength, combining the Rietveld method and selective dissolution method was investigated. They concluded that: 1) The Rietveld and selective dissolution methods could be successfully quantified. 2) LSP was produced mono-carbonate and hemi-carbonate. 3) The effect of LSP on the strength development was more significant than with other samples. The filling effect was greater. Carrasco et al. (2004) experimented with using LSP for compressive strength development. They concluded that the LSP–BFS–OPC system showed optimum strength at all curing ages. Singh (2000) investigated the compressive strength development of Portland slag cement with blended gypsum. The conclusion was that: 1) A decrease in setting time and increase in the compressive strength of cement was observed. 2) Maximum attainment of strength was achieved using blended gypsum. Menedez et al. (2003) experimented with ternary blended cement being used for the development of BFS concrete. LSP could improve the early strength. The combination of LSP and BFS can lead to energy saving.

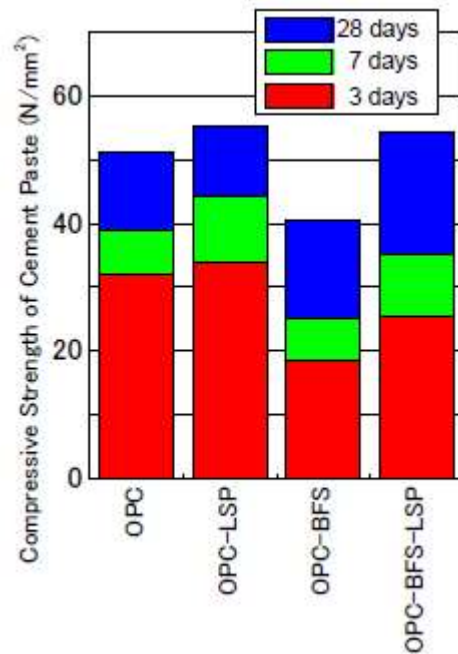


Fig. 1.2 Compressive strength development by LSP (Hoshino et al. 2006)

Rakhimova et al. (2014) investigated the compressive strength development of cement pastes by means of alkali activation. Sajedi and Razak (2010) also researched the influence of various kinds of alkali activators on the BFS blended cement properties. The results revealed that sodium hydroxide, sodium silicate, and potassium hydroxide could be used as the activators to increase BFS cement compressive strength. In addition, Gu et al. (2014) found that the mechanical and hydration properties of BFS blended cement could be increased by adding the chemical activator MgO–CaO mixtures.

At present, one promising approach that has been proposed involves limestone powder (LSP) being incorporated to improve the early strength of the BFS blended mixture. In the case of adding LSP, C3A reaction in the cement can accelerate at early curing age. Such properties are opposite to the characteristics of BFS cement, and when BFS and LSP are used in a mixture, the strength could be increased due to the LSP hydration at an early age while it increased due to the BFS upon long-term aging (Bonavetti et al., 2001; Menendez et al., 2003; Ghrici et al., 2007; Lothenbach et al., 2008; Courard & Michel, 2014; Scholer et al.,

2015). Additionally, some studies have been carried out using Gypsum (CS) as an alkali activator (Chang et al., 2005), and studies have been conducted to determine the effects of CS on the BFS blended cement. A disadvantage of replacing BFS cement with CS arises when the replacement ratio of CS exceeds optimum ratios, at which point the strength degrades (Antonio et al., 2010; Park et al., 2016).

1.2.3 Infulence of C-S-H type accelerator on strength

In recent years, calcium silicate hydrate (C-S-H) accelerators have revealed an entirely different mechanism than before, and they have been developed to serve the purpose of increased production efficiency, streamlining the manufacturing of secondary products of concrete, and showing an effect in all temperature ranges. There is a probability that C-S-H type accelerators can be utilized for cold weather conditions.

Imoto et al. found that C-S-H type accelerators had an effect in low-temperature curing environments, and they also affected C₃S hydration.

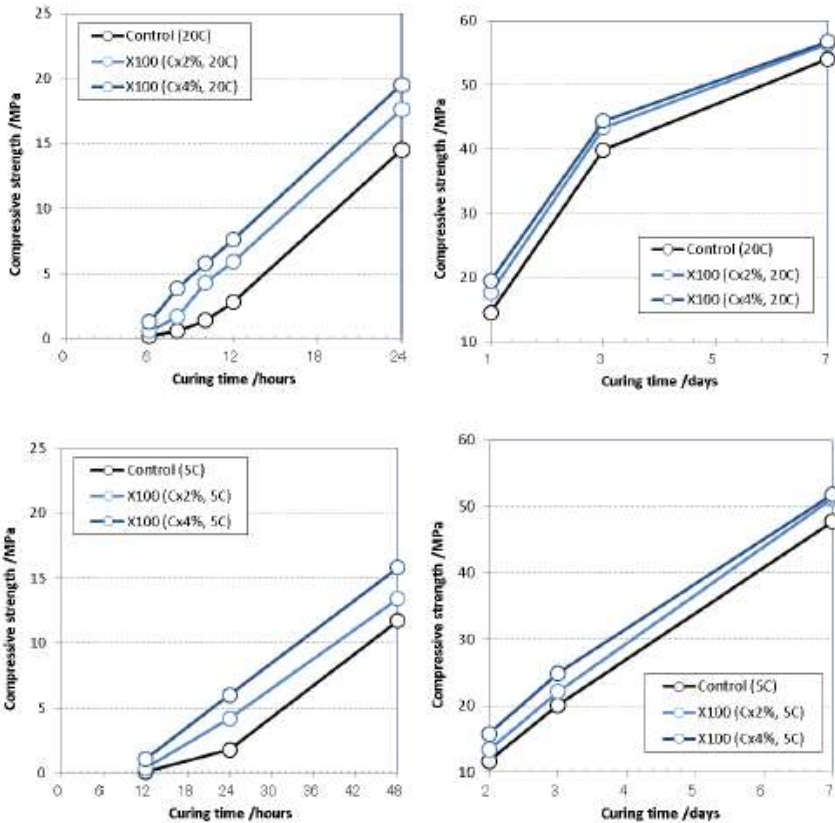


Fig. 1.3 Compressive strength development by C-S-H type accelerator (Imoto et al. 2006)

Onda et al. (2015) examined the strength development and heat generation characteristics at the initial age as a basic investigation of the applicability of each hardening promoting material, mainly for concrete used for PC upper work. Aggressive hardening was confirmed in the early strength development agent and various admixtures. The setting time accelerated, and the strength at the early curing age increased; however, the strength does not change in the long-term curing age. The estimated value of the adiabatic temperature rise amount in the simple adiabatic temperature rise test showed a slight increase tendency compared to the material not added.

Imoto et al. (2015) investigated the effect of C-S-H type accelerators on the type B blast furnace cement measurement setting and curing properties, and obtained the following results: 1) A C-S-H type accelerator can improve strength development. 2) C-S-H type accelerators promote initial hydration of BFS. 3) Even if the reaction of the BFS shows a similar trend by adding a C-S-H type accelerator, the pore structure showed densification.

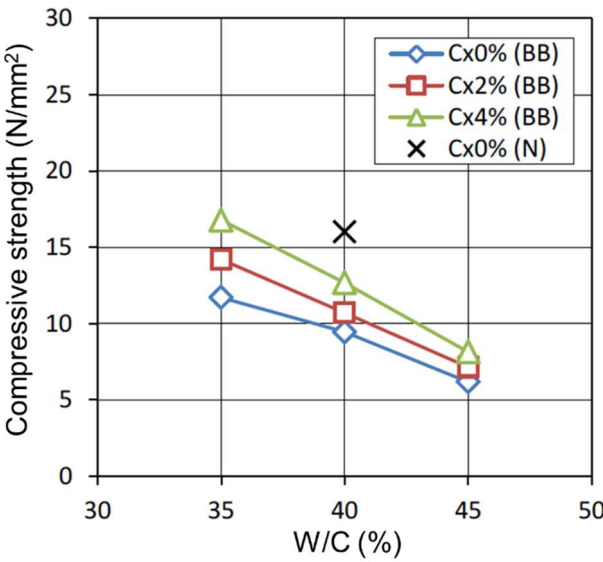


Fig. 1.4 Compressive strength development by C-S-H type accelerator on BFS cement (Imoto et al. 2015)

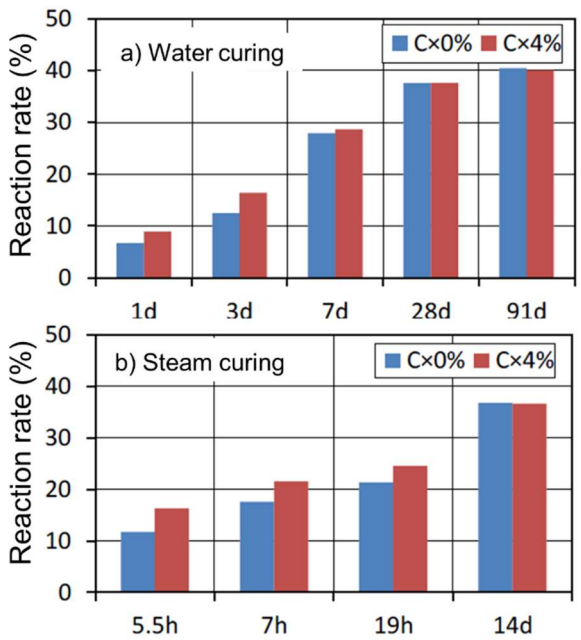


Fig. 1.5 Reaction rate by C-S-H type accelerator on BFS cement (Imoto et al. 2015)

Koyama et al. (2015) experimented with the focusing effect of steam curing. They concluded that: 1) The demold time can be shortened, or the steam curing temperature can be lowered. 2) The higher the maximum temperature of the steam curing, the higher the strength. 3) The C-S-H type accelerator was affected by the water binder ratio.

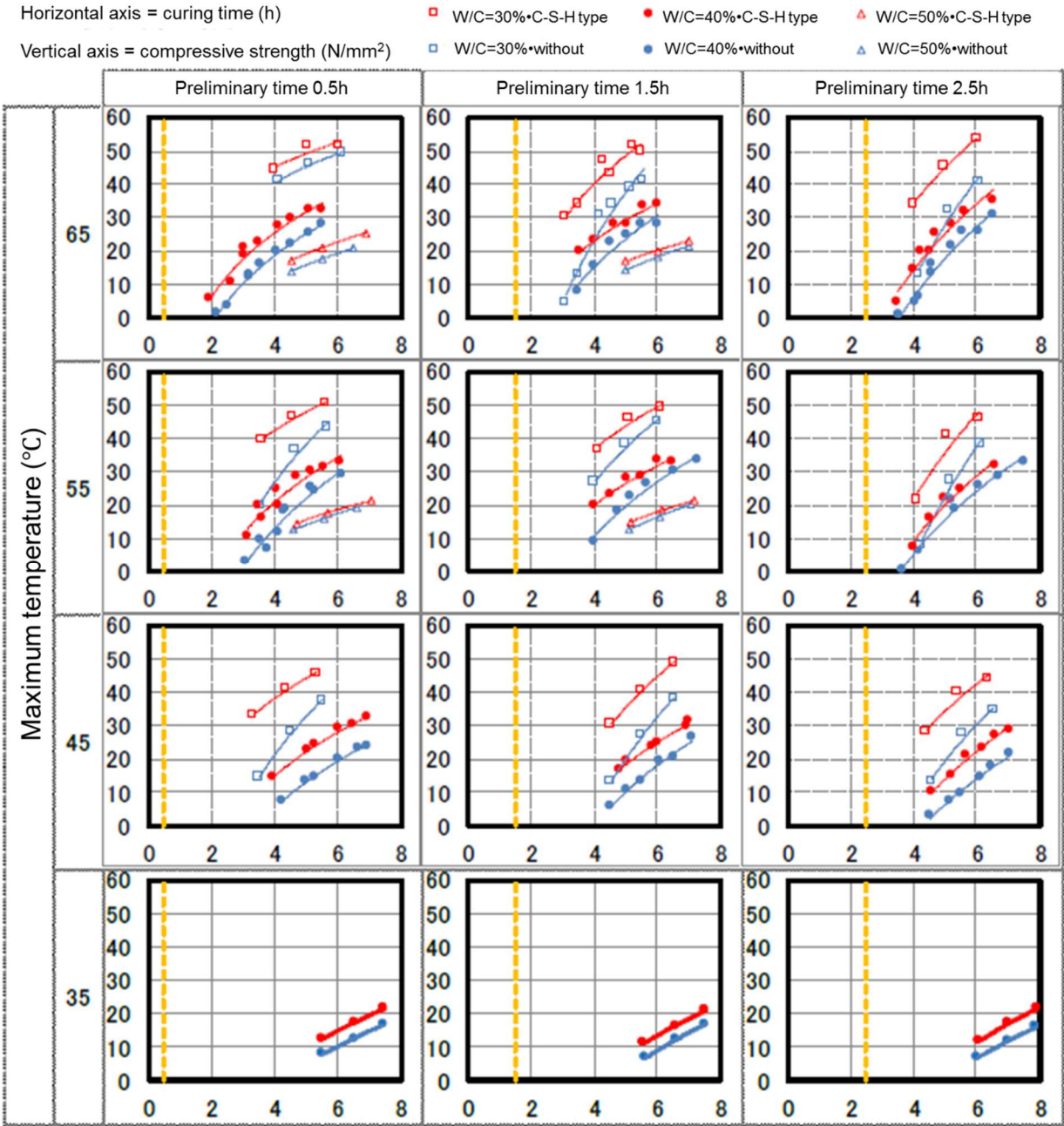


Fig. 1.6 Compressive strength development by C-S-H type accelerator on various water to binder ratio (Koyama et al. 2015)

Imoto et al. (2014) proposed the mechanism of the C-S-H type accelerator system. The nanoparticles of the binder in the liquid phase promote the hydration reaction. Therefore, nanoparticles are considered to move as crystals because they generate hydration products. Diffusion of ions is accelerated, and the initial hydration reaction of the cement is promoted.

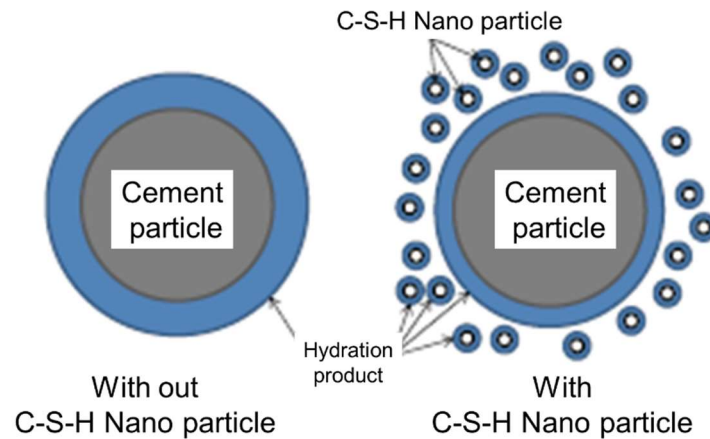


Fig. 1.7 Mechanism of the C-S-H type accelerator system (Imoto et al. 2014)

1.2.4 Influence of Ca/Si ratio of C-S-H

Ishida et al. (2013) investigated the carbonation behavior of C-S-H by exposing the simulated pore structure to CO₂ gas concentration environment under conditions of promoting carbonation by using a sample as a synthetic C-S-H with different Ca/Si ratios added. C-S-H remained even if the carbonation progressed and the pH nearly declined to the equilibrium value, and most of it was presumed to be low Ca type C-S-H, but only C-S-H with the initial Ca/Si ratio of 1.4, high Ca type C-S-H also remained. Although there was no difference in the carbonation rate due to the difference in the initial Ca/Si ratio, the lower the initial Ca/Si ratio, the more the residual amount of C-S-H was larger. This factor seems to be due to a large content of Si and a large amount of silica gel that inhibits carbonation.

Tanaka et al. (2009) investigated the density of C-S-H, the main hydrate of cementitious material, in order to evaluate the void volume in the cement hardened body more accurately. C-S-H, in which the Ca/Si ratio was varied, was pure chemically synthesized, and the density was measured. Furthermore, C-S-H, in which part of

the Si of the C-S-H was substituted with Al, was also synthesized, and the density was measured. In addition, calcium hydroxide added to C₃S or BFS fine powder was hydrated. From the density of the obtained cured product and the phase composition of the cured product, the density of C-S-H in the cured product was calculated. Taken together, the relationship between the Ca/Si molar ratio and the density of C-S-H with different production conditions was investigated. The density of C-S-H could be evaluated by Ca/Si ratio.

Suda et al. (2010) aimed to understand the physical properties such as C-S-H composition and density and specific surface area. The composition, density, and specific surface area of C-S-H were measured with a hydration sample of the synthetic C-S-H and the mixture of materials. As a result, it was confirmed that the H/S ratio of C-S-H does not depend on the material combination and is favorable to C/S. The density and specific surface area are proportional to the C/S ratio.

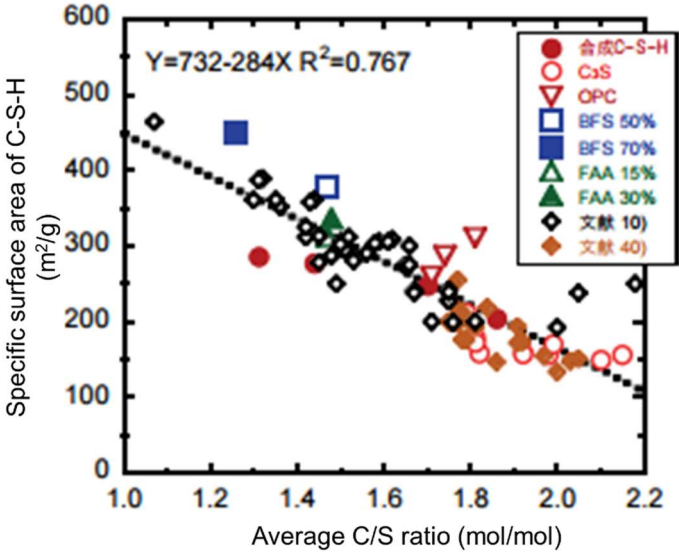


Fig. 1.8 relationship between C/S ratio and specific surface area (Suda et al. 2010)

1.2.5 Influence of affect carbonation deterioration on concrete

Hargis et al. (2014) reported that vaterite has low stability, high solubility, and large surface area, and that its reaction time is about three times faster than calcite. Vaterite is benefited from the mechanical properties of

the mortar. All of the mortars without gypsum increased the compressive strength of the mortar by reducing the expansion of the mortar with calcium carbonate. The timing of the increase in intensity corresponded to the reaction of calcium carbonate. Vaterite was more effective than calcite to reduce the loss of compressive strength.

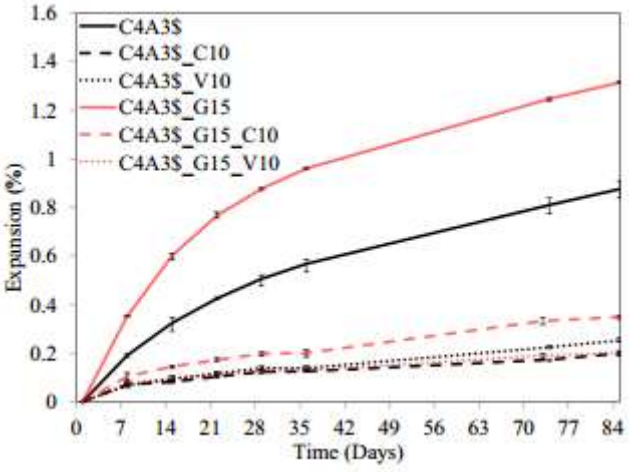


Fig. 1.9 relationship between expansion and various samples (hargis et al. 2014)

Igarashi et al. (2003) found that the formation process of the internal structure of cement paste made with a few cements with different particle sizes was studied by image analysis method of backscattered electron image with the characteristics of coagulation property, degree of hydration, and coarse capillary void structure. The cement particle size has a large influence on the space filling of the particles, and the initial degree of hydration increases as the particle diameter decreases. In addition, the coarse capillary void volume decreases with the formation of a large amount of cement gel. In addition, at long-term age, the difference in coarse capillary void structure is small, but the dispersion characteristics of unreacted particles characterize the difference in microscopic structure.

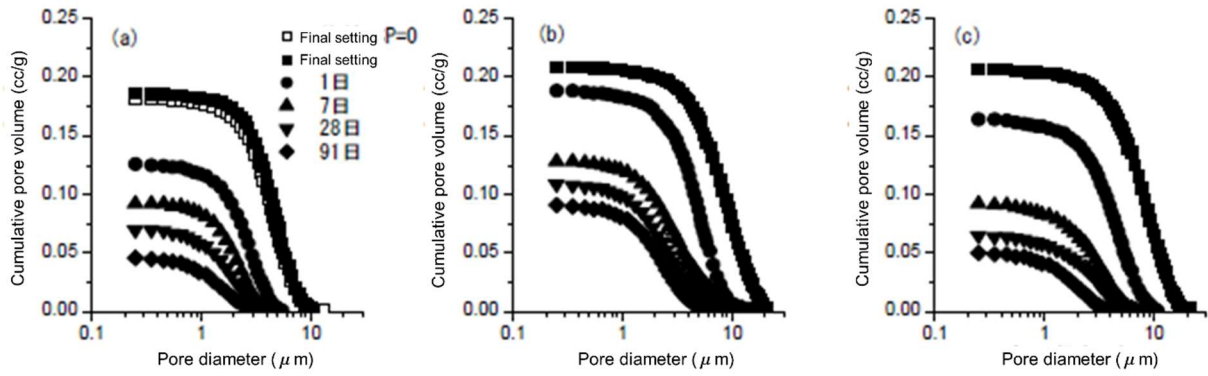


Fig. 1.10 relationship between curing age and pore volume (Igarashi et al. 2014)

Yoneyama et al. (2008) introduced the concept of spatial statistics to the image analysis of the backscattered electron image of cement paste, and the relation between the parameter relating to the change of the continuity of the solid phase was evaluated, and the relation between the strength development mechanism of the cement paste and the model of power's was investigated. The growth tendency of the solid phase corresponds to the development of strength, and the compressive strength of the cement paste is similar. The spatial structure of the solid phase and the coarse capillary voids are almost in agreement, too. It was also confirmed from the change of the spatial correlation function that the formation of a solid phase that reduces coarse voids is important for strength development.

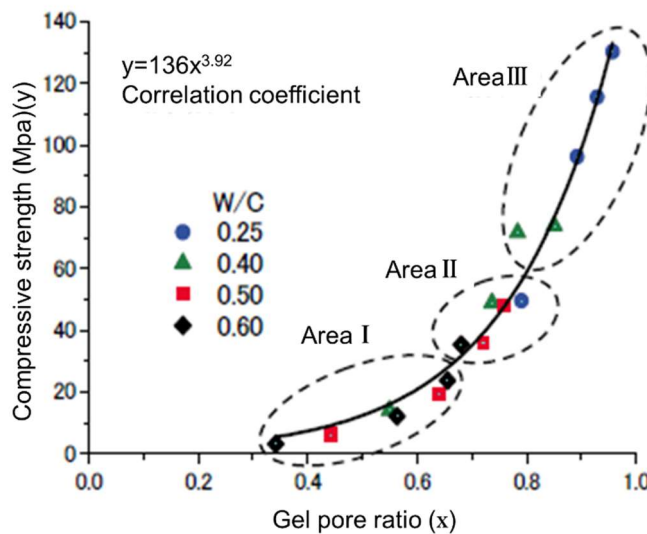


Fig. 1.12 relationship between gel pore and compressive strength (Yoneyama et al. 2008)

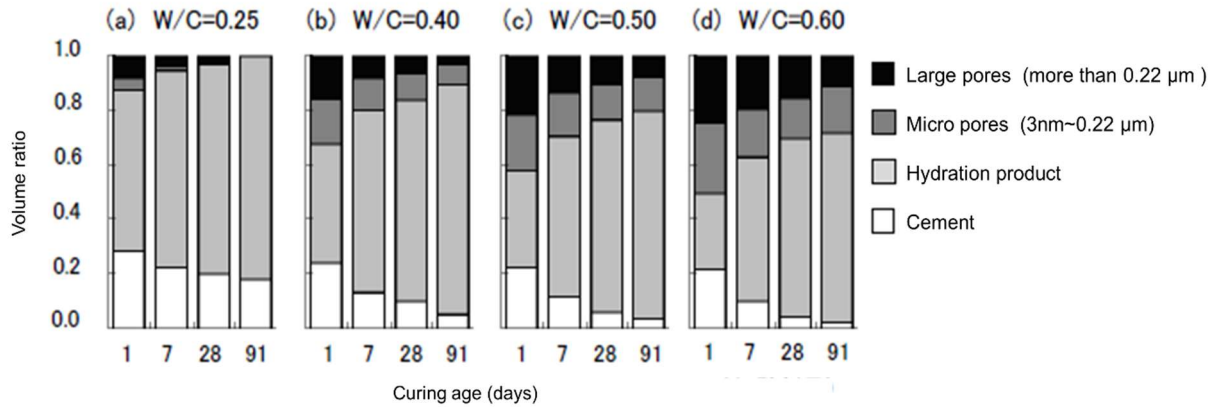


Fig. 1.13 relationship between curing age and pore structure (Yoneyama et al. 2008)

Li et al. (2009) conducted basic studies on the influence of carbonation during drying from the early stage on the pore structure and oxygen diffusion coefficient of the cement hardened body, focusing on the water cement ratio and the curing age of the samples. The cement hardened samples exposed to the dry environment from early curing age were evaluated for carbonation depth by accelerating carbonation, total pore volume, pore size distribution, and specific surface area. Saturation, oxygen diffusion coefficient, and the effect of carbonation progression from the early stage on the pore structure and oxygen diffusion behavior of the cement samples were examined as well. As a result, the carbonation progressed from the curing age, although the pore structure became denser. In both cases, the influence on the oxygen diffusion coefficient varied depending on the water cement ratio, and in the case of the water cement ratio of 30% and 45%, the diffusion coefficient decreased, and when the water cement ratio was 60%, the diffusion coefficient increased.

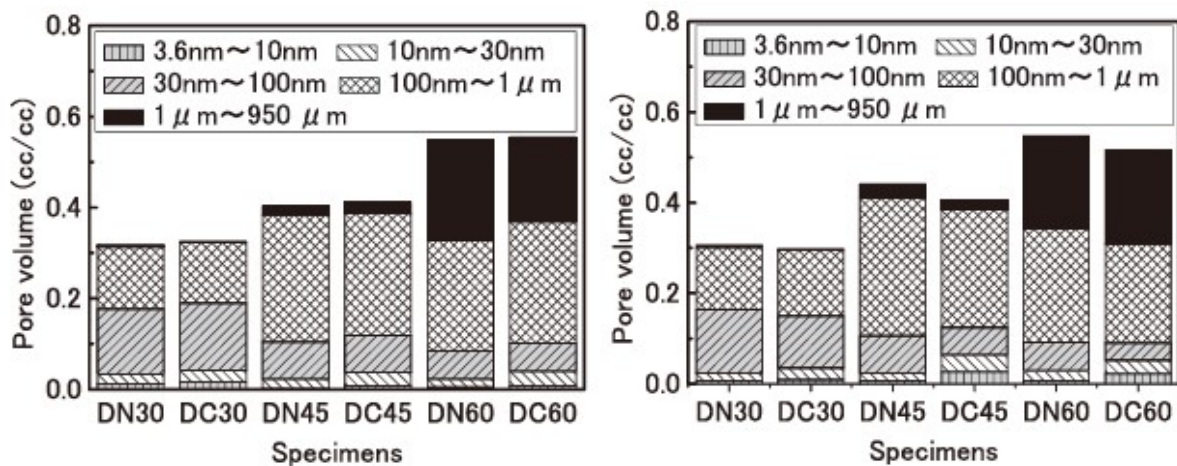


Fig. 1.14 relationship between various curing environment and pore volume (Li et al. 2009)

Saeki et al. (1990) investigated pore size distribution, the amount of calcium hydroxide, the amount of calcium carbonate, and weight change, respectively. After carbonation, the pore structure changes in terms of pore volume and pore size distribution. In addition, the difference in pore size distribution and pore size distribution by carbonation is different due to the difference in initial curing conditions of the water cement ratio. This is because the state of the matrix after the initial curing is different, and the rate of progress of the carbonation is different. When the carbonation test promoting dryness repetition is performed, the total amount of pores of the mortar decreases. In addition, the pore size distribution moves toward small diameters and increases the fine holes around 100A in diameter. The carbonation test was carried out, and the amount of the pores' volume changed or increased with time. This is due to the fact that there is little increase in the carbonation depth, and the dissolution of calcium hydroxide in the solid phase and the formation and dissolution of calcium hydrogen carbonate compensate for the consumption of calcium hydroxide by the carbonation reaction. With dry and wet repetition, if the water cement ratio is high in the carbonation test, pores around 1000A tend to increase. The pore size distribution changes due to the progress of carbonation, and the water cement ratio decreases with increasing water evaporation rate and water absorption rate in the specimen, while it tends to increase with higher water cement ratio. Densification of tissues by neutralization has the effect of suppressing the progress of neutralization thereafter.

1.3 Problem definition

From the above researches, some of the main problems of investigation on the BFS blended cement could be described as follows:

- (1) For the C-S-H type accelerator, the behavior and mechanism of the C-S-H type accelerator for BFS blended cement has not been fully clarified. Moreover, adding to the fact that most previous studies concerned ordinary Portland cement as high-temperature environment curing, while, the studies about the C-S-H type accelerator evolution in cementitious composites incorporating BFS are notably few.

- (2) For the compressive strength development using mineral admixture, the mixture amount of gypsum and limestone powder for BFS blended cement has not been clearly established. Moreover, investigations for compressive strength development of mineral admixture of quantification are not clear, either. In addition, calculations using power equations to compare pore volume and compressive strength incorporating BFS are few.
- (3) A different microstructure was formed in cementitious composites by carbonation deterioration compared with curing age. In spite of this, the clarification of incorporating BFS cement characteristics and curing age effects on the carbonation and microstructure formation has not been fully understood, which is quite important for studies on combined deterioration in cementitious composites with BFS.
- (4) According to the different mechanism of combined deterioration, the influence of pore structure on the carbonation and frost damage has not been completely unified, and it is necessary to propose a uniform pore structure involved in the combined deterioration, which could provide useful information for combined deterioration behavior.

1.4 Research aims and thesis organization

This thesis is organized into six chapters as follows:

Chapter 1 covers the research background of BFS blended cement and the durability of combined deterioration by carbonation and frost damage both in domestic and overseas contexts, and the logic for the thesis organization is also presented.

Chapter 2 discusses recent research to study the compressive strength developed method using the C-S-H type accelerator; it is an experiment for the availability in the BFS incorporation cementitious composite.

In addition, the experimental investigates the characteristics of thermal characteristics, chemical analysis, etc., in accordance with various cement types by using C-S-H type accelerator.

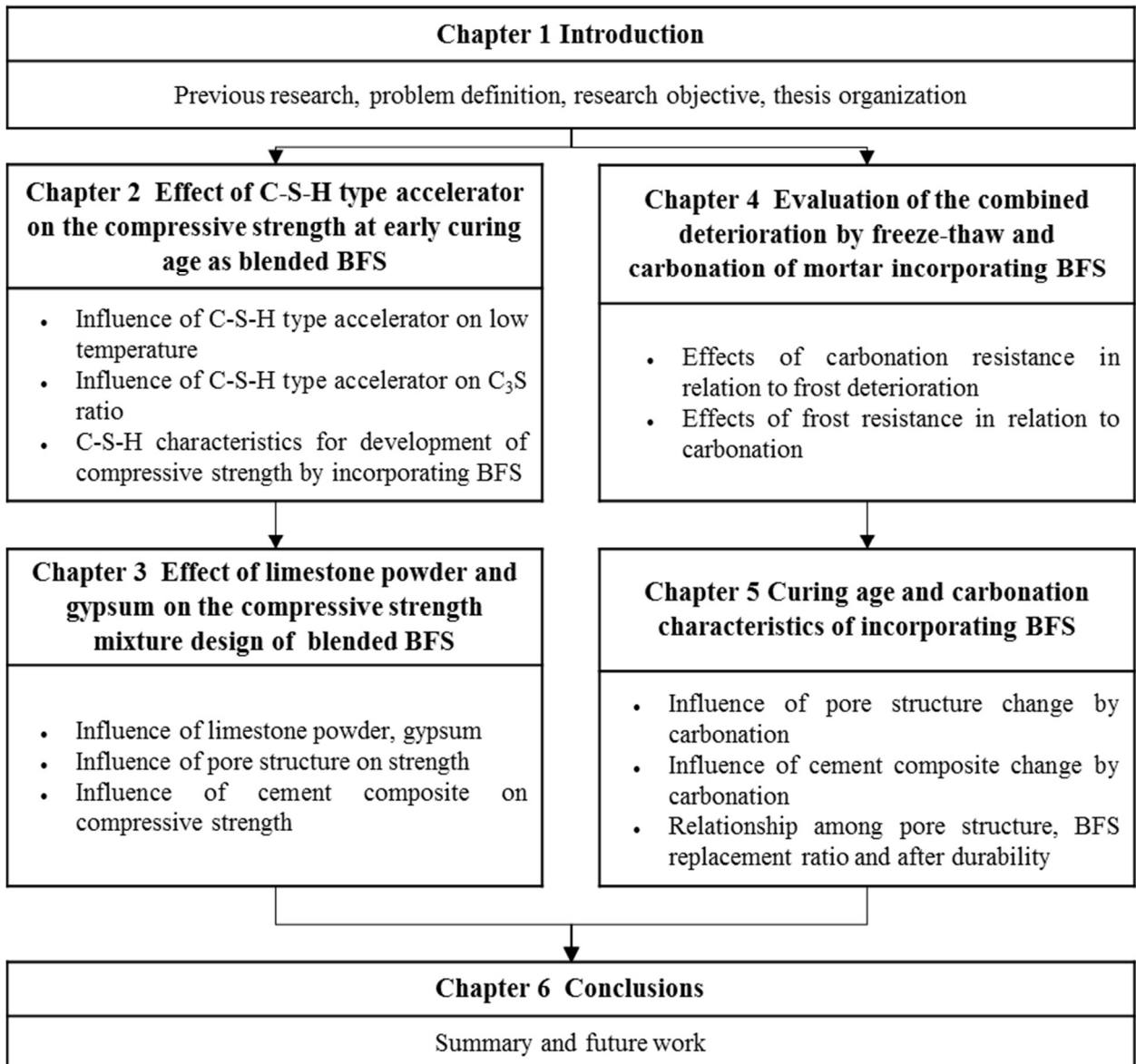
Chapter 3 investigates experimentally the mineral admixture by the compressive strength development of the BFS replacement mortar with the quantification of the cement hydrate by XRD/Rietveld method. In addition, it identifies that the compressive strength of cement-based composite depends on the porosity, which can be experimentally evaluated by calculation from XRD/Rietveld method analysis.

Chapter 4 obtains the applicable pore structure in the combined carbonation and frost damage deterioration of mortar samples, and investigates single deterioration and combined deterioration. Moreover, an experiment for the durability of mineral admixture incorporating limestone powder and gypsum was conducted, and the influence of the limestone powder and gypsum replacement in BFS cement in combined deterioration is investigated.

Chapter 5 experimentally confirms the effect of carbonation on cementitious composite to compare the with and without carbonation of BFS blended paste samples. Therefore, the porosity change of the pore structure and the total porosity by carbonation is identified. In addition, the changed chemical composite measurements by thermal analysis according to carbonation, and XRD method on cement composite by carbonation in the incorporating BFS cement, are considered.

Chapter 6 shows the thesis conclusion and further research work in the future.

The following is this thesis structure:



References:

- Barnett, S. J., Soutsos, M. N., Millard, S. G., and Bungey, J. H., Strength development of mortars containing ground granulated blast-furnace slag: Effect of curing temperature and determination of apparent activation energies, *Cement and Concrete Research*, 36, 2006, pp. 434–440
- Bonavetti, V. L., Rahhal, V. F., and Irassar, E. F., Studies on the carboaluminate formation in limestone filler-blended cements, *Cement and Concrete Research*, 31, 2001, pp. 853–859
- Borges, H.R. P., Costa, O. J., Milestone, B. N., Lynsdale, J. C., Streatfield, E. R., (2010). “Carbonation of CH and C-S-H in composite cement pastes containing high amounts.” *Cement and Concrete Research*, 40, 284-292.
- Çetin, C., Erdogan, S. T., and Tokyay, M., Effect of particle size and slag content on the early hydration of interground blended cements, *Cement and Concrete Composites*, 67, 2016, pp. 39–49
- Chang, J. J., Yeh, W., and Hung, C. C., Effects of gypsum and phosphoric acid on the properties of sodium silicate-based alkali-activated slag pastes, *Cement & Concrete Composites*, 27, 2005, pp. 85–91.
- Chen, H. J., Hung, S. S., Tang, C. W., Malek, M.A., and Ean, L. W., Effect of curing environments on strength, porosity and chloride ingress resistance of blast furnace slag cement concretes: A construction site study, *Construction and Building Materials*, 35, 2012, pp. 1063–1070
- Courard, L., and Michel, F., Limestone fillers cement based composites: Effects of blast furnace slags on fresh and hardened properties, *Construction and Building Materials*, 51, 2014, pp. 439–445
- Escalante-Garcia, J.I., Mendoza, G., Sharp, J.H., (1999). “Indirect determination of the Ca/Si ratio of the C-S-H gel in Portland cements.” *Cement and Concrete Research*, 29, 1999-2003.
- Gu, K., Jin, F., Abir, A. T., Shi, B., and Liu, J., Mechanical and hydration properties of ground granulated blast furnace slag pastes activated with MgO–CaO mixtures, *Construction and Building Materials*, 69, 2014, pp. 101–108
- Gu, Y. M., Fang, Y. H., You, D., Gong, Y. F. and Zhu, C. H., (2015). “Properties and microstructure of alkali-activated slag cement cured at below- and about-normal temperature.” *Construction and building*

Materials, 79, 1-8.

Hargis, C.W., Telesca, A., Monteiro P.J.M., (2014). "Calcium sulfoaluminate (Ye`elinite) hydration in the presence of gypsum, calcite, and vaterite." *Cement and Concrete Research*, 65, 15-20.

Ichitsubo, K., Yamashita, H., Tanosaki, T., Satake, S., Research of highly functional cement that reduced interstitial liquid phase content (part 2 study of further reduction of interstitial liquid phase content and increase of C3S content), *Cement Science and Concrete Technology*, Vol. 63, 2009, pp. 62-69 (in Japanese)

Imoto, H., Koizumi, S., Hanafusa, K., Baba, Y., Effect of a C-S-H type accelerator on the strength development of blast furnace slag cement, *Architectural Institute of Japan*, 2015, pp. 49-50 (in Japanese)

Imoto, H., Koizumi, S., Hanafusa, K., Baba, Y., Initial curing behavior of concrete using C-S-H type early strengthening agent and bleeding suppression effect, *Japan Concrete Institute*, Vol. 36(1), 2014, pp. 2248-2253 (in Japanese)

Ishida, S., Igarashi. S., (2012). "Influence of progress of neutralization on the capillary void structure of cement paste." *Concrete Research and Technology*, 34(1), 622-627.

Ishida, S., Igarashi. S., Koike, Y., (2011). "Effects of early-age carbonation on mechanical and electrical properties of cement pastes and concretes." *Japan Cement Association*, 65(1), 282-289.

Ishida, T., Ito, Y., Kawai, K., (2013). "Carbonation characteristics of the C-S-H with various Ca/Si ratios." *Japan Cement Association*, 67(1), 487-494.

Kakali, G., Tsvivilis, S., Aggeli, E., Bati, M., (2000). "Hydration products of C₃A, C₃S and Portland cement in the presence of CaCO₃." *Cement and Concrete Research*, 30, 1073-1077.

Koyama, H., Sasaki, H., Date, S., Initial Strength Development of Precast Concrete Using C-S-H System Early Strength Agent, *Japan Concrete Institute*, Vol. 37(1), 2015, pp. 331-336 (in Japanese)

Koyama, H., Uemura, S., Nakajima, N., Date, S., Influence of steam curing on curing properties of mortar using C-S-H type early strengthening agent, *Japan Concrete Institute*, Vol. 38(1), 2016, pp. 231-236 (in Japanese)

Li, C., Nakarai, K., Ishii, Y., Yokozuka, K., (2009). "Experimental study on effect of carbonation of early aged cement paste on micro-pore structure and effective diffusion coefficient of oxygen." *Cement Science and*

Concrete Technology, 63, 99-106.

Lothenbach, B., Saout, G. L., Gallucci, E., and Scrivener, K., Influence of limestone on the hydration of Portland cements, *Cement and Concrete Research*, 38, 2008, pp. 848–860

Menendez, G., Bonavetti, V., Irassar, E.F., (2003). “Strength development of ternary blended cement with limestone filler and blast-furnace slag.” *Cement & Concrete Composites*, 25, 61-67.

Miyazawa, S., Yokomuro, T., Sakai, E., Yatagai, A., Nito, N., and Koibuchi, K., Properties of concrete using high C₃S cement with ground granulated blast-furnace slag, *Construction and Building Materials*, 61, 2014, pp. 90–96

Ngala, V.T., Page, C.L., (1997). “Effects of carbonation on pore structure and diffusional properties of hydrated cement pastes.” *Cement and Concrete Research*, 27, 995-1007.

Nippon Slag Association, Use of blast furnace slag of steel slag, 2015 (in Japanese)

Özbay, E., Erdemir, M., and Durmus, H. I., Utilization and efficiency of ground granulated blast furnace slag on concrete properties – A review, *Construction and Building Materials*, 105, 2016, pp. 423–434

Park, H., Jeong, Y., Jun, Y., Jeong, J., and Oh, J., Strength enhancement and pore-size refinement in clinker-free CaO-activated GGBFS systems through substitution with gypsum, *Cement and Concrete Composites*, 68, 2016, pp. 57–65

Phung, Q.T., Maes, N., Jacques, D., Bruneel, E., Driessche, I. V., Ye, G., Schutter, G.D., (2015). “Effect of limestone fillers on microstructure and permeability due to carbonation of cement pastes under controlled CO₂ pressure conditions.” *Construction and Building Materials*, 82, 376-390.

Rakhimova, N. R., and Rakhimov, R. Z., Characterisation of ground hydrated Portland cement-based mortar as an additive to alkali-activated slag cement, *Cement & Concrete Composites*, 57, 2015, pp. 55–63

Rakhimova, N. R., and Rakhimov, R. Z., Individual and combined effects of Portland cement-based hydrated mortar components on alkali-activated slag cement, *Construction and Building Materials*, 73, 2014, pp. 515–522

Rostami, V., Shao, Y., Boyd, A. J., He, Z., (2012). “Microstructure of cement paste subject to early carbonation curing.” *Cement and Concrete Research*, 42, 186-193.

Saeki, T., Ohga, H., Nagataki, S., (1990). "Change in micro-structure of concrete due to carbonation." *Journal of Japan Society of Civil Engineers*, 420, 33-42.

Sajedi, F., and Razak, H. A., The effect of chemical activators on early strength of ordinary Portland cement-slag mortars, *Construction and Building Materials*, 24, 2010, pp. 1944–1951

Sajedi, F., Razak, H. A., (2010). "The effect of chemical activators on early strength of ordinary Portland

Scholer, A., Lothenbach, B., Winnefeld, F., and Zajac, M., Hydration of quaternary Portland cement blends containing blast-furnace slag, siliceous fly ash and limestone powder, *Cement & Concrete Composites*, 55, 2015, pp. 374–382

Suda, Y., Study on performance evaluation of hardened cement paste based on relation between chemical composition and physical property of C-S-H, Niigata University, doctoral dissertation, 2013 (in Japanese)

Suda, Y., Tanaka, Y., Saeki, T., (2010). "Fundamental study on chemical composition and physical properties." *Japan Society of Civil Engineers*, 66(4), 528-544.

Tanaka, Y., Saeki, T., Sasaki, K., Suda, Y. (2009). "Fundamental study on density of C-S-H." *Japan Cement Association*, 63(1), 70-76.

Taylor, H. F. W., *Cement Chemistry*, Thomas Telford, 2nd. Edition, 1997, pp. 262–271

Thiery, M., Villain, G., Dangla, P., Platret, G., (2007). "Investigation of the carbonation front shape on cementitious materials: Effects of the chemical kinetics." *Cement and Concrete Research*, 37, 1047-1058.

CHAPTER 2

EFFECT OF C-S-H TYPE ACCELERATOR ON THE COMPRESSIVE STRENGTH AT EARLY CURING AGE AS BLAST FURNACE SLAG BLENDED CONCRETE

2.1 Overview

Early curing age compressive strength was raised as a problem in blast furnace slag (BFS) blended concrete. The development of early curing age compressive strength was the main reason for increasing the amount of BFS blended concrete. Many researchers have studied the early curing age strength development of BFS blended concrete by using alkali liquid activators such as Na_2SO_4 , NaOH , and water glass (i.e., sodium silicate). Such liquid activators can increase the early curing age strength development of BFS blended concrete.

Recently, calcium silicate hydrate (C-S-H) type accelerators have been used for increasing the compressive strength of concrete. Imoto et al. (2014; 2015) investigated the properties of C-S-H type accelerators, including compressive strength, hydration reaction, bleeding, reaction rate, and setting time. Koyama et al. (2015; 2016) investigated the effect of C-S-H type accelerators under steam curing, with evaluation by compressive strength. Koizumi et al. (2014) investigated the effect of C-S-H type accelerators on concrete durability. Onda et al. investigated the strength and heating characteristics by using various accelerator agents, including C-S-H type accelerators. They were examined for their reactivity and compressive strength, and compared with ordinary Portland cement. These results showed that the properties of C-S-H type accelerators were dependent on the C_3S amount of the cement mineral, and that adding C-S-H type accelerators could increase the compressive strength and accelerate hydration reaction.

The present study attempts to improve the strength of BFS cement with the aim of increasing the amounts of BFS use. In addition, in order to determine the effect of the C_3S amount, various cement types were used in this study. Finally, XRD and a calorimeter were used for determining the reaction rate due to the C-S-H type accelerator on the compressive strength in the BFS blended mixture incorporating various cement types.

2.2 Experimental program and method

2.2.1 Materials and experimental design

Table 2.1 shows the used material, and the mix proportion of concrete is given in Table 2.2. Specimens were

prepared with 50% water-to-cement ratio (W/C) by using crushed stone, natural sand, and ordinary Portland cement, or BFS cement type B was used as per JIS. The additive amount of C-S-H type accelerator was 0, 2, 4, and 8 wt% of the cement weight. The samples were cured using a $\phi 50 \times 100$ mm plastic mold. OPC and BFS were used for the cement types.

Table 2.1 Material

Material	Symbol	Type	Density [g/cm ³]
Cement	N	Ordinary Portland cement	3.16
	BB	Blast-furnace slag cement type B	3.05
Fine aggregate	S	Land sand	2.66
Coarse aggregate	A	Crushed stone	2.62
Admixture	CA	Calcium Silicate Hydrate type accelerator (C-S-H nanoparticle Suspension)	

Table 2.2 Mix proportion of concrete

Symbol	Cement	W/C [%]	S/a [%]	Unit mass [kg/m ³]				CA [C×%]
				W	C	S	A	
N-P	N	50	47.6	175	350	891	967	-
N-C2			47.9	172	344	904		2
N-C4			48.8	165	330	935		4
N-C8			49.8	156	312	974		8
BB-P	BB		46.7	168	336	886	993	-
BB-C2			47.1	165	330	899		2
BB-C4			48.8	151	302	960		4
BB-C8			49.7	143	286	995		8

2.2.2 Fresh property, setting time and compressive strength

After the concrete was mixed, the freshness property was evaluated by a slump test (JIS A 1101-2005) and an air volume test (JIS A 1128-2005) in accordance with the evaluation quality standard of accelerators for freeze protection, and the quality of C-S-H type accelerator was measured. To extract cement mortar from concrete, the test sample was used under an environment of 20°C and 5°C. All specimens were cast into

φ100×200mm cylinder molds. The compressive strength test was conducted in accordance with JIS A 1108-2006. To test the samples' early age compressive strength, the top surface was capped with gypsum after 1 day curing at 20°C due to the fact that the early age compressive strength was too low to demold (20°C for 1, 3, 7, and 28 days, and 5°C for 2 days, respectively).

2.2.3 Heat of hydration

Cement paste was run into a 35mm film case (resin-made mold) with 50% W/C, and the heat of hydration has been measured at a constant temperature of 20°C since 72 hours of starting by a twin-type conduction calorimeter (CHC-OM6). A laxative called liquid paraffin was used as a reference, and the heat of hydration was obtained by comparative calculation between the reference heat quantity and unknown one of each sample.

2.2.4 X-ray diffraction

In XRD, ordinary Portland cement and blast furnace slag cement type B are used as cement, and the C-S-H type accelerator has been used at dosages of 0 and 4% by mass of the cement. Table 4 shows the synopsis for XRD analysis. It was kneaded under a specific amount of water, and the kneaded material was shaped into a 50ml plastic pillar sample bottle and a prescribed curing period at a certain temperature of 20°C. This was done for 3, 6, 10, and 24 hours in the case of using ordinary Portland cement, and for 3, 10, 20, and 30 hours in the case of blast furnace slag cement type B. After that, hydrate was put to a stop by acetone displacement for 24 hours (hydration reaction was stopped by immersing the cement sample in solution acetone within 24 hours). Then, these were suction-filtered, freeze-dried for 24 hours, and dried in a desiccator.

In addition, the samples were pulverized to a particle size of about 5 mm and analyzed by X-ray powder diffraction internal standard method. The measurement conditions were as following: CuKα radiation with scintillation detector, tube voltage 45kV, tube current 40 mA, scans range of 5~70 deg.2θ, step width 0.02 deg. and using by semiconductor high-speed detector.

Table 2.3 Synopsis for analysis of X-ray diffraction

Cement	ACX [C × %]	Age [h]					
		3	6	10	20	24	30
N	-	○	○	○	-	○	-
	4	○	○	○	-	○	-
BB	-	○	-	○	○	-	○
	4	○	-	○	○	-	○

2.3. Experimental results and discussion

2.3.1 Relationship among the C-S-H type accelerator and compressive strength development, and characteristics of low temperature

Figure 2.1 shows the results for the compressive strength of C-S-H type accelerator added to the sample with replacement ratios of 2%, 4%, and 8% by weight of cement. In the case of the N samples, the compressive strength was increased with increasing C-S-H type accelerator replacement ratio, even though the curing ages increased. However, in the case of the BB samples, they showed no effect compared to that of the C-S-H type accelerator. This suggests that a C-S-H type accelerator would depend on the amount of C₃S cement mineral (Imoto et al., 2014). Figure 2.2 shows the compressive strength ratio of the C-S-H type accelerator. It can be seen that the compressive strength of the N samples tends to increase with increasing C-S-H type accelerator. However, there was no correlation seen in the BB samples. Previous studies have confirmed that the compressive strength when using a C-S-H type accelerator with the BFS blended sample can depend on the water-to-binder ratio (Imoto et al., 2015). Consequently, the compressive strength development rate is lower at high water-to-binder ratios. Figure 2.3 shows the compressive strengths with curing temperatures of 20°C and 5°C for the investigation of the C-S-H type accelerator effect on the low temperature. In the case of the N sample, the results were similar to the compressive strength in Fig. 2.1, with the compressive strength increasing with increasing amount of C-S-H type accelerator at low curing temperature. The obtained results agree with those in previous studies reported in the literature (Imoto et al., 2014).

In the above compressive strength test results, with regard to the effects of using C-S-H type accelerator, the compressive strength increased with the increasing amount of C-S-H type accelerator in the N samples at an all-curing age, but had no effect in the BB samples in this study (W/B 50%). Regarding the effect at low temperature, it was found that the strength increased in the N samples.

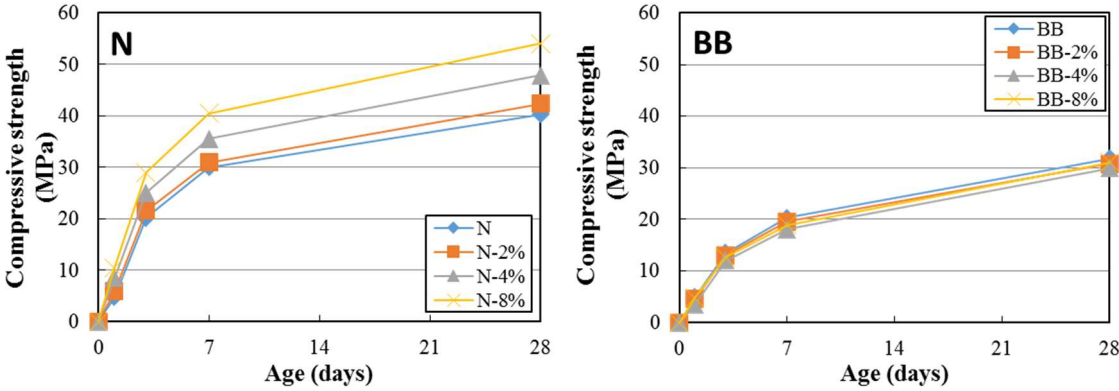


Fig. 2.1 Compressive strength according to C-S-H type accelerator content.

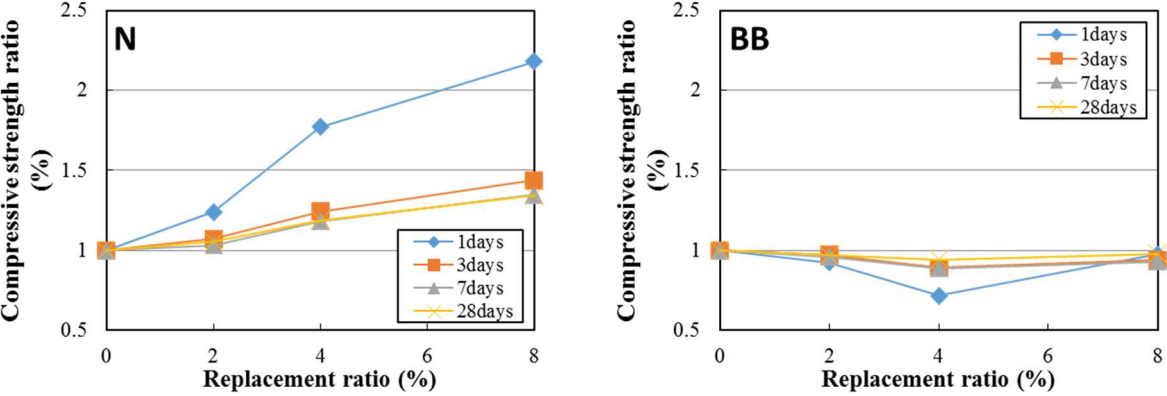


Fig. 2.2 Compressive strength ratio according to C-S-H type accelerator content.

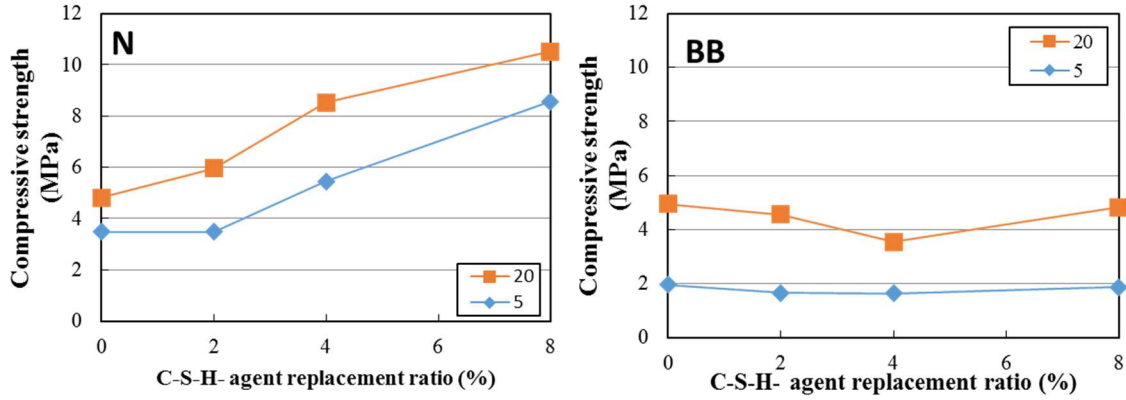


Fig. 2.3 Compressive strength result at low temperature.

2.3.2 Effect of C-S-H type accelerator on the setting time and cement composition

The results of the setting time under temperatures of 20°C and 5°C are given in Fig. 2.4. The initial setting time of the N and BB samples accelerates with elevation of C-S-H type accelerator usage. Depending on the C-S-H type accelerator usage, the N samples have a bias in that they shorten the time between initial setting time and final setting time. If they were under a 20°C condition, the time shortened for about 5 hours in the presence of a C-S-H type accelerator. However, in the case of the BB samples, the replacement ratio of the C-S-H type accelerator and the initial setting time had a clear relationship, and thus the C-S-H type accelerator can affect the shortening of the setting time (Imoto et al., 2014; Imoto et al., 2015). Similar results were obtained in this paper.

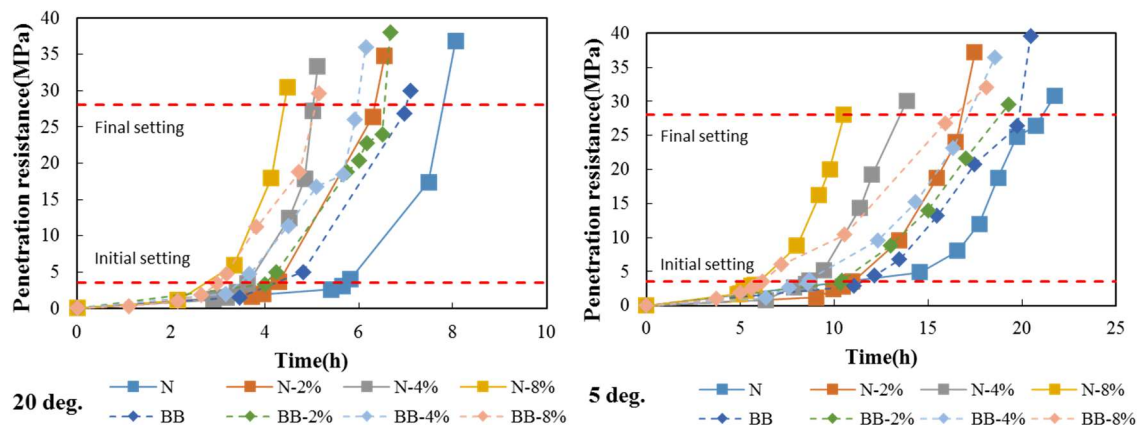


Fig. 2.4 Setting time result by various temperature.

Figure 2.5 shows the result of the analysis of the XRD paste samples: C-S-H type accelerator added 0 wt%

and 4 wt%, in relation to the cement mass in the N and BB samples. The XRD data for the N samples were collected after curing at 0, 3, 6, 10, and 24 hours, and the BB samples were collected after curing at 0, 3, 10, 20, and 30 hours. A calcium hydroxide (Ca(OH)_2 ; CH, peaks of $2\theta=18^\circ, 34^\circ, 47^\circ$) peak is found in all cement paste samples. However, it can be seen that there is a stronger peak by adding the C-S-H type accelerator to the cement paste samples. The CH was formed by reaction of a C_3S (peaks of $2\theta=29^\circ, 41^\circ, 52^\circ$) clinker mineral with water. It can be seen that the C_3S of the C-S-H type accelerator addition tends to be lower than without it at 10 hours. Moreover, in the case of adding C-S-H type accelerator 4 wt% in relation to the BB cement paste samples, the production of hydrotalcite (peaks of $2\theta=12^\circ$) was seen 0 and 3 hours. Moreover, monosulfate (AFm, peaks of $2\theta=9^\circ$) was seen after 20 hours in the case of the BB cement paste samples. In addition, the characteristics of adding C-S-H type accelerator in the cement paste samples meant that the intensity of the CH peaks is stronger than without C-S-H type accelerator.

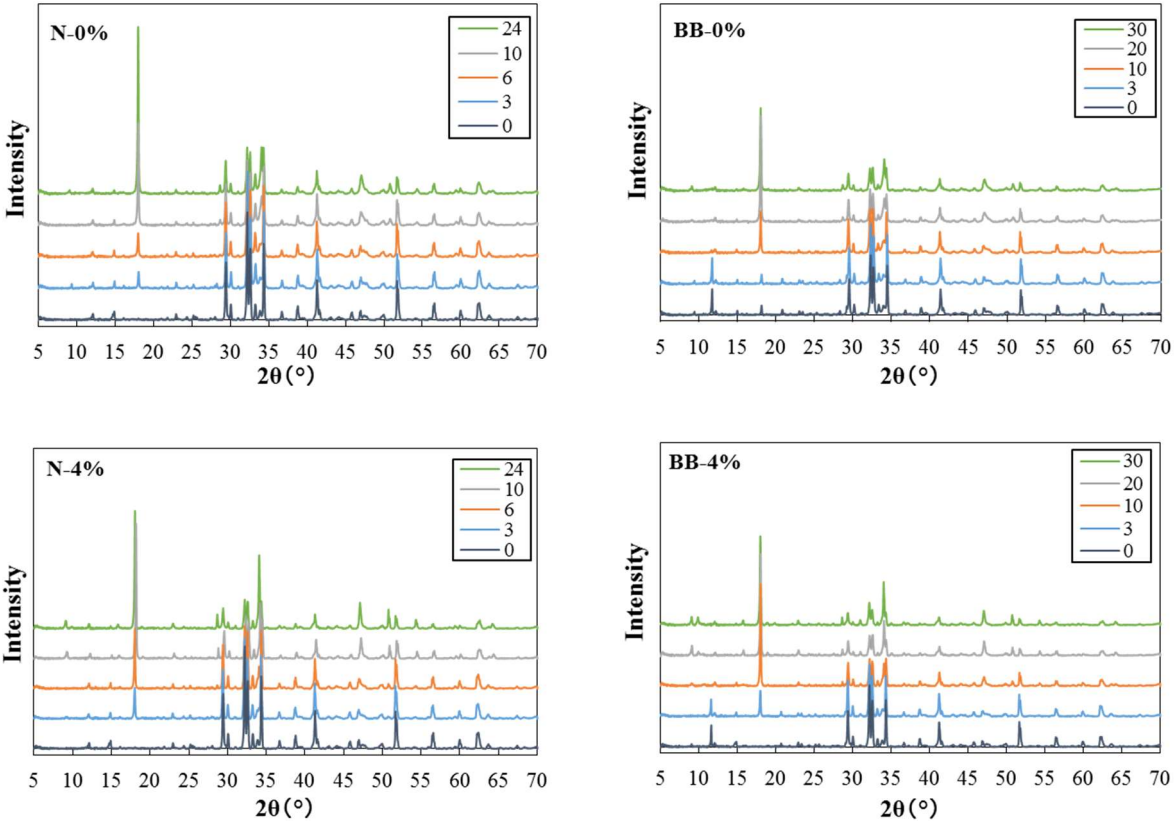


Fig. 2.5 X-ray diffractions patterns according to C-S-H type accelerator.

The effect of C-S-H type accelerator on the setting time and cement composition of the BFS blended

cement samples is as follows: The setting time can be shorter by the promotion of the reaction of C_3S , and the XRD result shows strong peaks of CH by adding C-S-H type accelerator. On the other hand, the peaks of C_3S were weaker than without C-S-H type accelerator by accelerate of CH products.

2.3.3 Optimization of C_3S ratio as C-S-H type accelerator reaction for compressive strength development

In this section, the investigation of the effect of C_3S ratio at compressive strength development by added C-S-H type accelerator in various cements is discussed. Figures 2.6 and 2.7 show the results for the compressive strength and strength development ratio for the various types of cement. In the case of the N samples, the compressive strength increased with increasing C-S-H type accelerator ratio. However, for the BB samples, with a C-S-H type accelerator, the compressive strength had little effect at all-curing days. This

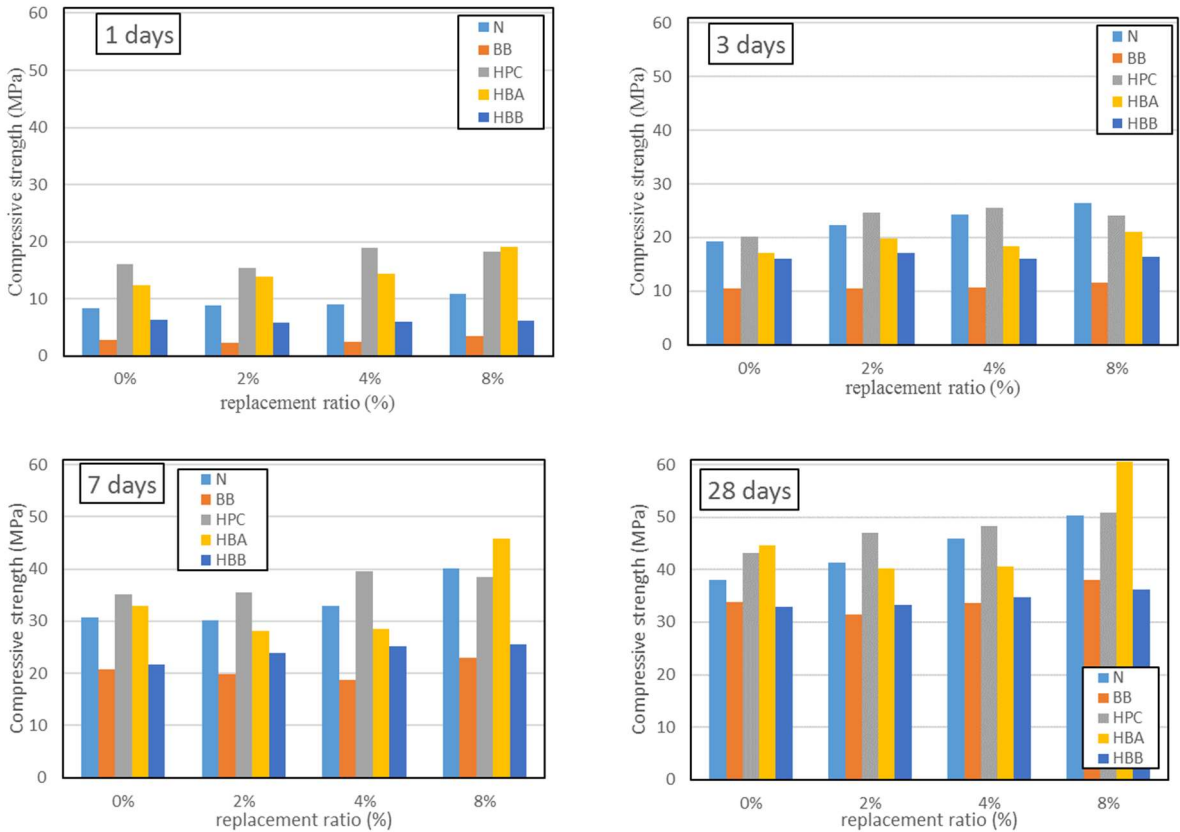


Fig. 2.6 Compressive strength results type of various cement.

finding is in good agreement with the results obtained in Section 2.3.1. For the HPC (high early strength

Portland cement) using mortar samples with different BFS replacement ratios, different trends of compressive strength with respect to the BFS replacement ratio can be observed. In the case of the HPC samples, the compressive strength increased after C-S-H type accelerator was added, from replacement ratio 2 wt%.

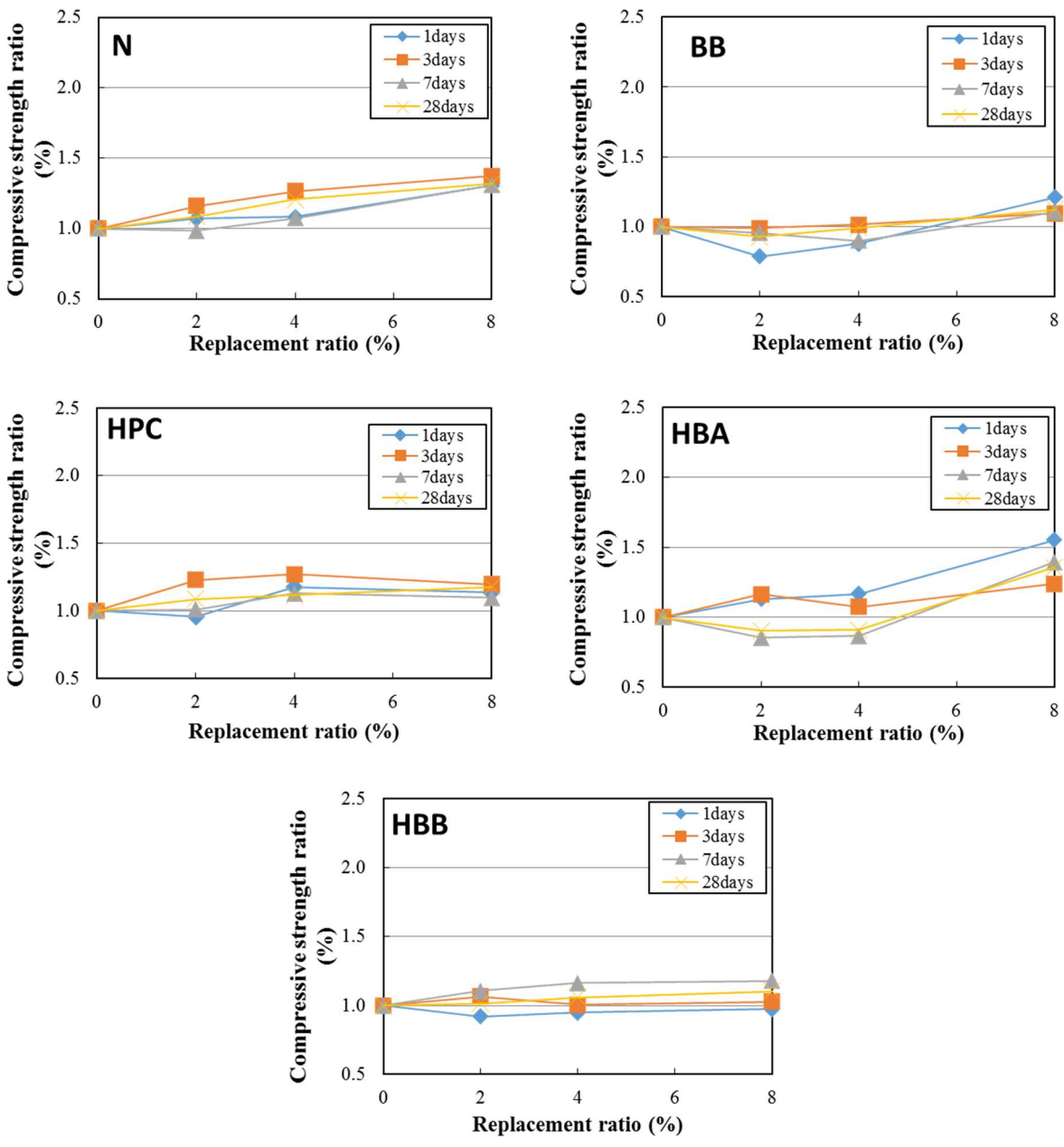


Fig. 2.6 Compressive strength results of various cement.

However, the ratio of compressive strength appeared to be similar to that of the replacement ratio 4 and 8

wt%. The compressive strength at a BFS replacement ratio of 20 wt% (the HBA samples) was highest in value with the C-S-H type accelerator replacement ratio at 8 wt%. In the case of the HBB samples (BFS replacement ratio of 40 wt%), the compressive strength increases with increasing replacement ratio of the C-S-H type accelerator at a curing age of 7 days. However, the effect of the C-S-H type accelerator was small, and the C-S-H type accelerator replacement ratio 0 wt% and 4 wt% was similar on the compressive strength result.

The effects of the C-S-H type accelerator on the compressive development of various cement types can be summarized as follows: In the case of the N, HPC, and HBA samples, the compressive strength at the early curing age of 1 and 3 days can be increased by the addition of C-S-H type accelerator. However, with the BB and HBB samples, the compressive strength results did not change, and were slightly increased in comparison to the C-S-H type accelerator ratio 0 wt%. It is well-known that, as mentioned above, when a C-S-H type accelerator is added to cement, it can be dependent on the C_3S (Imoto et al., 2014; Imoto et al., 2015). In addition to this observation, the minimum C_3S ratio for acceleration reaction of cement at C-S-H type accelerator.

2.3.4 Characteristics of the C-S-H type accelerator on X-ray diffraction and heat production

Heating production rate data from conduction calorimeters provide the chemical reaction rates between types of the cement and replacement ratio of the C-S-H type accelerator.

Figure 2.7 shows the heat evolution rate ($J/g \cdot h$) of the various cement types and C-S-H type accelerator ratios under isothermal conditions of $20^\circ C$ for 72 hours of the reaction rate, when the starting measurement shows high and narrow peaks, and the second peaks indicate a broad, slightly lower height. It is well-known that the first peaks on the heating rate were the effect of the C_3A amount in cement mineral (Ichitsubo et al., 2009), and the second peaks represent the reaction of the C_3S on the cement mineral (Yoda et al., 2013). In general, there was good agreement between the second peaks of the calorimeter and the final setting time of the penetration resistance. It can be seen that the heat evolution rate of the C-S-H type accelerator samples

tends to show faster and higher peaks with increasing C-S-H type accelerator replacement ratio at second peaks. In the case of the BFS blended samples, there appeared third peaks, which changed from ettringite to monosulfate.

Furthermore, when the addition of the C-S-H type accelerator was made to the N samples, there was a

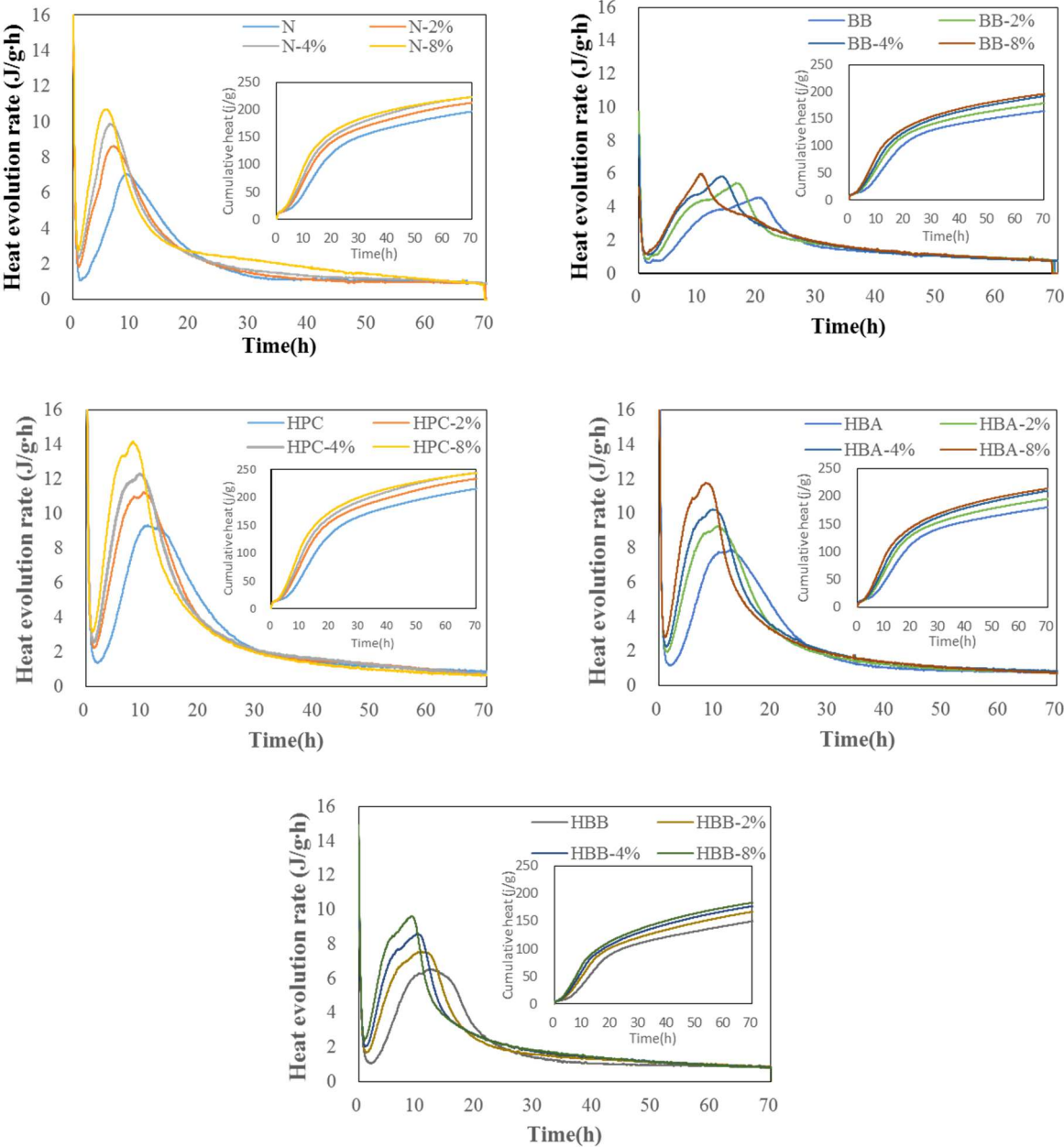


Fig. 2.7 Heat evolution rate results of various cement.

strong tendency toward the peak point being increased by the addition amount. Although slightly similar

characteristics can be seen, even in the BB samples, the additive amount cannot markedly affect the peak point. The acceleration period starts when C-S-H and CH is produced by the hydration reaction of C_3S , and the production rate is fast.

Among the C-S-H type accelerators studied so far, this admixture especially reacts with C_3S . Therefore, upon addition of the C-S-H type accelerator to blast furnace slag cement type B, the peak point had not changed; as the difference is believed to be due to it having a smaller amount of C_3S in this cement.

In addition, the cumulative heat shows the amount of heat generation for the investigated C-S-H type accelerator of the paste samples. It can be observed that the amount of cumulative heat tends to gradually increase according to the C-S-H type accelerator replacement amount, which agrees with earlier studies as described above (Imoto et al., 2014; Koyama et al., 2015; Koyama et al., 2016). On the other hand, in the case of the HPC-8% samples at 72 hours, the amount of heat is higher than for the other samples.

The effects of C-S-H type accelerator on the compressive development of various cement types can be summarized as follows: In the case of the N, HPC, and HBA samples, the compressive strength at the early curing age of 1 and 3 days can be increased by the addition of C-S-H type accelerator. However, with the BB and HBB samples, the compressive strength results did not change, and slightly increased in comparison to the C-S-H type accelerator ratio 0 wt%. It is well-known that, as mentioned above, a C-S-H type accelerator added to cement can be dependent on the C_3S (Imoto et al., 2014; Imoto et al., 2015). In addition to this observation, the minimum C_3S ratio for acceleration reaction of cement at C-S-H type accelerator.

Figure 2.8 shows the results for the crystalline phases in hardened cement paste of C-S-H- type accelerator replacement ratio 0 wt% and 4 wt% for various cements. It can be seen that the major CH peaks are stronger with curing age in the 2θ range of 18° in all samples. The intensity of the CH peaks of the paste samples also tends to be weak with the incorporation of the BFS at a curing age of 28 days, owing to the fact that the proportion of cement content decreases, and the BFS reaction rate is slow (Barnett et al., 2006; Boukendakdji et al., 2012; Miyazawa et al., 2014; Özbay et al., 2016; Çetin et al., 2016; Jaya Prithika & Sekar, 2016). However, when the BB 4 wt% samples were replaced by 4 wt% C-S-H type accelerator, the peaks of the CH

phase increased compared to the BB samples at a curing age of 28 days. In addition, it can be observed that the intensity of the C_3S phase peaks tend to decrease with curing age.

In the above XRD and heat production, with regard to the effect of using a C-S-H type accelerator, the heat evolution rate during 72 hours was higher with increased replacement ratio of the C-S-H type accelerator. This finding is in good agreement with the results obtained in the compressive strength test except for the case of the BB samples. Additionally, the XRD results were compared to C-S-H type accelerator 0 wt% and 4 wt%, and they were found to be structurally analogous to each other, but the BB samples were accelerated of CH phase by adding the C-S-H type accelerator.

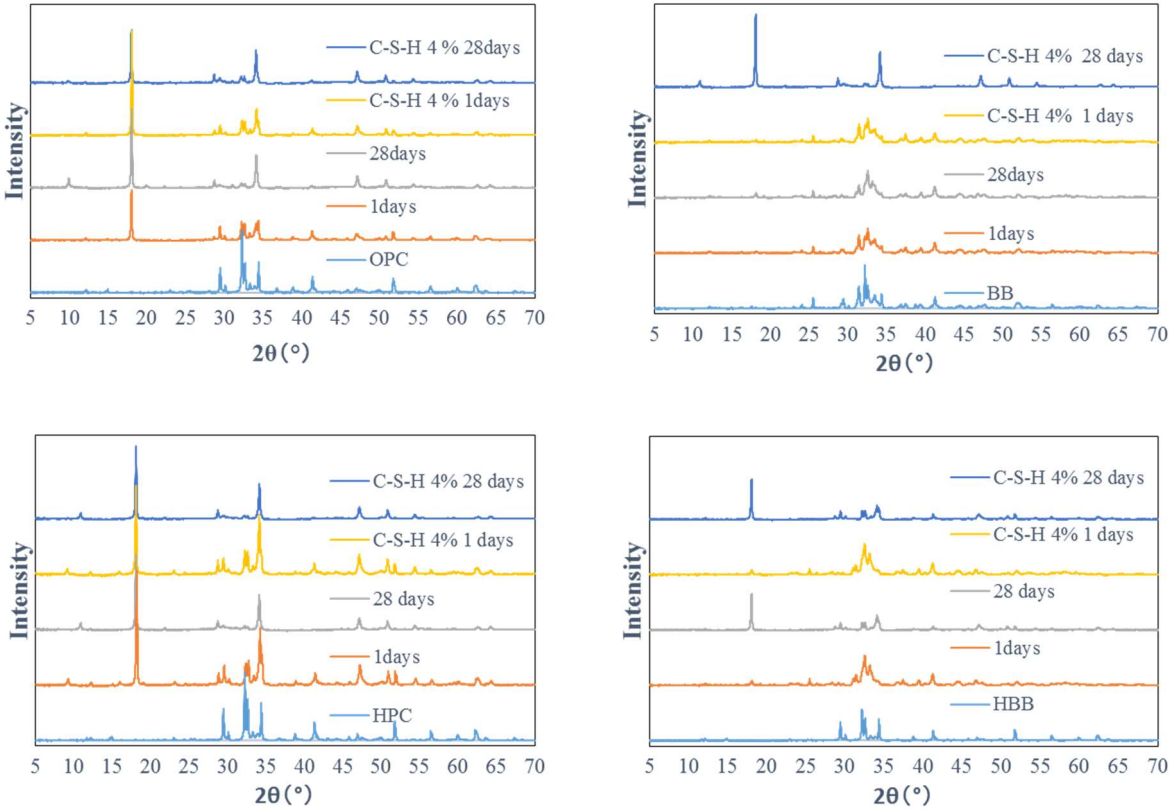


Fig. 2.8 X-ray diffraction patterns results of various cement.

2.4 Conclusion

In this study, in an effort to develop a blast furnace slag (BFS) blended cement that can replace ordinary Portland cement (OPC), its compressive strength development was investigated by varying the C-S-H type accelerator replacement ratios. Furthermore, the measurement between the heat evolution rate and the XRD was examined through chemical analyses of test samples and by investigating the relationship between compressive strengths. A summary of the results obtained in this study is given below:

- 1) Compressive strength test results under low temperature, with regard to the effects of using C-S-H type accelerator showed that in the case of using OPC, the compressive strength was increased with increasing C-S-H type accelerator at all curing ages. In the case of blended BFS, it had no effect on the water-to-binder ratio of 50% in this study. For the effect of low temperature, the N samples saw an increase by adding a C-S-H type accelerator.
- 2) From the results for the measured setting time and XRD, the setting time can be shorter by accelerated C_3S reaction. This is thought to be due to the contribution of C_3S to the cement hydration. The XRD result shows strong peaks of CH by adding C-S-H type accelerator.
- 3) With regard to the relationship between various cement types and compressive strength development, while the compressive strength development ratio increased with the amount of C_3S , in the case of the N, HPC, and HBA samples, the compressive strength at the early curing age of 1 and 3 days can be increased by the addition of C-S-H type accelerator. However, with the BB and HBB samples, the compressive strength results had no effect, and were slightly increased in comparison to 0 wt% of C-S-H type accelerator.
- 4) Consistent trends were observed for the results of the heat evolution rate and XRD. The heat evolution

rate was higher with increased amount of the C-S-H type accelerator. In the XRD results, they are structurally analogous to each other, but the BB samples saw accelerated CH phase by adding the C-S-H type accelerator.

References:

Yoda, Y., Teramoto, A., Kuroda, Y., Atarashi, D., Quality estimation method about foreign-made cement used conduction calorimeter, *Cement Science and Concrete Technology*, Vol. 67(1), 2013, pp. 116-122 (in Japanese)

Ichitsubo, K., Yamashita, H., Tanosaki, T., Satake, S., Research of highly functional cement that reduced interstitial liquid phase content (part 2 study of further reduction of interstitial liquid phase content and increase of C₃S content), *Cement Science and Concrete Technology*, Vol. 63, 2009, pp. 62-69 (in Japanese)

Imoto, H., Koizumi, S., Hanafusa, K., Baba, Y., Initial curing behavior of concrete using C-S-H type early strengthening agent and bleeding suppression effect, *Japan Concrete Institute*, Vol. 36(1), 2014, pp. 2248-2253 (in Japanese)

Imoto, H., Koizumi, S., Hanafusa, K., Baba, Y., Effect of a C-S-H type accelerator on the strength development of blast furnace slag cement, *Architectural Institute of Japan*, 2015, pp. 49-50 (in Japanese)

Koyama, H., Sasaki, H., Date, S., Initial Strength Development of Precast Concrete Using C - S - H System Early Strength Agent, *Japan Concrete Institute*, Vol. 37(1), 2015, pp. 331-336 (in Japanese)

Koyama, H., Uemura, S., Nakajima, N., Date, S., Influence of steam curing on curing properties of mortar using C - S - H type early strengthening agent, *Japan Concrete Institute*, Vol. 38(1), 2016, pp. 231-236 (in Japanese)

CHAPTER 3

EFFECT OF LIMESTONE POWDER AND GYPSUM ON THE COMPRESSIVE STRENGTH MIXTURE DESIGN OF BLAST FURNACE SLAG BLENDED CEMENT MORTAR

3.1 Overview

Blast furnace slag (BFS) has been widely used as a mineral admixture in cement and concrete in the concrete industry in order to reduce CO₂ emissions (Miyazawa et al. 2010; Chen et al. 2012; Kumar et al. 2008). In Japan, the replacement levels of BFS are categorized into type A (5–30 wt.%), type B (30–60 wt.%), and type C (60–70 wt.%) according to the Japanese Industrial Standard (JIS). However, only type-B BFS blended cement is actually used in construction and is mainly used for building foundations or underground structures and not in main structural elements, owing to its low compressive strength at an early age (Nippon Slag Association 2015). In order to widen the usefulness of BFS blended cement, type-A BFS blended cement is expected to be used in construction and the mechanical properties and hydration products need to be further discussed.

In the literature (Gu et al. 2015; Cetin et al. 2016; Rakhimova et al. 2014; Rakhimova et al. 2015; Gu et al. 2014), BFS blended cement is reported to have the advantages of reducing hydration heat, enhancing long-term strength, and providing some resistance to chloride-induced damage and sulfates. At present, to utilize these advantages effectively, studies to resolve the disadvantages of BFS blended cement are actively being pursued. Various studies are being conducted to resolve the issue of initial strength degradation and the temperature dependency of BFS was also investigated (Castellano et al. 2016). Rakhimova et al. (2014) investigated the compressive strength development of cement pastes by means of alkali activation. Sajedi and Razak (2010) also researched the influence of various kinds of alkali activators on the properties of BFS blended cement. The results revealed that sodium hydroxide, sodium silicate, and potassium hydroxide could be used as activators to increase the compressive strength of BFS cement. In addition, Gu et al. (2014) found that the mechanical and hydration properties of BFS blended cement could be increased by adding -MgO–CaO mixtures as a chemical activator.

At present, one promising approach that has been proposed is to incorporate limestone powder (LSP) to improve the early strength of the BFS blended mixture (Bonavetti et al. 2001; Menendez et al. 2003). When LSP is added, the C₃A reaction in the cement can be accelerated at an early curing age. Such properties are in contrast to the characteristics of BFS cement. When BFS and LSP are used in a mixture, the strength can be

increased as a result of LSP hydration at an early age and as a result of the BFS in long-term aging (Ghrici et al. 2007; Lothenbach et al. 2008; Courard and Michel 2014; Scholer et al. 2015). Additionally, some studies have been carried out using gypsum (CS) as an alkali activator (Chang et al. 2005), and studies have been conducted to determine the effects of CS on BFS blended cement (Melo Neto et al. 2010; Park et al. 2016). A disadvantage of replacing BFS cement with CS arises when the replacement ratio of CS exceeds an optimum ratio, after which point the strength is degraded (Melo Neto et al. 2010; Park et al. 2016).

In addition, in order to quantitatively determine the effect of the replacement binder, the XRD/Rietveld method is used in some studies. This method is widely used for cement binders by quantifying the cement's chemical composition and hydration product. Many researchers have also studied ordinary Portland cement (OPC) and BFS cement using the XRD/Rietveld method (Kondo and Ohsawa 1969; Matsushita et al. 2008; Hargis et al. 2014; Sagawa et al. 2010; Sagawa and Nawa 2014; Sagawa and Nawa 2014). Sagawa and Nawa (2006) quantified BFS hydration using the XRD/Rietveld method with crystallization of the slag at high temperatures in order to investigate the hydration product of BFS blended cement.

This study attempts to improve the strength of BFS cement to a level comparable to that of OPC, with the aim of increasing the amounts of BFS used, such that type-A BFS cement can serve as a replacement for OPC. In addition, LSP and CS are used to enhance the strength of type-A BFS cement. Finally, the XRD/Rietveld method is used to quantify hydration analysis of the BFS blended cement and determine the effect of hydration products on the compressive strength of the BFS blended mixture incorporating various mineral admixtures. Finally, Powers' equation was used to investigate the relationship between compressive strength and the gel/pore ratio.

3.2 Experimental

3.2.1 Experimental program

The experimental plan in this study consists of three parts. The first step deals with the development of compressive strength in BFS blended systems incorporating two types of mineral admixture, such as LSP and CS. The second part concerns the hydration degree and hydration products of BFS blended cement paste made

with different mineral admixtures with to respect to XRD/Rietveld analysis. Finally, the relationship between the experimental compressive strength results and the gel/pore ratio is investigated using Powers' gel/pore ratio model (1958). Details of the experimental plan and investigated BFS blended cement samples are given below.

3.2.1.1 Experimental materials

The cement and BFS were used as per the JIS. The physical properties and chemical compositions of the OPC and BFS are shown in Table 3.1; the two types of mineral admixtures are also presented. The Blaine specific surface areas of the LSP and CS were 4640 cm²/g and 3030 cm²/g, respectively.

Table 3.1 Chemical and physical properties of the materials.

		OPC	BFS	LSP	CS
Chemical composition (%)	SiO ₂	21.06	34.03	-	-
	Al ₂ O ₃	5.51	14.36	-	-
	Fe ₂ O ₃	2.69	0.83	-	-
	CaO	65.47	43.28	51.67	40.50
	MgO	1.66	6.51	-	-
	K ₂ O	0.40	-	-	-
	Na ₂ O	0.24	-	-	-
	SO ₃	1.91	-	-	55.68
Physical properties	Density (g/cm ³)	3.17	2.91	2.73	2.96
	Blaine fineness (cm ² /g)	3390	3930	4640	3030

3.2.1.2 Preparation of compressive strength test samples

Table 3.2 shows the experimental design of the mortar used in this study. The water–binder ratio (W/B) was 0.5 and the BFS replacement ratios were 0, 15, 20, and 25%. The mortar was cured using a $\phi 50 \times 100$ mm plastic mold. OPC and BFS were used for the cement types and LSP and CS were also used as mineral materials. The compressive strength levels of all mixtures were measured and curing temperatures were set to 20 °C. The compressive strength was tested after 1, 3, 7, 28, and 91 days under the 20-°C curing conditions.

Table 3.2 Mixture designations of the BFS blended cement mortar.

Mixture designation	W/B (%)	B:S	Unit content (kg/m ³)					S
			W	C	BFS	LSP	CS	
Control	0.5	1:3	324	515	-	-	-	1387
B15				438	77	-	-	
B15-L2				428	77	10	-	
B15-L3				423	77	15	-	
B15-L4				418	77	21	-	
B15-L5				412	77	26	-	
B15-C2				428	77	-	10	
B15-L2-C2				418	77	10	10	
B15-L3-C2				412	77	15	10	
B15-L4-C2				407	77	21	10	
B15-L4-C2				402	77	26	10	
B20				412	103	-	-	
B20-L2				402	103	10	-	
B20-L3				437	103	15	-	
B20-L4				392	103	21	-	
B20-L5				387	103	26	-	
B20-C2				402	103	-	10	
B20-L2-C2				392	103	10	10	
B20-L3-C2				387	103	15	10	
B20-L4-C2				381	103	21	10	
B20-L5-C2				376	103	26	10	
B25				387	129	-	-	
B25-L2				376	129	10	-	
B25-L3				371	129	15	-	
B25-L4				366	129	21	-	
B25-L5				361	129	26	-	
B25-C2				376	129	-	10	
B25-L2-C2				366	129	10	10	
B25-L3-C2				361	129	15	10	
B25-L4-C2				356	129	21	10	
B25-L5-C2				351	129	26	10	

Note: B: blast furnace slag, L: limestone powder, C: gypsum

B(replacement ratio wt.%) - L(replacement ratio wt.%) - C(replacement ratio wt.%)

3.2.1.3 Preparation of hydration product samples

For the measurement of the hydration product, a paste sample with different mineral materials was fabricated. Table 3.3 shows the experimental design of the chemical analysis used in this study. The sample was mixed for two minutes using a hand mixer. To stem material bleeding, it was cured after one hour before commencing curing. Sealed curing was utilized with this sample for six aging conditions (1, 3, 7, 28, 56, and 91 days) at 20 °C.

Table 3.3 Experimental design for the chemical analysis.

Mixture designation	W/B	Weight percentage (%)			
		OPC	BFS	LSP	CS
Control	0.5	100	-	-	-
B20		80	20	-	-
B20-C2		78	20	-	2
B20-L4-C2		74	20	4	2

3.2.2 Measurement methods

3.2.2.1 Compressive strength test method

The compressive strength test was conducted in accordance with the JIS A 1108. To test the mortar's compressive strength at an early age, the top surface of the mortar was capped with gypsum after 1 day of curing at 20 °C, owing to the fact that the early age compressive strength is too low to demold. After the gypsum was completely hardened, compressive strength testing of the mortar was conducted.

3.2.2.2 Reaction rate and hydration product measurement

An analysis of the hydration was conducted using the XRD/Rietveld method. To assess the BFS reaction rate and to check for alite ($3\text{CaO} \cdot \text{SiO}_2$; C_3S), belite ($2\text{CaO} \cdot \text{SiO}_2$; C_2S), an aluminate phase ($3\text{CaO} \cdot \text{Al}_2\text{O}_3$; C_3A), a ferrite phase ($4\text{CaO} \cdot \text{Al}_2\text{O}_3 \cdot \text{Fe}_2\text{O}_3$; C_4AF), and various cement hydration products, the XRD/Rietveld method was used to assess the effects of LSP and CS on the hydration of the BFS blended cement mortar samples. The X-ray diffraction and ignition loss characteristics were measured for samples that were 5 mm³ in size after curing for 1, 3, 7, and 28 days. For each aging condition, acetone replacement was carried out to stop the hydration reaction and the samples were dried before the measurements.

The drying procedure involved drying for 24 hours at 40 °C before the sample was measured. Powder was used for the X-ray diffraction and ignition loss measurements, and the samples were made into powder form using a vibration mill. The method for quantification of BFS was proposed by Sagawa and Nawa (2006) based on the heat treatment method, where the nonreactive BFS was crystallized by carrying out heat treatment for

30 minutes at 900 °C, and the heat loss through this was considered as ignition loss. Then XRD/Rietveld analysis was conducted on the sample.

Figure 3.1(a) shows the XRD results with respect to different BFS replacement ratios according to Sagawa and Nawa (2006). The peaks of gehlenite and akermanite near 31.4° were increased and the peak of C3S near 29.4° was decreased as the BFS replacement ratio increased. Figure 3.1(b) shows the BFS content found from Rietveld analysis. The amounts of gehlenite, akermanite, and merwinite determined from Rietveld analysis were calculated to be the BFS content. Figure 3.1(b) (Sagawa and Nawa 2006) shows that the calculated BFS content was highly consistent with the actual BFS content. Therefore, this method is reliable for the analysis results.

Moreover, for the test conditions for the ignition loss of the OPC, heat treatment was performed for 30 minutes at 950 °C. For the XRD measurement, a semiconductor-type high-speed detector was used with CuK α as a target, a tube voltage of 45 kV, a tube current of 40 mA, a 2 θ scan range of 5–70°, and a step width of 0.02°. For the Rietveld analysis, Siroquant Ver. 3.0 was used to measure the cement minerals, slag reaction rate, and amount of hydration product, with alumina (α -Al $_2$ O $_3$) at an average particle size of 3 μ m, following the standard methods used in the literature (Jansen et al. 2011a; Jansen et al. 2011b; Jansen et al. 2012).

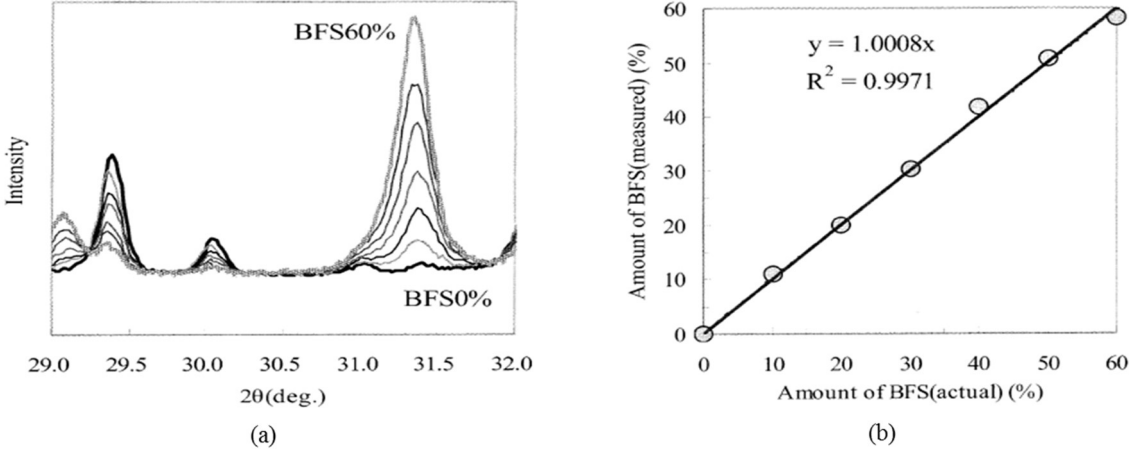


Fig. 3.1 Quantification results for BFS from Sagawa *et al.* (2006):
 (a) XRD profiles of tempered samples and
 (b) relationship between actual and measured amounts of BFS in unhydrated cement

3.3 Results and discussion

3.3.1 Characteristics of compressive strength development

3.3.1.1 Influence of blast furnace slag on the compressive strength

Figure 3.2 shows the results for the compressive strength of BFS blended cement mortar samples with replacement ratios of 15%, 20%, and 25% by weight of cement. It can be seen that the compressive strength of the mortar samples tends to decrease with increasing BFS replacement ratio at 1, 3, and 7 days, owing to the fact that the proportion of cement content decreases and the reaction rate of BFS is slow (Çetin et al. 2016; Barnett et al. 2006; Boukendakdji et al. 2012; Miyazawa et al. 2014; Özbay et al. 2016; Jaya Prithika and Sekar 2016). In fact, it may cause a decrease in the compressive strength at an early curing age. Moreover, the compressive strengths of the mortar samples with 15 and 20 wt.% of BFS at 91 days exceeded that of the OPC sample with no addition of BFS, implying that long-term curing in BFS blended mortar samples is efficient for the development of compressive strength. The above results clarify that curing age can affect the compressive strength development of mortar samples incorporating BFS (Barnett et al. 2006; Boukendakdji et al. 2012; Özbay et al. 2016). In the case of B20, the compressive strength data at 28 days is believed to be due to an experimental error.

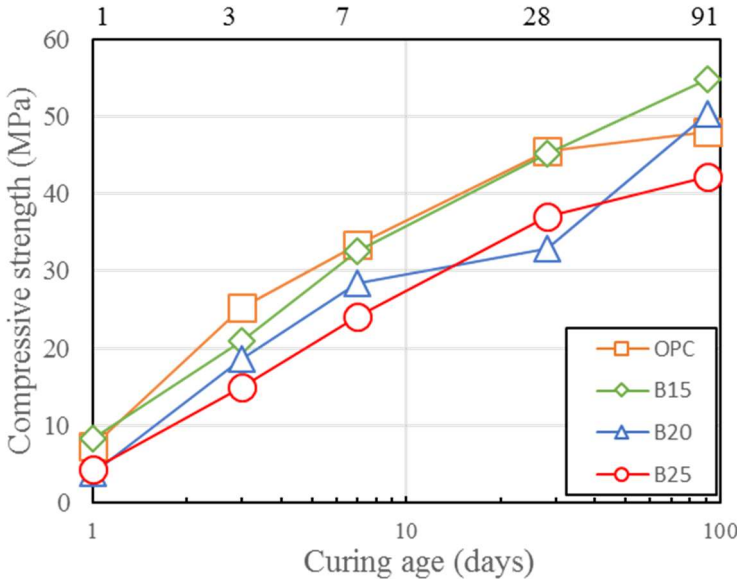


Fig. 3.2 Compressive strength of BFS blended mortar.

3.3.1.2 Influence of CS on the compressive strength

For the BFS blended cement mortar samples with different BFS replacement ratios and with the same CS contents of 2 wt.% for cement, as shown in Fig. 3.3, the compressive strength in the B20-C2 mortar sample (7.6 MPa) appeared to be similar to that of the reference mortar (7.3 MPa) without BFS, particularly at 1 day, suggesting that the addition of CS in BFS blended cement mortar samples would affect the development of compressive strength at an early curing age. It is known that gypsum will generate heat when mixed with water in an exothermic reaction. The particles possess high free energy at high temperature and, as a result, the chemical reaction rate is increased. In addition, the use of CS will provide additional calcium. As described above, high concentrations of CS lead to a higher incidence of C-S-H, which agrees with Chang et al. (2005); this is discussed in detail in Section 3.3.3.

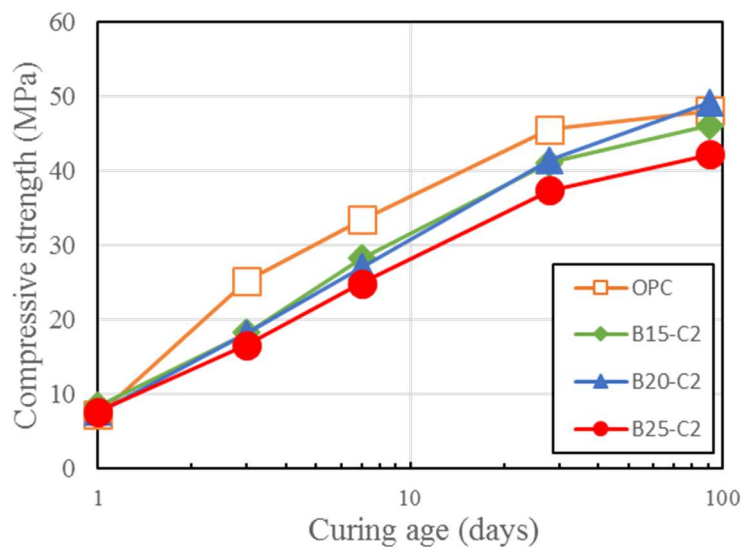


Fig. 3.3 Compressive strength of BFS blended mortar incorporating CS.

3.3.1.3 Influence of LSP on the compressive strength

Figure 3.4 shows the results for the compressive strength of all BFS blended cement mortar samples with different replacement ratios of 0, 2, 3, 4, and 5 wt.% of LSP. Different trends of compressive strength with respect to the BFS replacement ratio can be observed. In the case of a mortar sample incorporating 15 wt.% BFS by weight of cement, the compressive strength was decreased with the increasing LSP replacement ratio, even

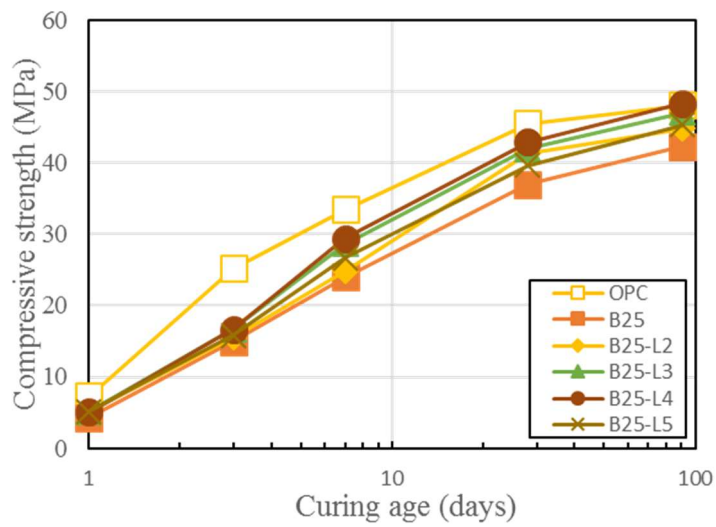
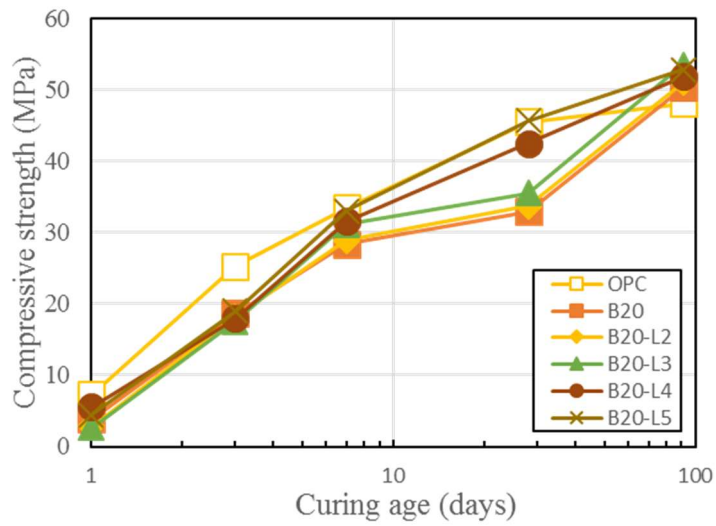
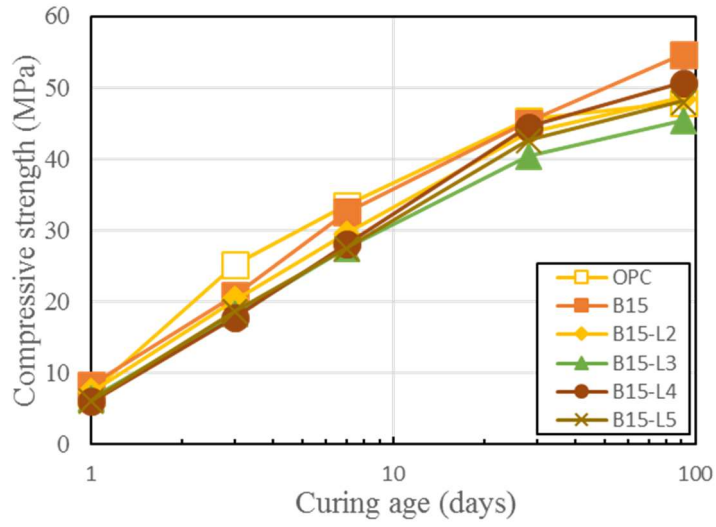


Fig. 3.4 Compressive strength of BFS blended mortar incorporating LSP.

though the curing ages increased. The compressive strength of mortar at a BFS replacement ratio of 20 wt.% was increased with increasing LSP replacement ratio at all curing ages. However, when the BFS replacement ratio is 25 wt.%, the strength also increased with increasing LSP replacement ratio, except for B25-L5. Previous studies have confirmed that the strength can be improved by using a BFS replacement ratio of 40 wt.% (Sagawa and Nawa 2006), showing a similar trend to that of the BFS replacement ratios of 20% and 25% in this study. However, for a BFS replacement ratio of 15 wt.%, the strength is lowered, indicating a need for further research.

3.3.1.4 Combined influence of limestone powder and CS on the compressive strength

Figure 3.5 shows the compressive strength of BFS blended cement mortar with LSP and CS as replacements. It shows that a BFS replacement ratio of 15 wt.% yields almost the same compressive strength value as OPC mortar. The compressive strength was reduced slightly as the BFS replacement ratio increases from 20 wt.% to 25 wt.%, which shows the same trend as the BFS cement mortar without LSP and CS until a curing age of 91 days. Furthermore, all of the mortar samples prior to 1 day showed the same value of compressive strength as OPC.

In the above strength test results, with regard to the effects of using CS as a replacement material, the strength at an early curing age (1 day) was identical to that of OPC, and it was determined that the low initial strength stemming from the use of BFS as a replacement material can be improved. Regarding the effect of LSP, it was found that the strength was increased at BFS replacement ratios of 25 wt.% as the LSP replacement ratio increased. In addition, the compressive strength was greater than that of OPC at both an early curing age and after long-term curing. When using a combination of LSP and CS, a trend similar to that of BFS replacement was observed, where the strength decreased slightly as the amount of binder increased, except for the use of OPC. However, for all mixtures, it was observed that the strength at the early curing age (1 day) was similar to that of OPC.

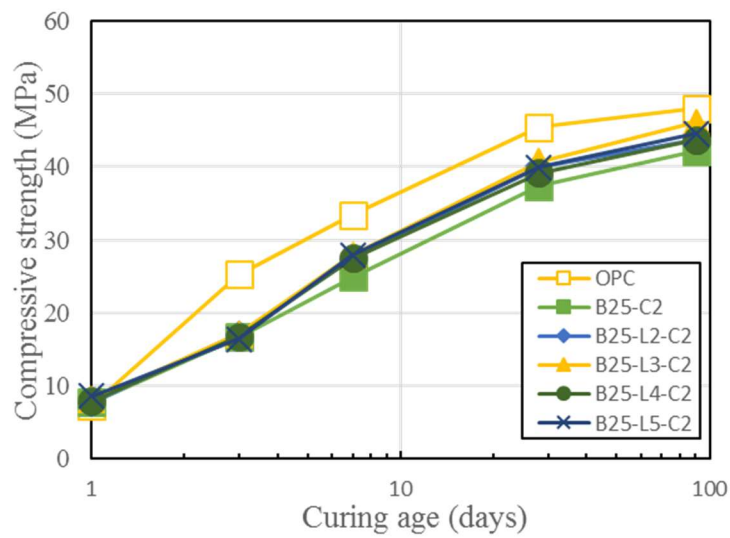
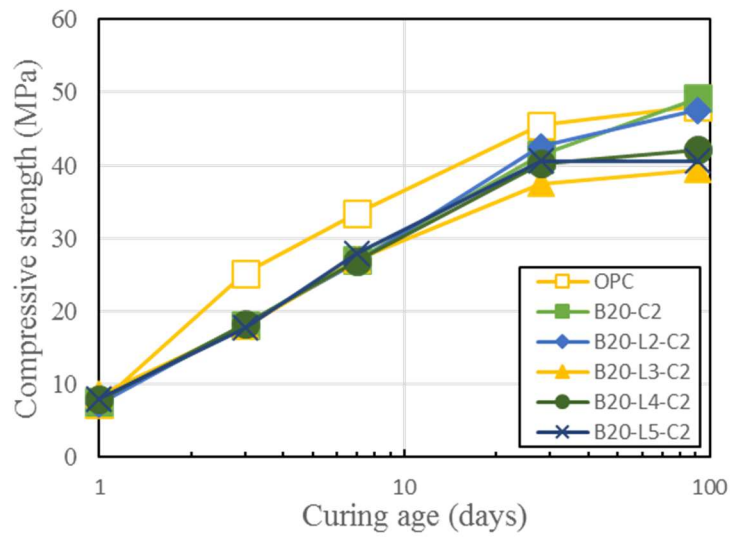
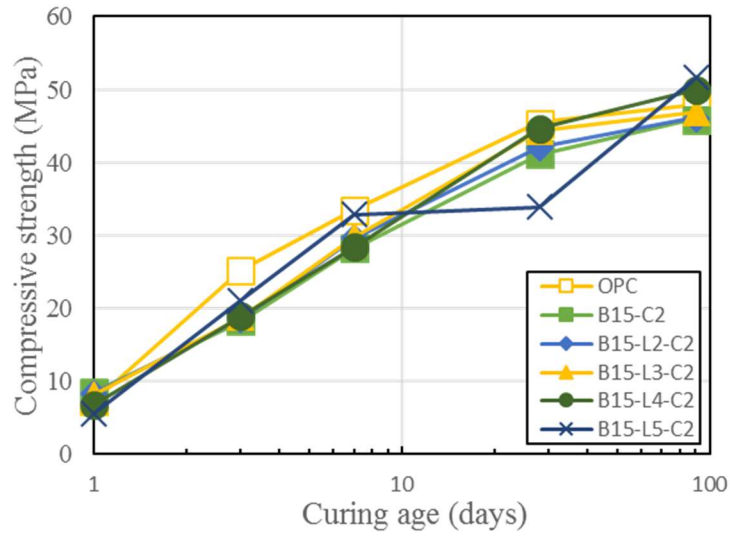


Fig. 3.5 Compressive strength of BFS blended mortar incorporating CS and LSP.

3.3.2 Compressive strength of BFS blended paste samples incorporating various mineral admixtures

Figure 3.6 shows the compressive strengths of BFS blended paste samples with mineral admixtures at curing ages of 1, 3, 7, 28, and 91 days. The compressive strength at 1 day was measured to be 7.3 MPa, 5.4 MPa, 7.6 MPa, and 7.9 MPa for OPC, B20, B20-C2, and B20-L4-C2 mortar samples. In the case of the B20 mortar sample, with a BFS replacement ratio of 20 wt.%, the compressive strength at 1 day showed an initial strength lower than that of the OPC mortar sample, but after 91 days its compressive strength was recorded to be 50 MPa, exceeding that of the OPC sample. This finding is in good agreement with the results obtained in the mortar strength tests in Section 3.3.1. For the B20-C2 sample, with a CS replacement ratio 2 wt.%, the compressive strength at 1 day was measured to be 7.6 MPa and similar to that of OPC, while the same compressive strength development as for the B20 sample was observed after 3 to 91 days, suggesting that the use of CS in BFS blended mortar can help to accelerate the hydration reaction of BFS. The obtained results agree with those in previous studies reported in the literature (Chang et al. 2005).

In addition, the B20-L4-C2 mortar sample exhibited the same compressive strength as the B20-C2 samples for curing ages of 1, 3, 7, and 28 days, but not 91 days.

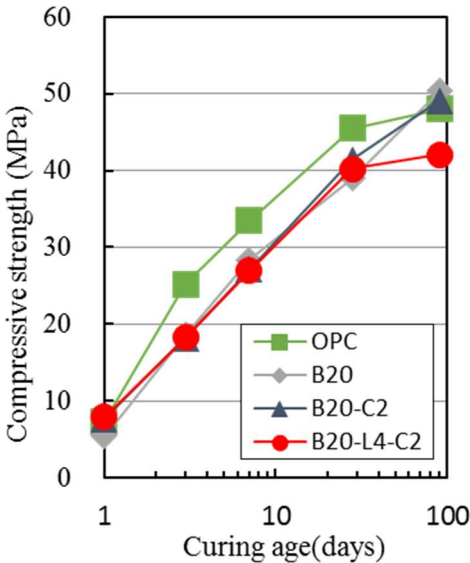


Fig. 3.6 Compressive strength of BFS blended cement paste.

3.3.3 Hydration reaction analysis of paste samples

3.3.3.1 Hydration degree of cement

Figure 3.7 shows the hydration degree calculated by XRD/Rietveld analysis for the four types of BFS blended pastes incorporating LSP, CS, and OPC. It can be seen that by incorporating CS and LSP the hydration degree of the cement minerals in the BFS blended paste after 1 day of curing was higher than that of the reference pastes, suggesting that CS and LSP can accelerate the hydration of cement minerals at an early curing age of 1 day. The change of hydration degree for each cement mineral will be described in following sections.

Figure 3.8 presents the hydration degree of BFS in the investigated paste samples. It shows that the hydration degree of the paste was approximately 63.7% after 91 days of curing. It was reported by Sagawa et al. (2006) that the hydration degree of cement is increased when the BFS replacement ratio is decreased. In this research, a BFS replacement ratio of 20 wt.% was used, in Sagawa et al. (2006) studies the results of paste produced with a BFS replacement ratio of 40 wt.%, the hydration degree of the slag was recorded for 40 wt.% to 50 wt.%. Moreover, for pastes made with LSP and CS, the hydration degree was high until a curing age of 7 days, and then low for curing ages from 28 to 91 days, as compared to the B20 paste.

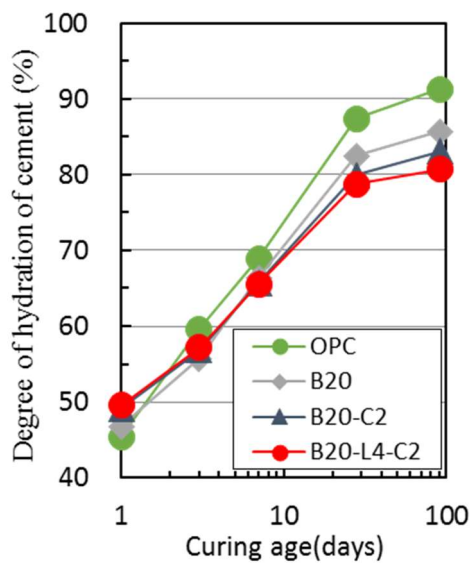


Fig. 3.7 Hydration degree of cement.

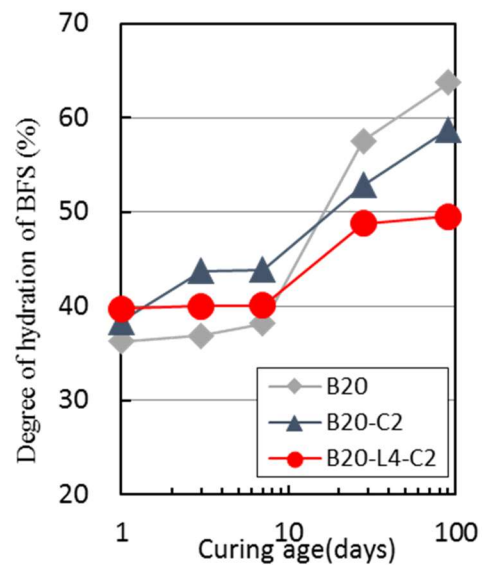


Fig. 3.8 Hydration degree of BFS.

3.3.3.2 Hydration degree of C_3S , C_2S , C_3A , and C_4AF

Figures 3.9(a) and (b) show the results for the hydration degree of C_3S and C_2S for the investigated BFS blended paste samples. It has previously been reported that the addition of BFS to cement accelerates the hydration of C_3S and slows the hydration of C_2S , and thus the BFS can affect the hydration reaction of cement minerals (Sagawa and Nawa 2006; Hoshino et al. 2006b). Similar results were obtained in this paper. In the case of the B20 sample incorporating 20% by weight of BFS for cement, the hydration degree of C_3S in the paste sample did not change and was slightly increased in comparison to OPC without BFS, implying that the hydration of C_3S tends to accelerate, owing to the addition of the slag, which agrees with earlier studies as described above (Sagawa and Nawa 2006; Hoshino et al. 2006b).

In addition, when the B20-C2 samples were replaced by combinations of 20-wt.% BFS with 2-wt.% CS, the hydration degree of C_3S was increased above 10% compared to the OPC and B20-C2 samples at curing ages of 1 and 3 days, which justifies the result of Fig. 3.6. Therefore, it is considered that the addition of BFS and CS can affect the development of compressive strength.

It is also observed that, in the case of the B20-L4-C2 samples made with LSP, CS and BFS, the hydration degree of C_3S did not differ from that of the B20-C2 sample. According to Hoshino et al. (2006b), when comparing OPC and OPC-LSP samples, the hydration degree of C_3S in cement did not change. However, in the case of the OPC-BFS-LSP sample, the hydration degree of C_3S was higher than that of OPC, suggesting that the addition of LSP for binder had a negligible effect on the hydration of C_3S . Figure 3.9(b) presents the hydration degree of C_2S for the investigated paste samples. It is concluded that, except for the B20-C2 paste sample, the same results for the hydration degree of C_3S were also observed in these pastes. Figure 3.9(b) shows that incorporating BFS and LSP for cement had an insignificant effect on the hydration of C_2S .

It is well known that, as mentioned above, a BFS replacement ratio of 40 wt.% in the cement would delay the hydration of C_2S , but, in this research, different results were obtained. From Fig. 9(b), in comparison to the OPC paste, the hydration degree of C_2S in B20 cement paste slightly increases up to 28 days, which implies that BFS would accelerate the hydration of C_2S .

In addition to this observation, in the cases of addition of CS and LSP, the hydration of C_2S is low compared

to the B20 cement paste. This suggests that C₂S would delay hydration.

Figures 3.9(c) and (d) show the hydration degree of C₃A and C₄AF for the investigated BFS blended paste samples. Previous studies on the hydration reaction of C₃A and C₄AF in cement (Sagawa and Nawa 2006) have reported that it was accelerated when BFS was used. It can be seen that the hydration degree of C₃A and C₄AF for the BFS cement paste sample was accelerated and similar to that of OPC cement paste (Hoshino et al. 2006a; Hoshino et al. 2006b). However, for samples using LSP and CS, the hydration reaction of C₄AF is slightly low in comparison to both OPC and B20 paste samples.

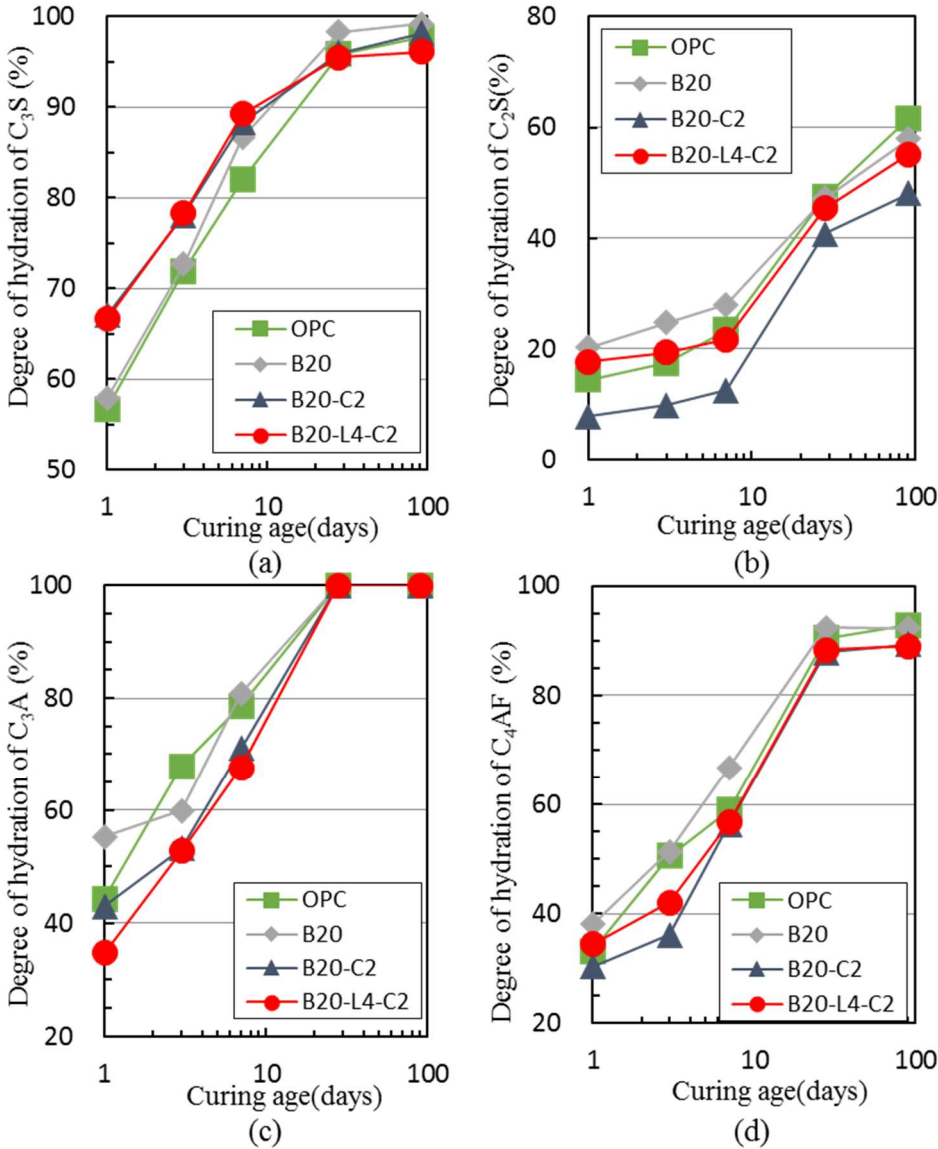


Fig. 3.9 Degree of hydration of the BFS blended cement minerals.

3.3.3.3 Hydration products

Figure 3.10 shows the amounts of hydration products of ettringite (AFt), mono-sulfate (AFm), katoite, monocarbonate (MC), and hemiacarbonate (HC) for the investigated BFS blended paste samples. Figure 3.10(a) shows the results for the amount of AFt produced. It can be observed that the amount of AFt tends to gradually decrease with curing age. On the other hand, in the case of the B20-L4-C2 samples at a curing age of 3 days, the amount produced is higher than for the other samples.

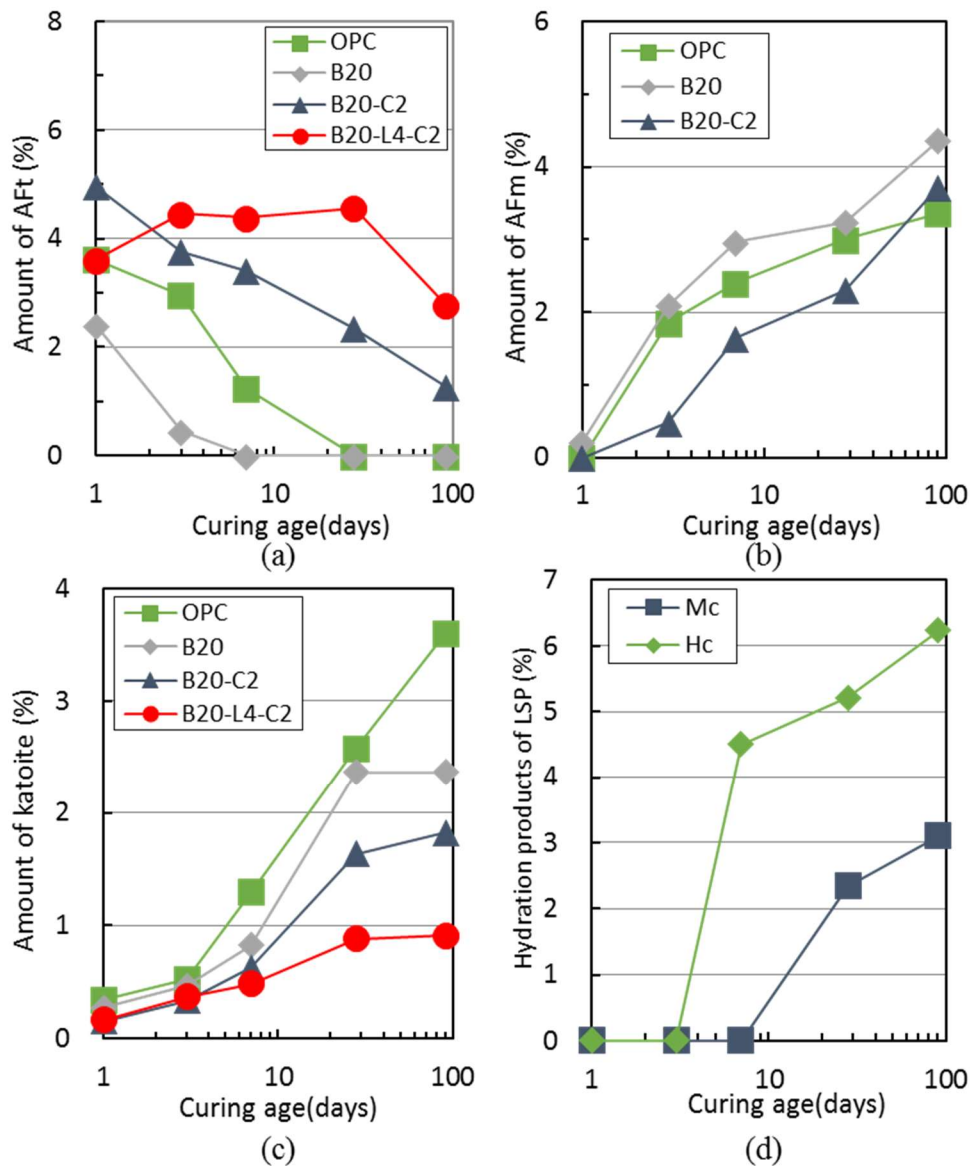


Fig. 3.10 Amounts of hydration products of the BFS blended cement minerals.

Figure 3.10(b) shows the produced amounts of AFm in the OPC, B20, and B20-C2 samples. For the B20-L4-C2 sample mixed with LSP mineral, AFm was not identified during the hydration process. In contrast to the AFt trends, the amount of AFm displayed a trend of increasing with curing age, which agrees with previous studies. It is considered that for the sample without LSP, the AFm hydration product is generated by AFt reacting with C₃A from an early curing age. However, if the sample is replaced with LSP, then C₃A preferentially reacts with the LSP mineral, which causes it to generate carbonate hydrates (MC, HC), as shown in Fig. 3.10(d) (Hoshino et al. 2006b). Figure 3.10(c) shows the produced amounts of katoite. It is concluded that the OPC sample yields the greatest amount of katoite, which decreases as the cement is replaced by the minerals.

The effects of CS and LSP on the compressive strength development of type-A BFS blended cement can be analyzed from the above reaction rates and amounts of hydration products. The conclusions are as follows. The compressive strength at a curing age of 1 day can be increased by the promotion of the reaction of C₃S and BFS. The compressive strength development of samples with LSP of at a curing age of 91 days is found to stagnate, owing to the suppression of the reaction of the BFS. In addition, in order to examine the relationship between the void volume and strength, the porosity can be calculated by assuming a density of C-S-H.

3.3.4 Relationship between porosity and compressive strength

It is well known that the compressive strength of a cement-based composite depends on the porosity, which can be experimentally evaluated using mercury intrusion porosimetry, drying methods, and so on. However, a different approach considering the hydration mechanism was adopted in this study in order to investigate the porosity and compressive strength in the investigated paste samples. Powers suggested the gel/pore equation, in which the porosity can be calculated from the hydration degree of cement minerals, the contents of hydration products, and the density of the C-S-H gel with respect to the results of XRD/Rietveld analysis:

$$X(t) = \frac{V_{hydrates}(t)}{V_{hydrates}(t) + V_{pore}(t)} \quad (1)$$

and:

$$S(t) = S_0 X(t)^N \quad (2)$$

where:

$X(t)$: gel/pore ratio (vol./vol.),

$V_{\text{hydrates}}(t)$: hydration amount (vol.),

$V_{\text{pore}}(t)$: pore volume (vol.),

$S(t)$: strength (MPa), and

S_0 , N : integers.

When the gel/pore ratio is considered to be a function of the hydrate, S_0 denotes the strength when the capillary pores of the hydrate are completely filled. This is normally known as the ultimate strength or the highest strength. Moreover, the value of N represents the pore dependency of the strength. However, the relationship between gel/pore ratio and strength is identical regardless of the type of Portland cement used (Maruyama and Igarashi 2012). In this study, the relationship between gel/pore ratio and strength can be expressed in the same way regardless of the binder type.

The volumes of unreacted cement mineral (V_{un}) and hydration products (V_{hyd}) can be calculated using the quantitative value of density of each compound obtained from XRD/Rietveld analysis. In addition, the volume of the C-S-H can be estimated by considering the amount of C-S-H gel that is found to be amorphous via XRD/Rietveld analysis. The pore amount is calculated by subtracting V_{un} , V_{hyd} , and V_{CSH} from the unit cement paste volume. In other words, the volume and the pore volume of the C-S-H the density as the unknown C-S-H is calculated, and it is possible to calculate the gel/pore ratio from this value.

Figures 3.11(a) and (b) show the relationship between the calculated gel/pore ratio and the compressive strength and the relationship between the calculated density of C-S-H and curing age, respectively. Table 3.4 summarizes the values of the densities of the produced hydrates taken from the literature. It can be seen that, regardless of the types of materials used, the relationship between gel/pore ratio and strength is similar to the calculated values and these values of S_0 and N are almost the same as those found in previous studies. Moreover, in the literature, the CaO/SiO_2 molar ratio in C-S-H (hereafter denoted the C/S ratio) has been reported to exhibit a correlation with the density of the C-S-H (Sagawa et al. 2010).

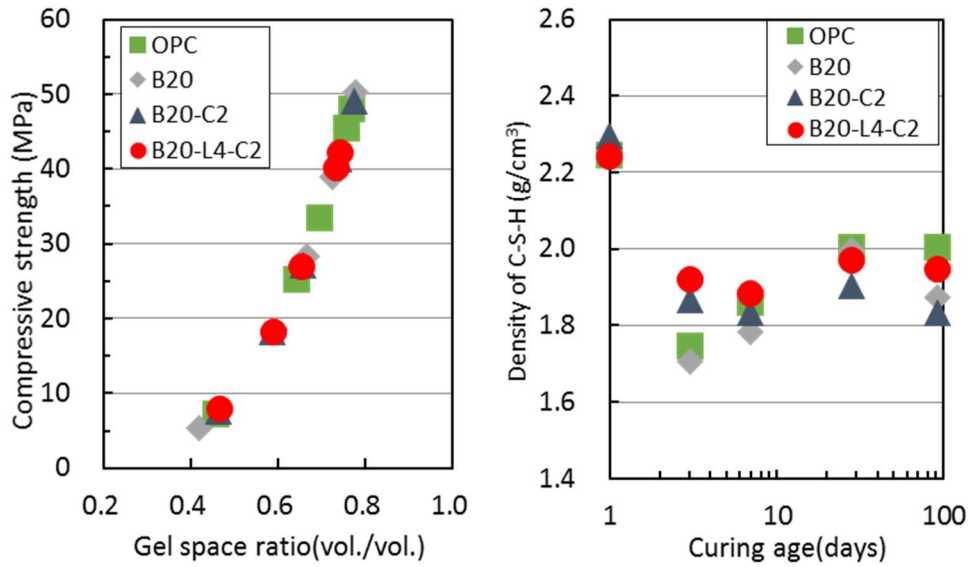


Fig. 3.11 Compressive strength versus gel/space ratio and density of C-S-H versus curing age.

Table 3.4 Densities of the hydrates.

Hydrate	Density (g/cm ³)
Calcite	2.71
CH	2.24
AFt	1.79
AFm	2.02
Hc	1.83
Mc	2.18
Katoite	2.53
HT	2.13

Figure 3.12 presents the relationship between the C/S ratio and the density of C-S-H, comparing the results of this study to those reported by Sagawa et al. (2010). The C/S ratio is calculated from the mass balance of SiO₂ and CaO, including the amount of CH remaining in the cement paste after hydration. For a BFS blended cement paste, the calculation of the C/S ratio was carried out in the same manner as previously reported by Taylor (1997) for the phase composition model of BFS blended cement. It is confirmed that the density of C-S-H obtained in this study is slightly different from that previously recorded at 1 day but, after 3 days, the values are roughly equal to the values from the previous study. Moreover, Fig. 3.12 implies that the density of

C-S-H decreases with increasing curing age and that the density of the BFS blended cement paste tends to be low compared to that of OPC paste, which agrees with the findings of Sagawa et al. (2010) and Suda (2013).

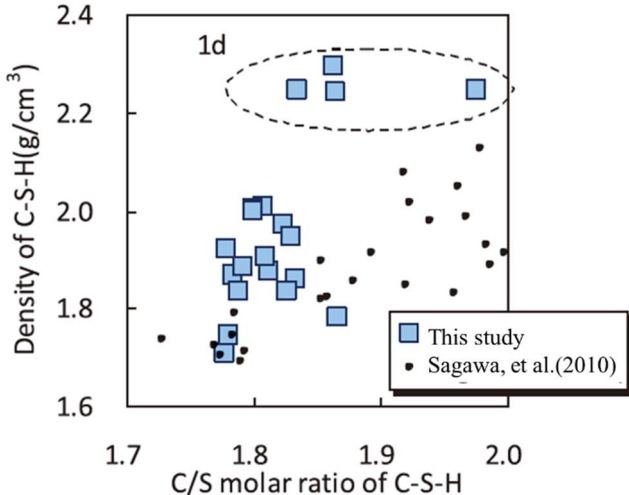


Fig. 3.12 Relationship between the C/S ratio and the density of C-S-H.

The hydration product of calcium aluminate (CA) are presented in Figs. 3.13 and 3.14. The hydration products are calculated from the volume of the cement paste, considering the density of C-S-H. It is obvious that for LSP, even though the hydration product of CA would increase, the volume of the C-S-H was found to be small in comparison to other samples, which justifies the compressive strength result shown in Fig. 3.6.

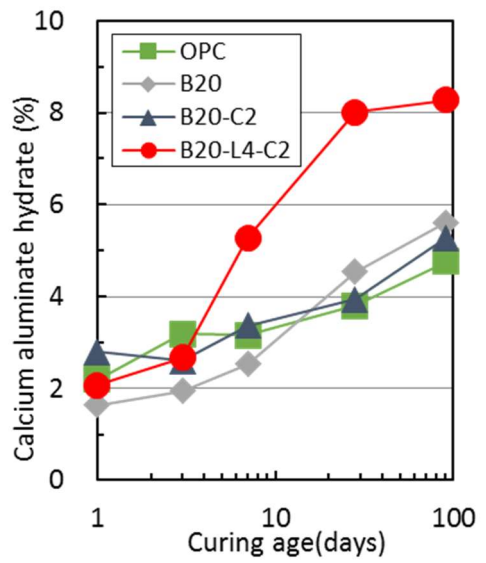


Fig. 3.13 Calcium aluminate hydrate.

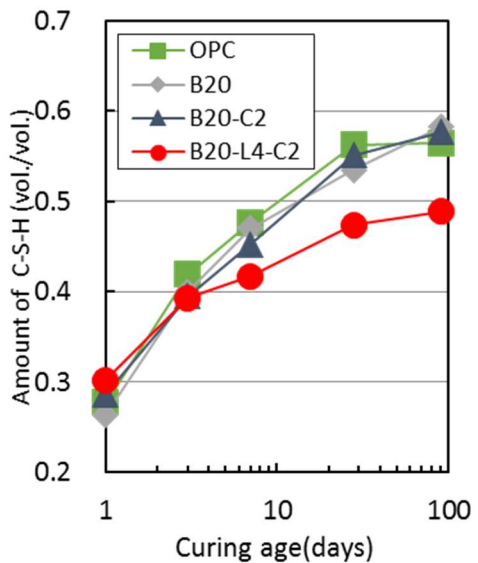


Fig. 3.14 C-S-H volume.

Figure 3.15 shows the results for capillary pore volume calculated using the amounts of hydration products. It is possible to estimate the change in pore ratio of each formulation from the change in C-S-H density. Figure 3.15 shows that, although the hydration content of B20 and B20-C2 paste samples at 91 days may decrease compared to that of an OPC sample, almost the same compressive strength was obtained as that reported in the results above, implying that low-density C-S-H is produced by the slag and thus fills the pore in the paste matrices.

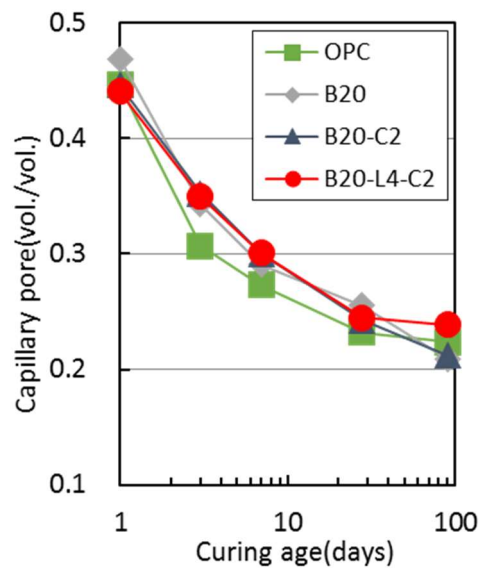


Fig. 3.15 The calculated capillary pore volume.

The reaction rate of the compound in each binder and the transition of the hydration product can be shown as a phase change in the composition in the paste with respect to curing age until 91 days, as shown in Fig. 3.16. The figures imply that a) the volume of C-S-H is high in the paste samples, even though the materials are different; b) the addition of slag to the mixture leads to small amount of CH hydration product; and c) the addition of LSP increases the amount of CA hydration product, but the hydration product of C-S-H decreases throughout the curing period in comparison to other paste samples with respect to the paste variation model.

The reactivity behavior of each compound was obtained through XRD/Rietveld analysis. The amount of hydration product is used to calculate the pore volume by assuming the density of C-S-H. As a result, the relationship between the compressive strength and the pore volume proposed by Powers can be examined with

the gel/pore ratio. The compressive strength at a curing age of 91 days of the B20 and B20-C2 samples is the same for OPC, which is considered to be the influence of the low C-S-H density generated by the BFS.

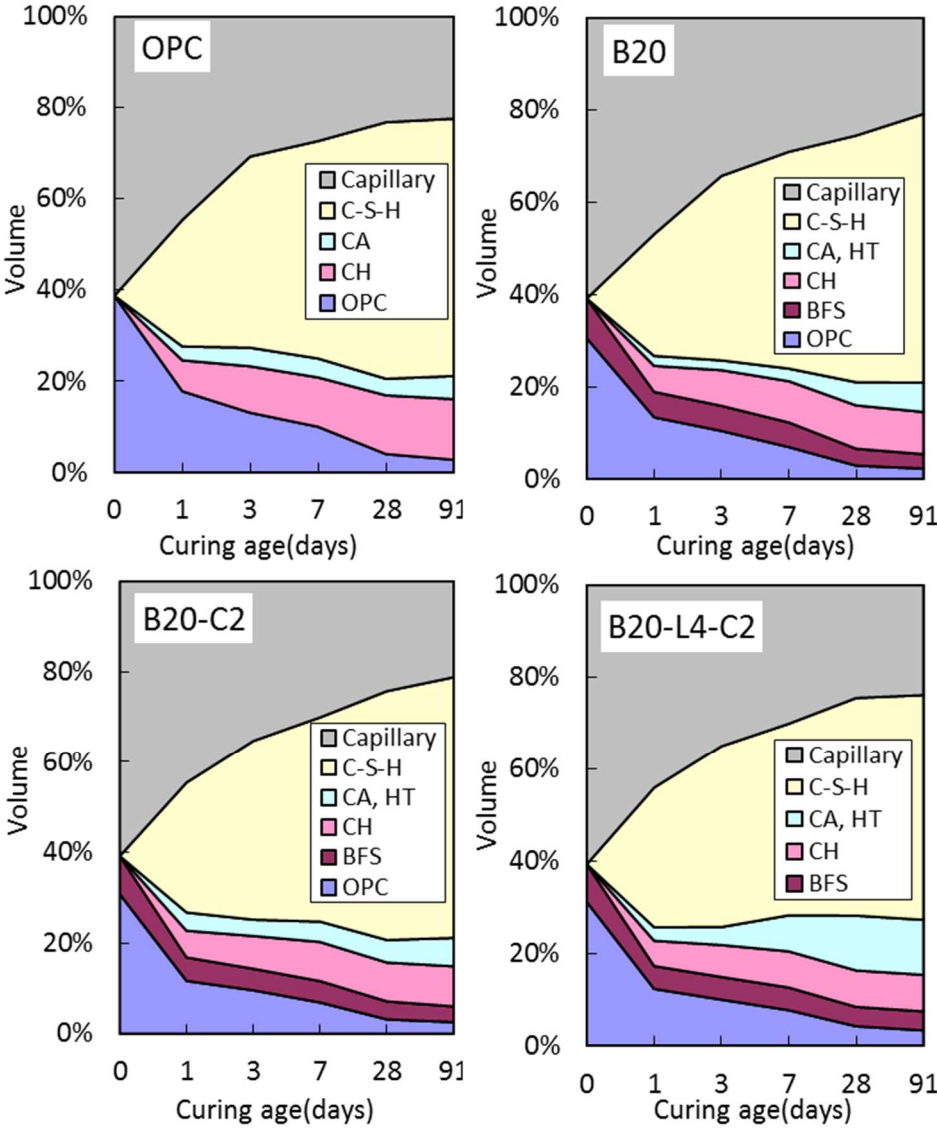


Fig. 3.16 Calculation results for composition of each mixture.

3.4 Mixture design of blast furnace slag concrete based on high early strength cement using the limestone powder and CaSO4

Tables 3.5 and 3.6 summarize the experimental plan and mix proportions of concrete used in this study. Blast furnace slag is used the two types. (1) ground granulated blast furnace slag, (2) blast furnace slag cement type B. And BFS were used with the replacement ratio amount 20% and 40%, respectively. BB50, BB90 sample

used BFS, and BF20, BF40 sample used BFS cement type B, And the BF15LS, BF35LC sample used LSP and CS. The slump and air content were measured on fresh concrete. For the hardened concrete mixes, the compressive strength was measured at 30, 90, 210, 840 and 2730 ° D · D of maturity and, the durability was evaluated in terms of the accelerated carbonation, resistance to free-thaw, dry shrinkage. The tests methods were conducted in compliance with the JIS standards of Japan. Compressive strength JIS A 1108, free-thaw resistance JIS A 1148 A and accelerated carbonation JIS A 1153 and dry shrinkage JIS A1129-30.

Table 3.5 Experimental Plan

	W/B (%)	S/a (%)	Binder ratio(%)					Air (%)	Slump (cm)	Curing Temperature (°C)	Maturity (°D · D)	Measurement	
			Cement			Admixture							
			OPC	HPC	BB	BFS	LSP						CS
N	55	46	100	-	-	-	-	-	5.0	18	5 20	30,90,210, 840,2730	Compressive strength
H			-	100	-	-	-	-					
BB50			-	50	50	-	-	-					
BB90			-	10	90	-	-	-					
BF20			-	80	-	20	-	-					
BF40			-	60	-	40	-	-					
BF15LC			-	80	-	15	3	2					
BF35LC			-	60	-	35	3	2					

Table 3.6 Mix proportions of the concrete

	W/B (%)	S/a (%)	Unit water (kg/m ³)	Unit content(kg/m ³)								AE (B×wt.%)
				OPC	HPC	BB	BFS	LSP	CS	S	G	
N	55	46	175	319	-	-	-	-	-	797	957	0.004
H				-	319	-	-	-	-	796	957	
BB50				-	160	160	-	-	-	795	954	
BB90				-	32	287	-	-	-	793	953	
BF20				-	255	-	64	-	-	795	954	
BF40				-	191	-	128	-	-	793	952	
BF15LC				-	255	-	48	10	6	794	954	
BF35LC				-	191	-	112	10	6	792	952	

3.4.1 Experimental results and discussion

3.4.1.1 Compressive strength

Figure 3.17 and 3.18 shows the results of compressive strength for BFS replacement cement concrete samples. It can be seen that the investigation of each mortar sample includes two curing cases, which are cured in air 5°C or 20°C at 30, 90, 210, 840 and 2730 °D · D maturity (1, 3, 7, 28 and 91 days). Maturity method in this study was used to investigate the effect of curing conditions on the compressive strength of all investigated mortar sample, which is expressed as follows Equation (3.3):

$$M = \sum_{Z=1}^n (\theta_Z + 10) \quad (3)$$

M= Maturity (°D · D)

Z= Curing age (day)

θ_Z = Temperature of concrete at Z days (°C)

It can be revealed that the compressive strength of mortar samples tends to decrease with the increasing the BFS replacement ratio at 30, 90 and 210 °D · D maturity due to the fact that proportion of cement content decreases and the fact that the reaction rate of BFS is late, in fact that may cause a decrease of the compressive strength at early age. The compressive strength is reduced as BFS replacement rate increases. In the case of BFS replacement 50% cured at 20°C, it shows an almost same compressive strength value with N concrete at the whole curing ages. In the case of BFS replacement 15% and replacement LSP, CS was higher than the other BFS replacement samples. BFS B type samples was similar compressive strength was N samples, without the BB90 sample. Because, BB90 sample was replacement ratio 10% of HPC. Moreover, compressive strength of concrete samples with replacing LSP, CS in maturity 2730 °D · D was higher in comparison with the other samples. The addition of CS in BFS blended mortar samples would affect the development of compressive strength at early curing age. In previous studies, the gypsum will generate heat when mixed in water, thermodynamically, the particles can own high free energy at high temperature, as a result, the chemical

reaction rate is increased. In addition, the use of CS, will provide additional Calcium. As described above, high concentrations of CS, a higher incidence of C-S-H which agrees with Ref (Chand et al. 2005).

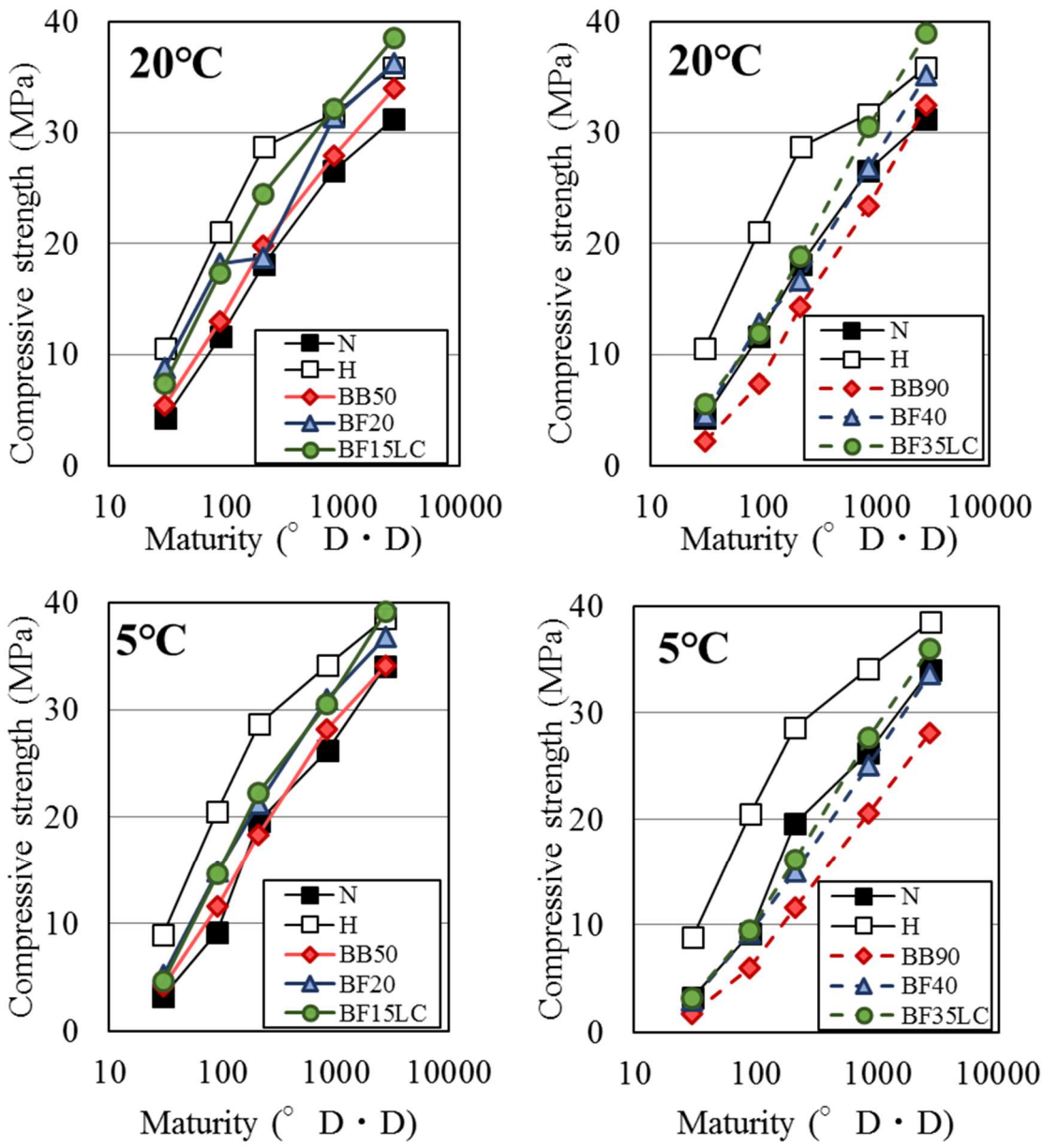


Fig. 3.17 Compressive strength of BFS blended mortar incorporating CS and LSP (base cement HPC).

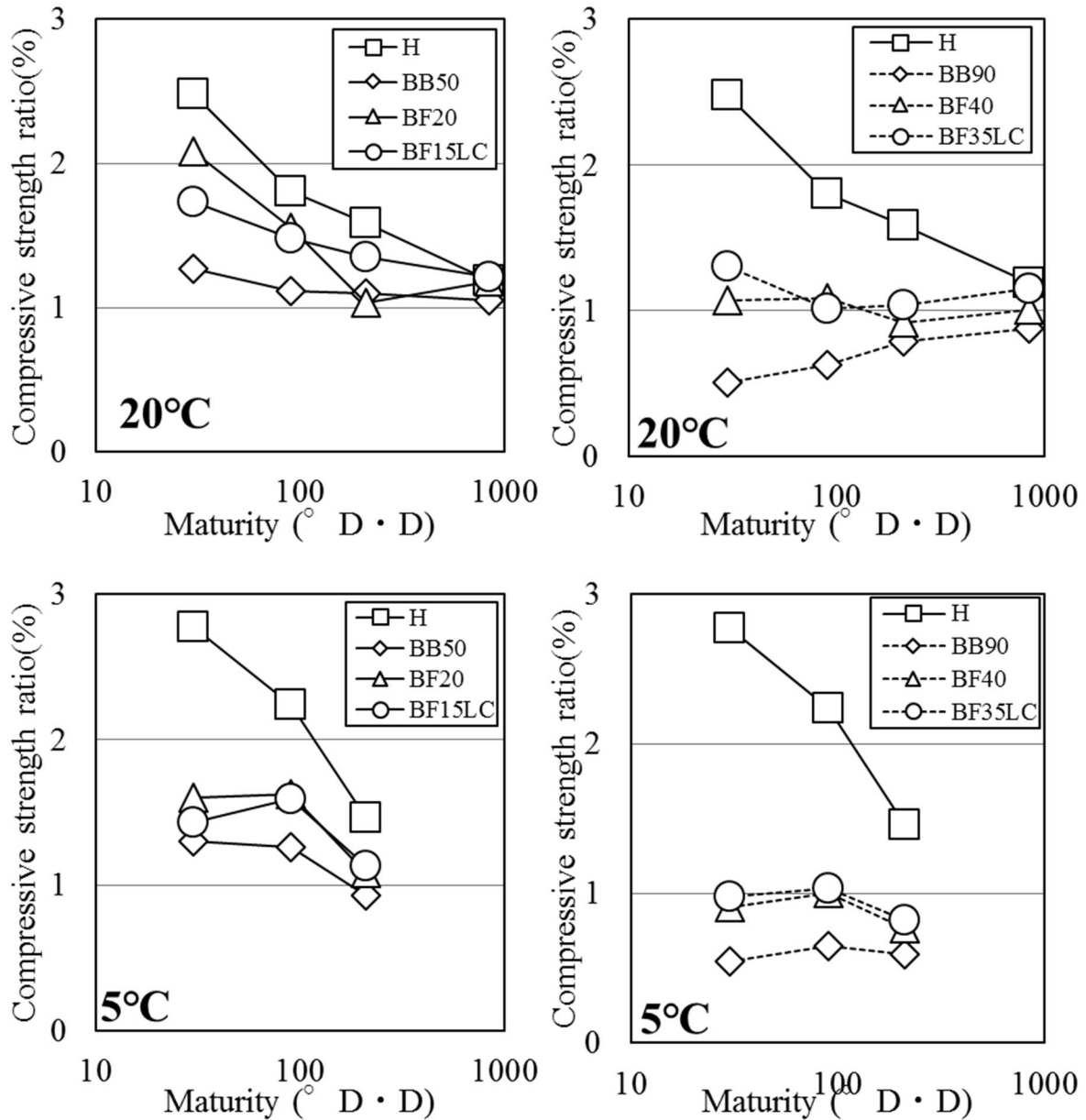


Fig. 3.18 Compressive strength ratios of BFS blended mortar incorporating CS and LSP (base cement HPC).

3.5 Conclusion

In this chapter, in an effort to develop a type-A of blast furnace slag (BFS) blended cement that can replace ordinary Portland cement (OPC), its strength development was investigated by varying the limestone powder (LSP) and gypsum (CS) replacement ratios. Furthermore, the correlation between the amounts of minerals produced in the cement and the compressive strength was examined through chemical analyses of test samples and by investigating the relationship between porosity and strength. A summary of the results obtained in this study is given below.

- (1) A mortar with BFS replacement exhibited a low early-age strength, which is thought to be due to the dependency of the initial strength of the slag cement on the OPC amount. For long-term aging, the strength obtained was high, in agreement with the literature.
- (2) When using CS as a replacement, the initial strength at a curing age of 1 day was equal to that of OPC. When CS was used as a replacement, significant heat was observed initially; this was determined to be an effect of the addition of calcium.
- (3) When using LSP as a replacement, the strength increased at replacement ratios of 20 and 25 wt.%. However, at a BFS replacement ratio of 15 wt.%, the strength decreased slightly. In comparison to findings in the literature (at 40 wt.% BFS), this result was thought to be due to the effect of LSP on the strength enhancement for BFS replacement ratios above a certain value.
- (4) From the results for the measured cement mineral reaction rate, the C_3S reaction amount increased for the case of CS replacement. This increase was thought to have affected the strength enhancement of the CS replacement mixture.
- (5) From the results for the measured hydration product, AFt was not converted to AFm as a result of LSP replacement. This is thought to be due to the contribution of AFt to the initial production of MC or HC in the LSP replacement case.
- (6) With regard to the relationship between porosity and strength, while the amount of capillary pores decreased with additional aging, the strength increased. Therefore, it was determined that, as the degree of hydration increased, the amounts of capillary pores decreased with aging and the strength increased accordingly.

- (7) With regard to the effect of using BFS cement as a replacement, the compressive strength development of the BFS type A was similar or higher than N. In long-term curing age strength development has been increase by the replacement Limestone powder and CaSO₄.

References:

- Barnett, S. J., Soutsos, M. N., Millard, S. G., and Bungey, J. H., Strength development of mortars containing ground granulated blast-furnace slag: Effect of curing temperature and determination of apparent activation energies, *Cement and Concrete Research*, 36, 2006, pp. 434–440
- Bonavetti, V. L., Rahhal, V. F., and Irassar, E. F., Studies on the carboaluminate formation in limestone filler-blended cements, *Cement and Concrete Research*, 31, 2001, pp. 853–859
- Boukendakdji, O., Kadri, E. H., and Kenai, S., Effects of granulated blast furnace slag and superplasticizer type on the fresh properties and compressive strength of self-compacting concrete, *Cement & Concrete Composites*, 34, 2012, pp.583–590
- Castellano, C. C., Bonavetti, V. L., Donza, H. A., and Irassar, E. F., The effect of w/b and temperature on the hydration and strength of blast furnace slag cements, *Construction and Building Materials*, 11, 2016, pp. 679–688
- Çetin, C., Erdogan, S. T., and Tokyay, M., Effect of particle size and slag content on the early hydration of interground blended cements, *Cement and Concrete Composites*, 67, 2016, pp. 39–49
- Chang, J. J., Yeih, W., and Hung, C. C., Effects of gypsum and phosphoric acid on the properties of sodium silicate-based alkali-activated slag pastes, *Cement & Concrete Composites*, 27, 2005, pp. 85–91.
- Chen, H. J., Hung, S. S., Tang, C. W., Malek, M.A., and Ean, L. W., Effect of curing environments on strength, porosity and chloride ingress resistance of blast furnace slag cement concretes: A construction site study, *Construction and Building Materials*, 35, 2012, pp. 1063–1070
- Courard, L., and Michel, F., Limestone fillers cement based composites: Effects of blast furnace slags on fresh

and hardened properties, *Construction and Building Materials*, 51, 2014, pp. 439–445

Ghrichi, M., Kenai, S., and Sai-Mansour, M., Mechanical properties and durability of mortar and concrete containing natural pozzolana and limestone blended cements, *Cement & Concrete Composites*, 29, 2007, pp. 542–549

Gu, K., Jin, F., Abir, A. T., Shi, B., and Liu, J., Mechanical and hydration properties of ground granulated blast furnace slag pastes activated with MgO–CaO mixtures, *Construction and Building Materials*, 69, 2014, pp. 101–108

Gu, Y. M., Fang, Y. H., You, D., Gong, Y. F., and Zhu, C. H., Properties and microstructure of alkali-activated slag cement cured at below- and about-normal temperature, *Construction and Building Materials*, 79, 2015, pp. 1–8

Hargis, C. W., Telesca, A., and Monteiro, P. J.M., Calcium sulfoaluminate (Ye’elinite) hydration in the presence of gypsum, calcite, and vaterite, *Cement and Concrete Research*, 65, 2014, pp. 15–20

Hoshino, S., Hirao, H., and Yamada, K., A study on the hydration reaction of cement paste by XRD/Rietveld method, *Proceedings of the Japan Concrete Institute*, 28(1), 2006a, pp. 41–46

Hoshino, S., Yamada, K., and Hirao, H., XRD/Rietveld analysis of the hydration and strength development of slag and limestone blended cement, *Japan Concrete Institute*, 4(3), 2006b, pp. 357–367

Jansen, D., Goetz-Neunhoeffler, F., Lothenbach, B., and Neubauer, J., The early hydration of ordinary Portland cement (OPC): An approach comparing measured heat flow with calculated heat flow from QXRD, *Cement and Concrete Research*, 42, 2014, pp. 134–138

Jansen, D., Goetz-Neunhoeffler, F., Stabler, C., and Neubauer, J., A remastered external standard method applied to the quantification of early OPC hydration, *Cement and Concrete Research*, 41, 2011a, pp. 602–608

Jansen, D., Stabler, C., Goetz-Neunhoeffler, F., Dittrich, S., and Neubauer, J., Does ordinary Portland cement contain amorphous phase? A quantitative study using an external standard method, *Powder Diffraction*, 26(1), 2011b, pp. 31–38

Jaya Prithika, A., and Sekar, S.K., Mechanical and fracture characteristics of eco-friendly concrete produced using coconut shell, ground granulated blast furnace slag and manufactured sand, *Construction and Building*

Materials, 103, 2016, pp. 1–7

Jiang Jhy Chand, Weichung Yeih and Chi Che Hung, Effects of gypsum and phosphoric acid on the properties of sodium silicate-based alkali-activated slag pastes, *Cement & Concrete Composites*, 27, pp. 85-91, 2005

Kondo, R., and Ohsawa, S., Studies on a method to determine the amount of granulated blast furnace slag and the rate of hydration of slag in cements, *The Ceramic Society of Japan*, 77, 1969, pp. 39–46 (in Japanese)

Kumar, S., Kumar, R., Bandopadhyay, A., Alex, T. C., Kumar, B. R., Das, S.K., and Mehrotra, S. P., Mechanical activation of granulated blast furnace slag and its effect on the properties and structure of Portland slag cement, *Cement & Concrete Composites*, 30, 2008, pp. 679–685

Lothenbach, B., Saout, G. L., Gallucci, E., and Scrivener, K., Influence of limestone on the hydration of Portland cements, *Cement and Concrete Research*, 38, 2008, pp. 848–860

Maruyama, I., and Igarashi, G., Prediction of strength of concrete in long-lived concrete member, *Architectural Institute of Japan*, 77(673), 2012, pp. 323–332

Matsushita, T., Hirao, H., Maruyama, I., and Noguchi, T., Quantitative analysis of cement hydration by XRD/Rietveld analysis, *Journal of Structural and Construction Engineering*, 73(623), 2008, pp. 1–8

Melo Neto, A.A.M, Cincotto, M.A., and Repette, W., Mechanical properties, drying and autogenous shrinkage of blast furnace slag activated with hydrated lime and gypsum, *Cement & Concrete Composites*, 32, 4, 2010, pp. 312–318

Menéndez, G., Bonavetti, V., and Irassar, E. F., Strength development of ternary blended cement with limestone filler and blast-furnace slag, *Cement & Concrete Composites*, 25, 2003, pp. 61–67

Miyazawa, S., Yokomuro, T., Fujiwara, H., and Koibuchi, K., Properties of concrete using blast-furnace slag cement type A with modified chemical composition, *Cement Science and Concrete Technology*, 64, 2010, pp. 244–250 (in Japanese)

Miyazawa, S., Yokomuro, T., Sakai, E., Yatagai, A., Nito, N., and Koibuchi, K., Properties of concrete using high C3S cement with ground granulated blast-furnace slag, *Construction and Building Materials*, 61, 2014, pp. 90–96

Nippon Slag Association, Use of blast furnace slag of steel slag, 2015 (in Japanese)

Özbay, E., Erdemir, M., and Durmus, H. I., Utilization and efficiency of ground granulated blast furnace slag on concrete properties – A review, *Construction and Building Materials*, 105, 2016, pp. 423–434

Park, H., Jeong, Y., Jun, Y., Jeong, J., and Oh, J., Strength enhancement and pore-size refinement in clinker-free CaO-activated GGBFS systems through substitution with gypsum, *Cement and Concrete Composites*, 68, 2016, pp. 57–65

Powers, T. C., Structure and physical properties of hardened Portland cement paste, *Journal of the American Ceramic Society*, 41, 1958, pp. 1–6

Rakhimova, N. R., and Rakhimov, R. Z., Individual and combined effects of Portland cement-based hydrated mortar components on alkali-activated slag cement, *Construction and Building Materials*, 73, 2014, pp. 515–522

Rakhimova, N. R., and Rakhimov, R. Z., Characterisation of ground hydrated Portland cement-based mortar as an additive to alkali-activated slag cement, *Cement & Concrete Composites*, 57, 2015, pp. 55–63

Sagawa, T., and Nawa, T., Determined the hydration ratio of slag by Rietveld method and selective dissolution method, *Concrete Research and Technology*, 28(1), 2006, pp. 209–214 (in Japanese)

Sagawa, T., and Nawa, T., Quantitative hydration analysis of blast furnace slag cement by Rietveld method, *Concrete Research and Technology*, 17(3), 2006, pp. 1–11 (in Japanese)

Sagawa, T., and Nawa, T., Hydration analysis and phase composition of cement-based materials by X-ray diffraction/Rietveld method using an external standard, *Cement Science and Concrete Technology*, 68, 2014, pp. 46–52 (in Japanese)

Sagawa, T., and Nawa, T., Quantitative determination of blast-furnace slag content in slag-blended cement by combination method of heat-treatment and XRD/Rietveld analysis, *Cement Science and Concrete Technology*, 68, 2014, pp. 38–45 (in Japanese)

Sagawa, T., Ishida, T., Luan, Y., and Nawa, T., Hydrate composition analysis and micro structure characteristics of Portland cement–blast furnace slag system, *Concrete Research and Technology*, 66(3), 2010, pp. 311–324 (in Japanese)

Sajedi, F., and Razak, H. A., The effect of chemical activators on early strength of ordinary Portland

cement-slag mortars, *Construction and Building Materials*, 24, 2010, pp. 1944–1951

Scholer, A., Lothenbach, B., Winnefeld, F., and Zajac, M., Hydration of quaternary Portland cement blends containing blast-furnace slag, siliceous fly ash and limestone powder, *Cement & Concrete Composites*, 55, 2015, pp. 374–382

Suda, Y., Study on performance evaluation of hardened cement paste based on relation between chemical composition and physical property of C-S-H, Niigata University, doctoral dissertation, 2013 (in Japanese)

Taylor, H. F. W., *Cement Chemistry*, Thomas Telford, 2nd. Edition, 1997, pp. 262–271

CHAPTER 4

EVALUATION OF THE COMBINED DETERIORATION BY FREEZE-THAW AND CARBONATION OF MORTAR INCORPORATING BFS

4.1 Overview

Assessing the durability of concrete structures is a major concern of building owners because it is related to safety, economy and sustainability. In cold regions, the action of freeze–thaw cycles significantly lowers the performances of concrete structures by destroying the compactness of the superficial concrete in reinforced concrete, developing the propagation of internal cracks in the cement paste, and accelerating the process of ice formation in the internal structure, thus causing serious and unacceptable loss (Zhao et al. 2014; Chung et al. 2010; Gerard et al. 2000; Özbay et al. 2012; Ahmet 2014). Moreover, one of the foremost issues (Neves et al. 2015; Parrott et al. 1996) affecting the durability of concrete structures is steel corrosion caused by the carbonation of concrete (Thomas et al. 1999; ACI 2003; Liu et al 2016), which also reduces the durability of reinforced concrete structures.

In previous studies, the carbonation and frost resistance characteristics of concrete have been investigated in detail both experimentally and theoretically (Zhang et al. 2008; Kumar and Paulo 2006). It is well-understood that the carbonation of concrete is related to the diffusion of CO₂ through the connectivity of pores on the surface of concrete, and also to its hydration products, such as calcium hydroxide and calcium silicate hydrates, a process that consumes hydroxyl ions and alters the physical and chemical properties of the concrete. Furthermore, the pore structure can be redistributed because of the carbonation of concrete (Leemann et al. 2017; Cizer et al. 2012; Chao and Gu 2016), which may reduce concrete porosity because the concrete surface may experience densification due to the production of CaCO₃. In addition, it is suggested (Lim and Mondal 2015) that the refinement of the pore structure may decrease the permeability. However, the influence of the pore structure change caused by carbonation on the freezing and thawing performance has not yet been clarified. In frost conditions, the hydraulic pressure governs the deterioration due to freezing, and pore solution in the frozen concrete pores induces a large internal hydraulic pressure and severe frost damage, resulting in cracks in the matrix. Furthermore, research into the effects of the freeze–thaw resistance of cement composites mixtures exposed to carbonation conditions was not encountered in the literature (Shirota and Murakami 2014; Wachi et al. 2011). Hence, it is necessary to investigate the influence of carbonation resistance on the frost

damage of reinforced concrete structures, especially in areas easily subjected to freeze–thaw damage. There is also little investigation in the literature concerning the combined effects of these two phenomena. The combined effects of freeze–thaw cycle damage and carbonation may increase the complexity of the durability design and the prediction of concrete structures located in cold areas. Additionally, it has been reported that the deterioration of concrete structures subjected to multi-damage processes could be significantly accelerated (Zhao et al. 2014; Sun et al. 2002; Zhao et al. 2011). Therefore, the cement type and mineral admixture of concrete members are expected to contribute to improving the degree of cement hydration and creating a more compact pore structure with lower permeability and higher performance (Sagawa et al. 2015; Pang et al. 2016; Zomeren 2011).

As a sustainable solution, the use of supplementary cementitious materials such as blast furnace slag, silica fume, limestone powder and calcium sulfate, as partial replacement of cement, is a common practice to reduce the environmental impact of the cement and concrete industry. The use of these materials often results in eco-friendly mixes with better durability and improved long-term mechanical properties (Hesami et al. 2016; Aprianti et al. 2015; Zhang et al. 2015; Na et al. 2012; Moura et al. 2007). In Japan, Portland blast furnace-slag cement (BFS cement) is classified into three categories according to the Japan Industrial Standards (JIS R 5211), i.e., Types A, B and C, which contain BFS from 5% to 30%, 30% to 60% and 60% to 70% by weight, respectively (Zhang et al. 2015). However, BFS cement has rarely been used for reinforced concrete buildings, primarily because concrete incorporating BFS leads to slower strength development at an early age and lower carbonation resistance compared to normal concrete. Additionally, the frost resistance of concrete is also affected by the addition of BFS. Although sufficient curing of BFS type B cementitious composite at an early age is required to increase resistance to freezing and thawing, the carbonation problem in BFS cementitious composite has been a topic of study for a long time; however, there is little agreement as to the combined deterioration effects of accelerated carbonation and freeze–thaw resistance. As one method of improving the strength development of the CaO-activated GGBFS system, the addition of sulfate sources, e.g., gypsum or calcium sulfate (CS), has been proposed (Sagawa et al. 2015; Park et al. 2016). Considerable work has been

undertaken on the use of limestone powder (LSP) as a cement replacement, and most of the previous research concluded that a large amount of limestone powder replacement has a negative effect on concrete compressive strength, which may be due to the cement content dilution effect (Ahmed et al. 2016; Dhiri et al. 2007; Ramezaniapour et al. 2009; Cyr et al. 2006; Guemmadi et al. 2009). Additionally, previous research has indicated that, generally, as the content of limestone powder increases, the sodium sulfate and corrosion resistance of concrete decrease (Lee et al. 2009; Pipilikaki et al. 2009; Moon et al. 2004). However, the influence of LSP and CS in controlling the durability of BFS cementitious composite has not been systematically investigated. In summary, there is a lack of information on the effects of mineral additions on the durability and combined deterioration properties of slag cement concrete.

The experimental program in this study is designed to assess the interaction between accelerated carbonation and freeze-thaw resistance in BFS mortar with limestone powder (LSP) and calcium sulfate (CS). First, the influence of mineral admixtures as cement replacement on the mechanical properties, carbon resistance and freeze-thaw resistance of mortar is determined. Furthermore, the combined deterioration under the combined effects of carbonation and frost damage is investigated. Mortar subjected to different degrees of frost damage is examined to assess the influence of frost damage on carbonation resistance and the pore structure change in BFS cement mortar. Then, the influence of pre-carbonation on the frost resistance is investigated, and the pore structure change with the accelerated carbonation progress is also measured. Through the above investigations, the obtained results from this study provide invaluable information regarding concrete durability, offering a better understanding of the durability performance of cementitious composite.

4.2 Experimental program

4.2.1 Materials and mixture proportions

In the present study, ordinary Portland cement (with a density of 3.16 g/cm^3) and land sand (with a surface-dry density of 2.67 g/cm^3 and a water absorption of 1.57%) were used as the fine aggregates. The compositions of mineral admixtures used as cemen

t replacement, i.e., BFS, LSP and CS, are shown in Table 5.1. All mortar specimens were casted into 40 x 40 x 160 mm prisms with a water-to-binder ratio (W/B) of 0.55 and a binder-to-sand ratio of 1:3 without any chemical admixture. BFS with a fineness of 4000 cm²/g was used to replace cement at 15% and 45% by weight of cement. The mixture proportions of mortar and the dosage of mineral admixtures are shown in Table 4.1. The air content, as the fresh property of mortar incorporating mineral admixtures, was measured by the pressure method, in accordance with ASTM C231.

Table 4.1 Mixture proportions of mortar and fresh property

Sample	W/B	B:S	Binder (%)				Air content (%)
			OPC	BFS	LSP	CS	
N	55	1:3	100	-	-	-	5.0
BA			85	15	-	-	5.0
BB			55	45	-	-	3.4
BC			15	85	-	-	2.3
BA-C			83	15	-	2	4.2
BA-L			81	15	4	-	4.2
BA-LC			79	15	4	2	4.1

4.2.2 Experimental program for the combined deterioration

To measure the single deterioration property, specimens were demolded after 1 day and cured in water at 20°C for 27 days. The compressive strength and frost damage properties for the single deterioration were then measured. The carbonation resistance of mortar cured in a control chamber at 20°C and 60% relative humidity for 28 days was also measured. Subsequently, the mortar was placed in a carbonation chamber with a carbonation concentration of 5%, a temperature of 20°C, and 60% relative humidity at carbonation depths of 1 weeks, 4 weeks and 8 weeks.

The experimental program for the combined deterioration process is detailed in Table 4.2. Series 1 is to investigate the effect of the degree of deterioration, evaluated with a freezing and thawing program, on the carbonation resistance of mortar. Before the accelerated carbonation test, the specimens were degraded by frost

damage, with measurements taken after 0, 12, 30 and 60 cycles. Then, the specimens that suffered from deterioration were cured in a control chamber at 20°C and 60% relative humidity and placed in a carbonation chamber with a carbonation concentration of 5%, a temperature of 20°C and 60% relative humidity for the evaluation of the carbonation resistance at depths up to 8 weeks. The pore size distribution and pore volume were also measured after 0 and 60 cycles of frost damage deterioration to analyze the pore structure effects on the carbonation resistance.

Series 2 is to explore the influence of accelerated carbonation degradation on the frost resistance of mortar. Frost damage in mortar specimens were also analyzed after pre-carbonation at 8 weeks. After the accelerated carbonation tests, the pore size distribution and pore volume were also measured to assess the pore structure change with the accelerated carbonation.

Table 4.2 The experimental program

combined deterioration process			
Series 1	Freeze-thaw	-	Carbonation
		12 cyc.	
		30 cyc.	
		60cyc.	
Series 2	Carbonation	7 w	Freeze-thaw
	Air curing	7 w	

4.2.3 Testing method

4.2.3.1 Freeze-thaw test

The dynamic modulus of elasticity was measured by maintaining the minimal temperature of -18°C and the maximal temperature of 5°C, which is based on the JIS A 1148 A method (2010), which is similar to ASTM C 666 Procedure B (rapid freezing in air and thawing in water) (Nam et al. 2016). The relative dynamic modulus of elasticity was determined by measuring the resonant frequency and then calculated as the percentage fraction of transverse frequency after n cycles of freeze-thaw squared to the square of the transverse frequency

at 0 cycles. The frost resistance is the measure of the durability factor of the test specimen until the relative dynamic modulus of elasticity falls to less than 60% or the specimen is subjected to 300 cycles.

4.2.3.2 Accelerating carbonation test

According to JIS A 1153 (2013), the accelerating carbonation test samples were cured in a control chamber at 20°C and 60% relative humidity for 28 days. The specimens were subsequently placed in a carbonation chamber with a carbonation concentration of 5%, a temperature of 20°C, and 60% relative humidity. After 4 weeks, the samples were dried. The mortar samples were cut at 1, 4, 8, and 13 weeks, and the carbonation depths were determined by spraying the broken mortar surfaces with a phenolphthalein indicator. The carbonation speed coefficient is calculated from the carbonation depth results of the investigated samples using the following equation:

$$x = k\sqrt{t} \quad \text{Eq. (1)}$$

where, x is the depth of carbonation (mm); t is the time at which carbonation has taken place (week); and k is the carbonation speed coefficient ($\text{mm} \cdot \text{weeks}^{-0.5}$).

4.2.3.3 Mercury intrusion porosimetry test

The pore size distribution was determined by the mercury intrusion porosimetry (MIP) method, which is a method commonly used to measure the pore size distribution in cement-based materials (Zhang et al. 2015; Kayyali 1985; Zhang et al. 2013) using an Autopore Master33 porosimeter, which can function pressures from 0 to 220 MPa. The surface tension of the mercury and the mercury density were 0.480 N/m and 13.546 g/ml, respectively, assuming a contact angle of 140°. The samples for Series 2 measurements were taken from carbonated areas of the mortar bars after an exposure at 5% CO₂ in the control chamber. The MIP technique requires that the hardened cement-based materials should be thoroughly treated to remove water and then evacuated prior to testing. After the specified curing time, the mortar prisms were cut into 5-mm cubic samples. The samples were subsequently dried to stop the cement hydration reaction with acetone, followed by a

D-drying pretreatment. The pore size of the samples were measured using the Autopore Master33 porosimeter in which a hydraulic pump was used to generate the pressure and a contact sensor was used to measure the mercury volume.

4.3 Experiment result and discussion

4.3.1 Compressive strength

The results of the compressive strength test for all mortar samples incorporating mineral admixtures with BFS replacement ratios of 15 to 45% by weight and two types of mineral admixtures with LSP and CS are shown in Fig. 4.1. Five mortar mixtures were prepared with the proportions listed in Table 4.1. The data show that the compressive strength decrease as the BFS replacement ratio increases. In the case of LSP and CS addition, the compressive strength in the BA-C and BA-L samples is increased to the value of N mortar without incorporating mineral materials. With respect to the addition of CS, it is inferred that CS helps to accelerate the hydration reaction of BFS at an early age, also increasing the strength (Jawed and Skalny 1978). With respect to the replacement ratio of LSP in the binder, a filling effect can occur in which the pores are filled, leading to improved mechanical properties. These above results show that the behavior of LPS and CS

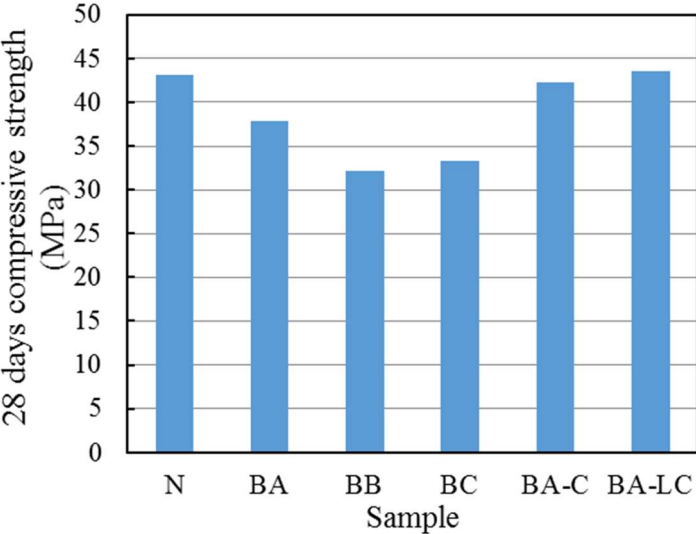


Fig. 4.1 Compressive strength result at 28 days.

can contribute to the development of compressive strength. Replacement ratios of 2% and 4% by weight for CS and LPS, respectively, in the binder are verified to be appropriate for increasing the compressive strength of the BFS blended mortar mixture.

4.3.2 Frost resistance

Results for the relative dynamic modulus of elasticity of mortars after curing in water for 28 days are given in Fig. 4.2. The frost damage with respect to the relative dynamic modulus of elasticity is found to be significantly reduced with the increase in the BFS dosage from 0 to 45 wt. %, implying that the addition of BFS to the binder has a negative effect on the frost resistance of the BFS blended mortar. A difference is observed in the relative dynamic modulus of elasticity of the mortar by incorporating a minor mineral mixture component. The frost damage of BA-L incorporating LSP is less than that of BA-C mixed with CS, which is similar to the durability of the N sample without mineral admixtures.

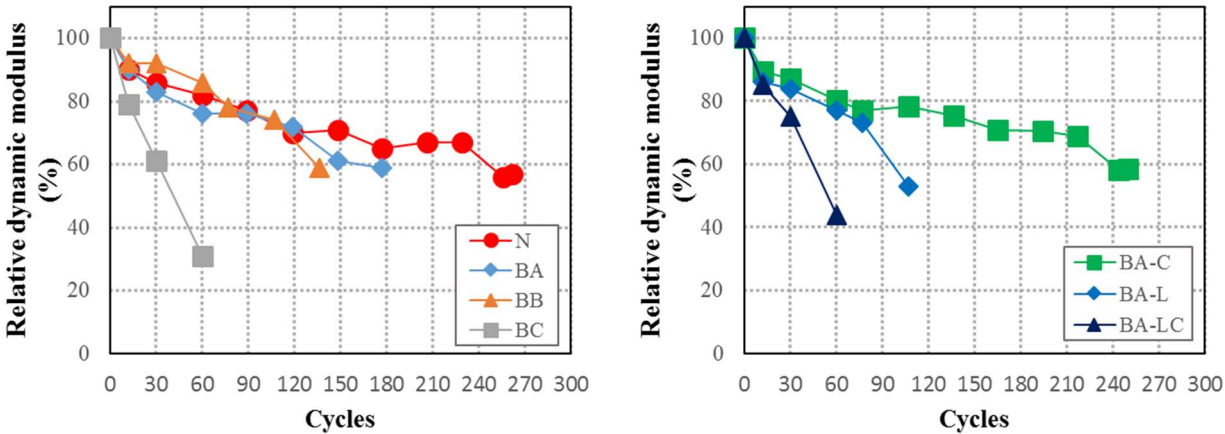


Fig. 4.2 Relative dynamic modulus of elasticity result of the mortar.

In this experiment, the air content of the mortar without the use of chemical admixtures was fitted to $4.2 \pm 1.0\%$. It is known that the frost resistance depends on the air content; thus, proper air content is necessary to enhance freeze and thaw resistance. Fig. 4.3 provides the relationship between durability factors and air

content for all of the mortars. The BB mortar with 3.4% air content exhibits a lower durability than the BA and N mortar with 5% air content. In this experiment, the air contents of the BA-C and BA-L mortar specimens with different mineral admixtures have the same values; however, different durability factors can also be obtained. The results also show that the frost resistance of mortar was reduced by the use of the LSP admixture in comparison with the BA and BA-C samples. It is inferred that with the addition of the LSP, the porosity of BFS mortar was increased and the pore size was also enlarged, as identified in the previous research (Zhang and Ye 2012). The pore structure is presented in Fig. 4.4. Fig. 4.4 (a) shows the cumulative pore volume result of mortar, and Fig. 4.4 (b) is the log differential pore volume result of mortar with LSP and CS as the mineral admixture. Previous research has noted that the freeze and thaw durability of cement, which strongly depends on the pore structure in the mixture, tends to increase with the decrease in pore volume in diameter from 40 to 2000 nm (Kabada 1988). It is observed in Fig. 4 (a) that the total pore volume is increased with the addition of LSP, and Fig. 4 (b) indicates that the pore size distribution peak of BA-L shifts to approximately 40 nm compared to the BA sample that presents the pore size distribution peak at 80nm. That is, the addition of LSP increases the coarse capillary pores and the total porosity of the BFS mortar. Therefore, the larger pore volume of the pore structure is considered to be the cause of the decreased freeze-thaw resistance.

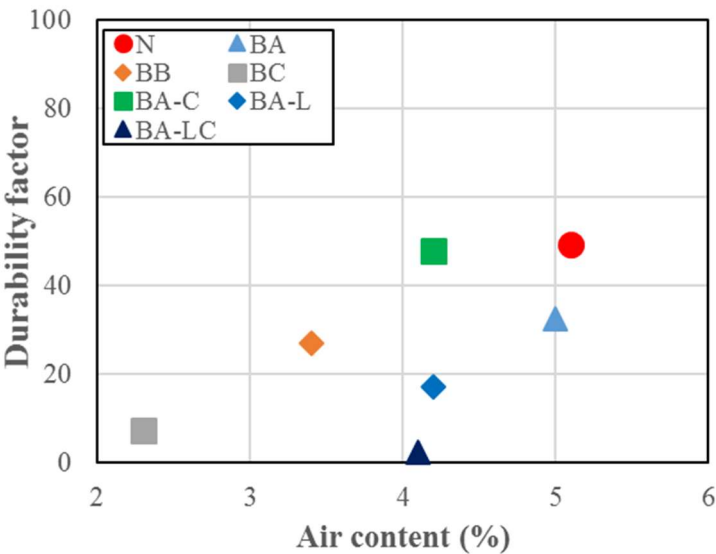


Fig. 4.3 Influence of air content on the durability.

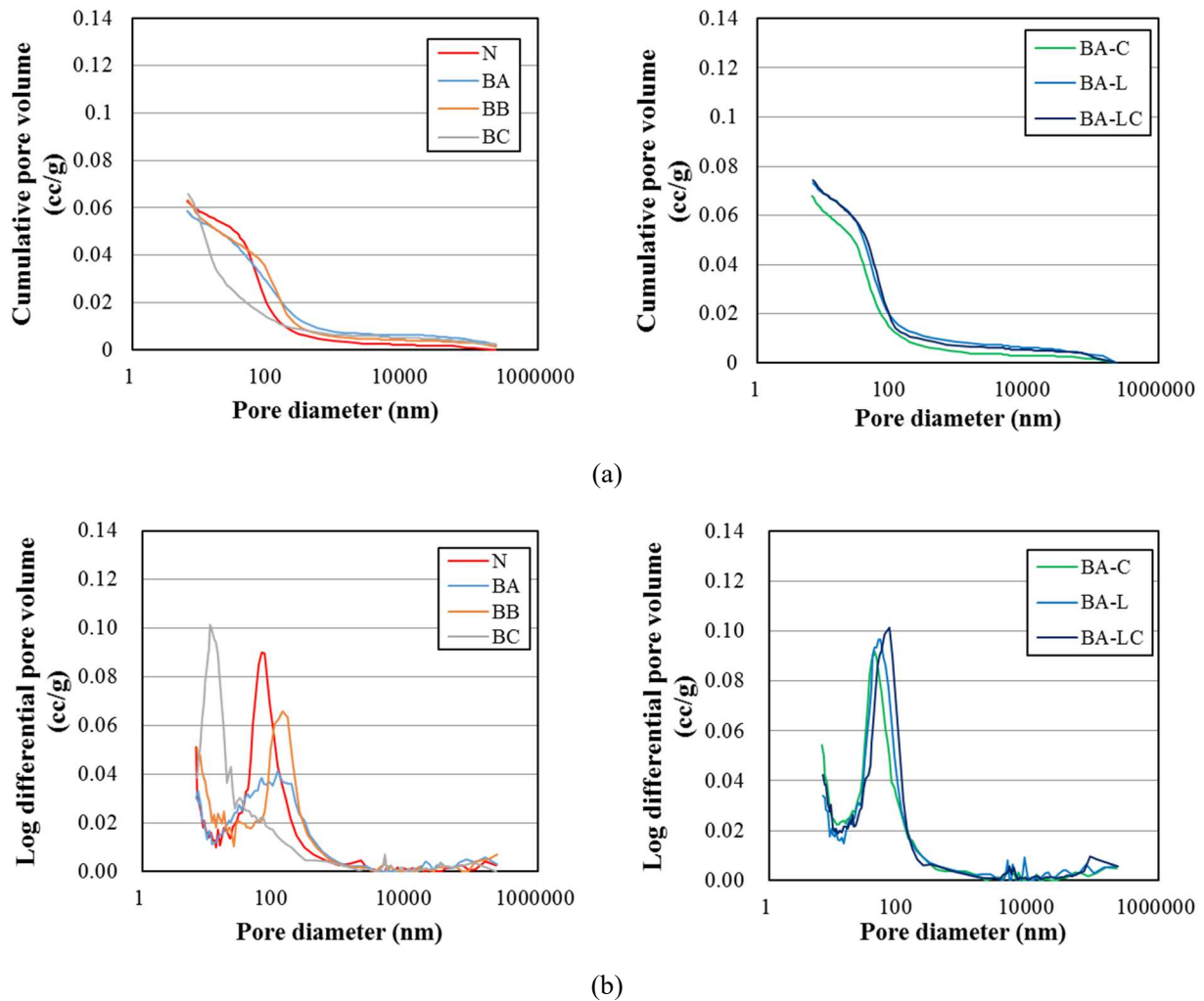


Fig. 4.4 Pore size distribution result of the mortar with different mineral materials. (a) Cumulative pore volume result. (b) Log differential pore volume result.

4.3.3 Carbonation result

The results of the carbonation tests to a depth of 8 W versus the carbonation period for all of the mortar samples are shown in Fig. 4.5. The data in Fig. 4.5 show that the carbonation resistance decrease as the BFS dosage increases; the BB sample with 45% BFS by weight of cement presents the greatest carbonation depth among all of the samples. However, the use of the mineral admixture of LSP and CS in the mortar sample leads to the same carbonation resistance as that of the BA sample. As a whole, the mortar with ordinary Portland cement shows higher carbonation resistance than blast furnace slag cement mortars. Although carbonation performance is known to be dependent on capillary pores having a radius of 0.05-0.1 μm (Harada

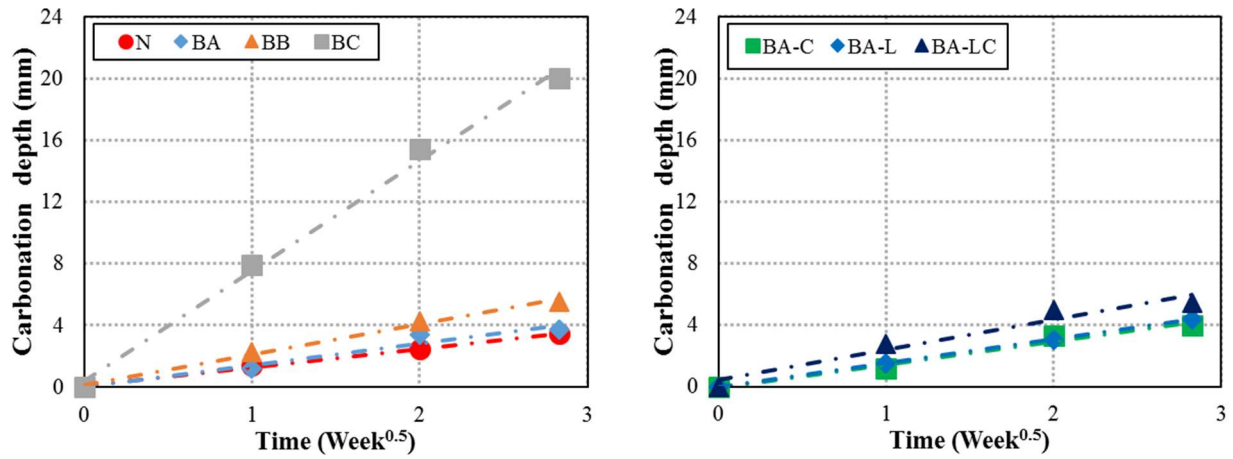


Fig. 4.5 Carbonation depth result.

1996), the relationship between capillary pores and the carbonation speed coefficient is shown in Fig. 4.6. It could be observed that there is no significant relationship between the carbonation coefficient and capillary pores of the mortar samples. From the perspective of the LSP, the poor active effect of hydration will increase the coarse capillary pores and the total porosity of the mortar, as demonstrated in Fig. 4.4. The coarse porosity is detrimental to improving the performance of carbonation resistance of mortar. In addition, because of the additional hydration process of BFS, a large amount of $\text{Ca}(\text{OH})_2$ is consumed, and the alkali content decreases,

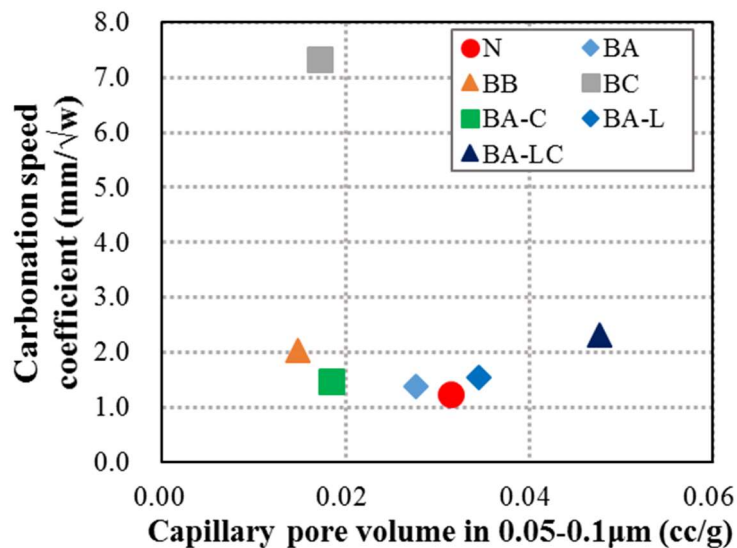


Fig. 4.6 Relationship between the carbonation speed coefficient and pore volume at 0.05-10 μm.

which causes the carbonation process to accelerate, thus increasing the speed of carbonation. Hence, in general, the addition of LSP has no beneficial effect on carbonation performance, and carbonation resistance is decreased.

4.4 Combined deterioration

4.4.1 Effects of the degree of frost damage and the pore structure on carbonation resistance

To assess the influence of different degrees of frost damage on the carbonation resistance of mortar, all of the measured mortar samples in Series 1 were degraded for 12, 30, and 60 cycles using the frost and thaw method according to ASTM C666. The different relative dynamic moduli of elasticity versus the repeated freezing and thawing cycles up to 60 cycles for mortar are the same as the result shown in Fig. 4.2. This indicates that the relative dynamic modulus of elasticity decreases in the range of 75% to 90% up to 60 cycles, and the mortars with different mix proportions show slightly different frost damage degrees corresponding to the degradation cycles. Then, the specimens subjected to the different degrees of frost damage were performed to the measurement of the carbonation resistance.

Fig. 4.7 gives the comparison result for the carbonation speed coefficient of mortar without frost damage and with frost damage after 60 cycles. As a whole, there is a tendency for the mortar carbonation speed coefficient to increase after 60 cycles of frost damage. To determine the influence of the deterioration degree on the carbonation property, the carbonation speed ratio versus the relative dynamic modulus of elasticity is plotted in Fig. 4.8. This carbonation speed ratio was determined as the percentage fraction of the carbonation speed coefficient after 12, 30, and 60 freeze-thaw cycles to the initial carbonation speed coefficient without freeze-thaw deterioration. In this study, the relative dynamic modulus of elasticity of mortar specimens varies from 75% to 90% under different freeze-thaw cycles, and it could be observed in Fig. 5.8 that the carbonation ratio increases as the deterioration degree increases, regardless of whether the mortar is mixed with BFS or with a mineral admixture of CS and LSP. As a whole, when the specimens were degraded by frost damage for

12, 30, and 60 cycles, it could be observed that the carbonation increases with the degree of frost damage for all of the investigated mortar samples.

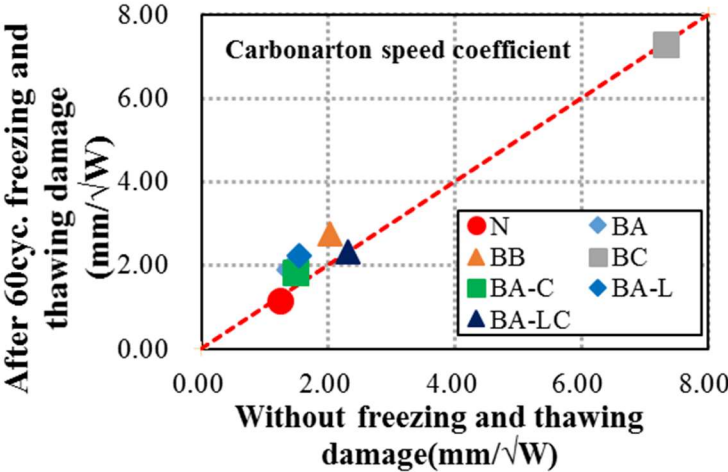


Fig. 4.7 Comparison of the carbonation speed coefficient of mortar without frost damage and with frost damage after 60 cycles.

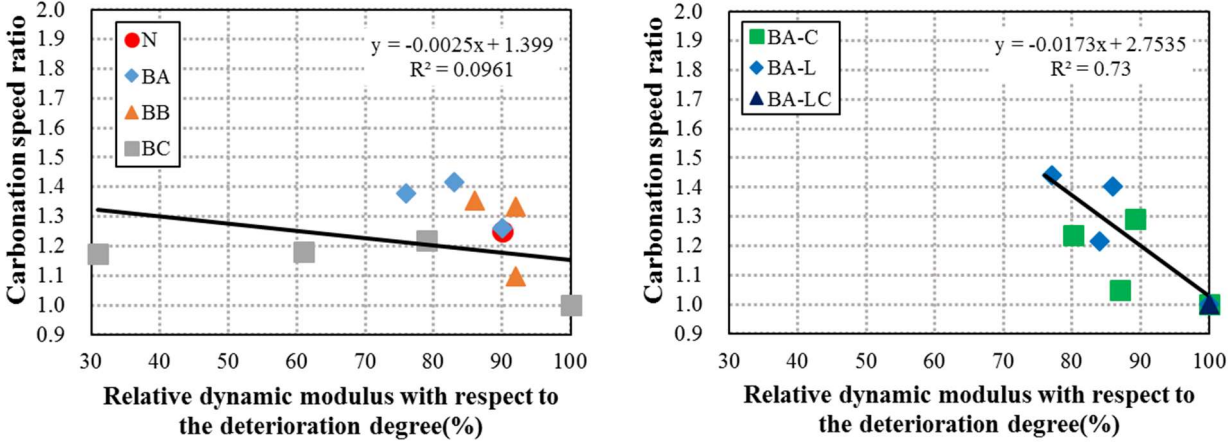


Fig. 4.8 Carbonation speed ratio of mortar with different relative dynamic moduli of elasticity.

Mortar is a porous material, and the carbon dioxide pathway depends primarily on the capillary pores. It has been noted that the inkbottle pore has water retention characteristics, which block this pathway, thereby decreasing the continuity of the pores and blocking the transfer of CO₂. According to the classical model, inkbottle pores consist of two cylindrical pores with different diameters, that is, the opening into the pore (D1) is smaller than the diameter of the pore (D2), as shown in Fig. 4.9. The MIP method has been widely used until

present; however, it is well-known that mercury pressure porosimetry does not describe the actual pore structure (Kaufmann et al. 2009; Moro and Bohni 2002; Tsakiroglou and Payatakes 1990; Vocĭka et al. 2000). Therefore, the size distribution of inkbottle type pores is analyzed by executing a second mercury cycle. The inkbottle pore volume is evaluated by the subtraction of the second intrusion curve from the first intrusion curve. Additionally, it has also been revealed that the pores with a diameter above 50 nm play an important role in the carbonation phenomena. Then, the change in the inkbottle pore volume above 50 nm in diameter caused by freeze-thaw deterioration is shown in Fig. 4.9. The influence of the inkbottle pore volume above 50 nm on the carbonation depth is shown in Fig. 4.10. The inkbottle pore volume of mortar samples without deterioration at 0 freeze-thaw cycle and after 60 freeze-thaw cycles were measured. The data in Fig. 4.10 show that the pore volume of inkbottle pores above 50 nm in diameter in the mortar clearly decrease after freeze-thaw deterioration. That is, the ability to retain water decreases and the continuity of the pores is increased. CO₂ could then more easily permeate the transfer path in the mortar samples. Fig. 4.10 shows that the carbonation speed coefficient increases as the inkbottle pore volume above 50 nm decreases. Therefore, the carbonation speed coefficient tends to increase, which is caused by the water retention property decrease in the inkbottle pores with diameter above 50 nm.

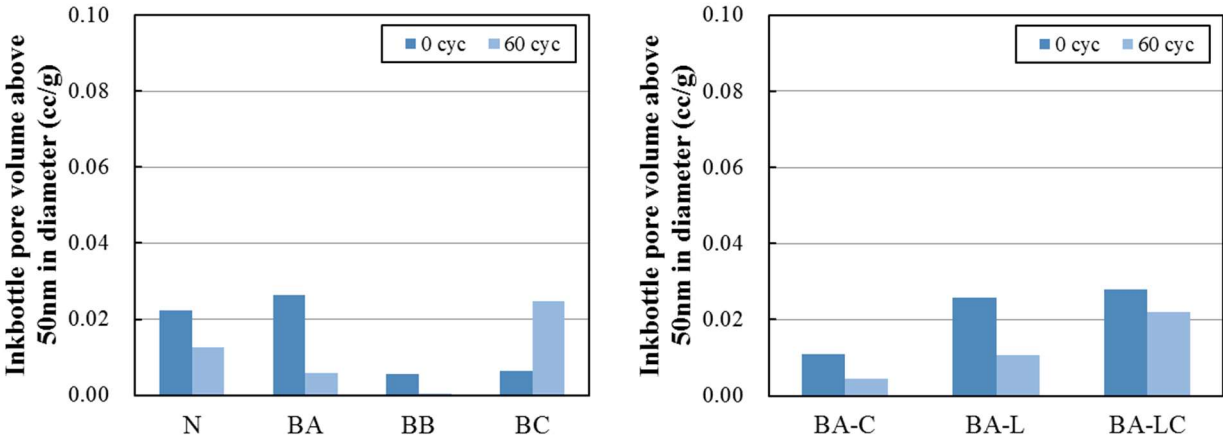


Fig. 4.9 Inkbottle pore volume change above 50 nm in diameter corresponding to the frost damage degree.

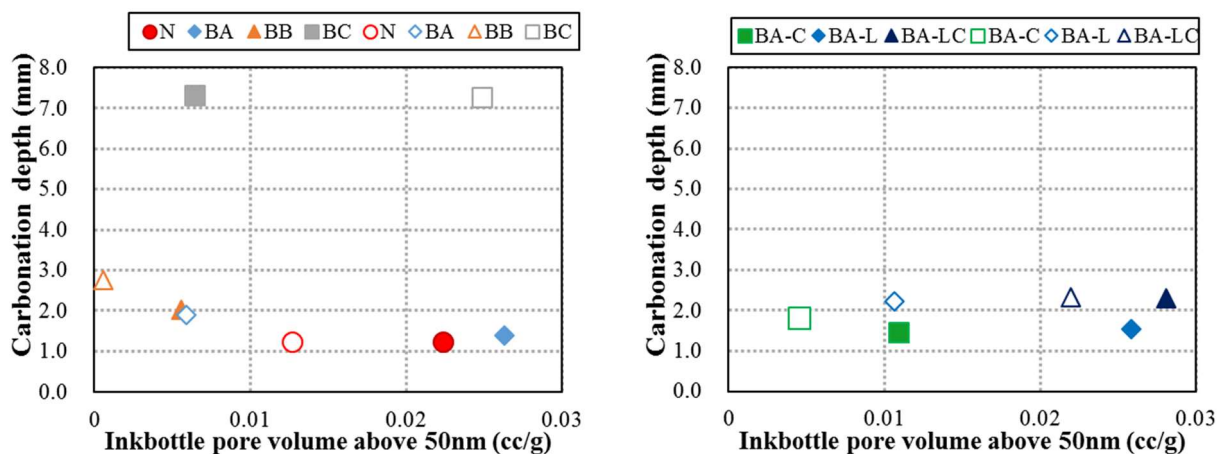
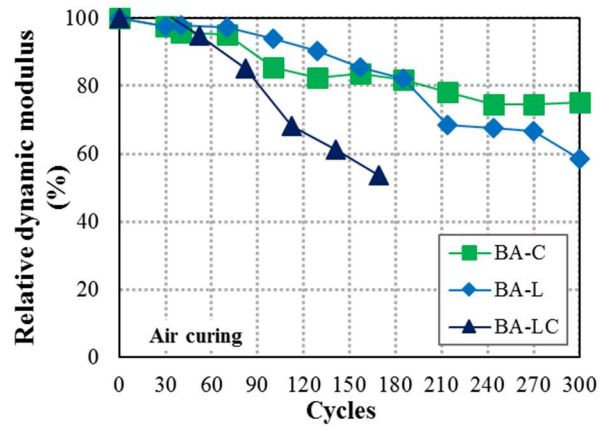
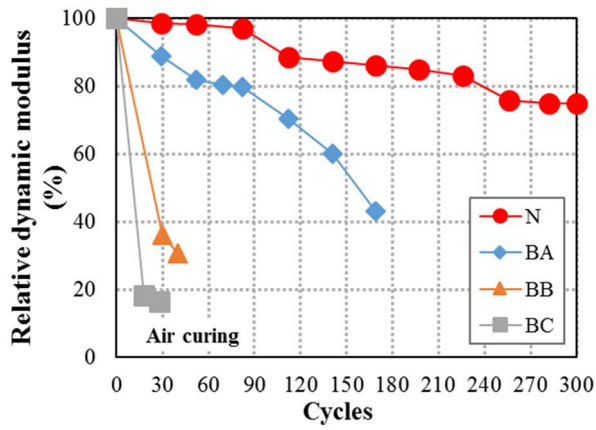


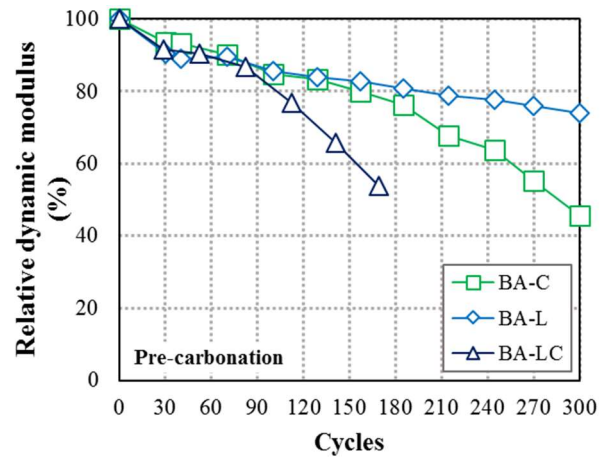
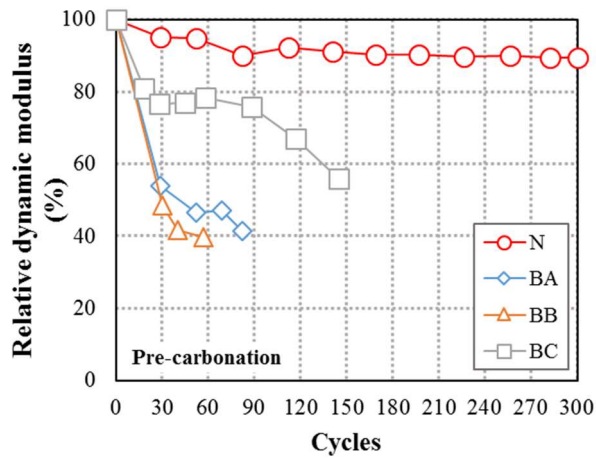
Fig. 4.10 Influence of inkbottle pore volume above 50 nm on the carbonation depth.

4.4.2 Effects of the pre-carbonation deterioration and the pore structure on frost resistance

To detect the influence of pre-carbonation deterioration on the frost resistance, mortar specimens were subjected to frost damage after pre-carbonation for depths up to 8 weeks. Some mortar samples were also cured in standard air as reference specimens. Fig. 4.11 presents the relative dynamic modulus of elasticity of mortars after air curing and after pre-carbonation. It could be found that an apparent decline of the relative dynamic modulus occurs for BA after pre-carbonation compared to that for air curing; the data for the other samples show a similar deterioration tendency regardless of air curing or pre-carbonation. Additionally, the mass loss change during the freeze-thaw process is shown in Fig. 4.12, which was measured and calculated for different numbers of freeze-thaw cycles. In Fig. 4.12, the symbol of C means the specimens after pre-carbonation; and non-means the specimens cured in air without accelerated carbonation. The mass loss ratio change is found to be significantly decreased after pre-carbonation deterioration. It is likely that the addition of BFS reduces the relative amount of cement and also reduces the $\text{Ca}(\text{OH})_2$ that can be carbonized simultaneously, weakening the ability of the mortar to absorb CO_2 and accelerate CO_2 diffusion. Because of the carbonization reaction, calcium carbonate and other solid products fill in the pores of the cement mortar, which can decrease the porosity and number of large pores.



(a)



(b)

Fig. 4.11 Relative dynamic modulus of mortar after air curing and after pre-carbonation. (a) mortar samples after air curing (b) mortar samples after pre-carbonation.

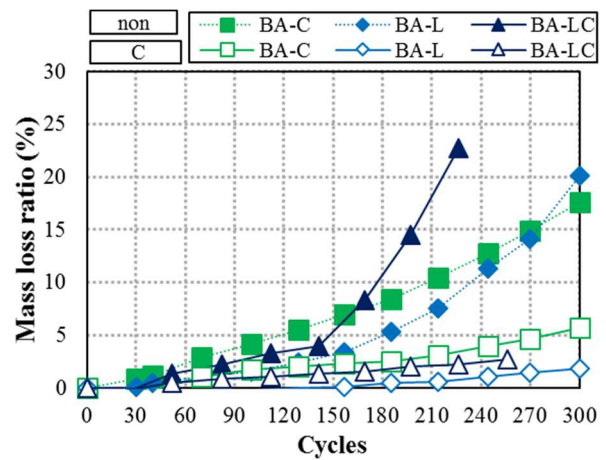
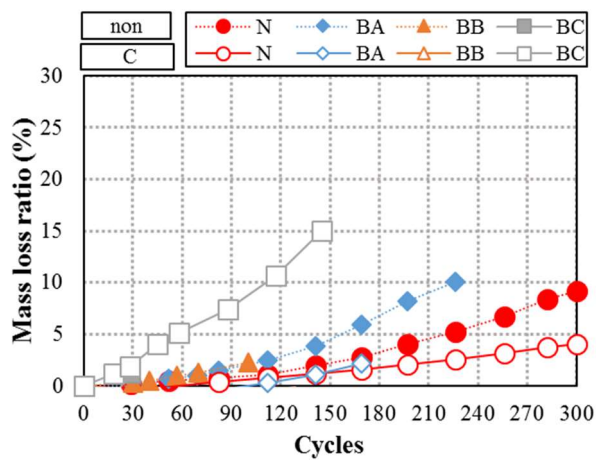


Fig. 4.12 Mass loss ratio with respect to the free-thaw process.

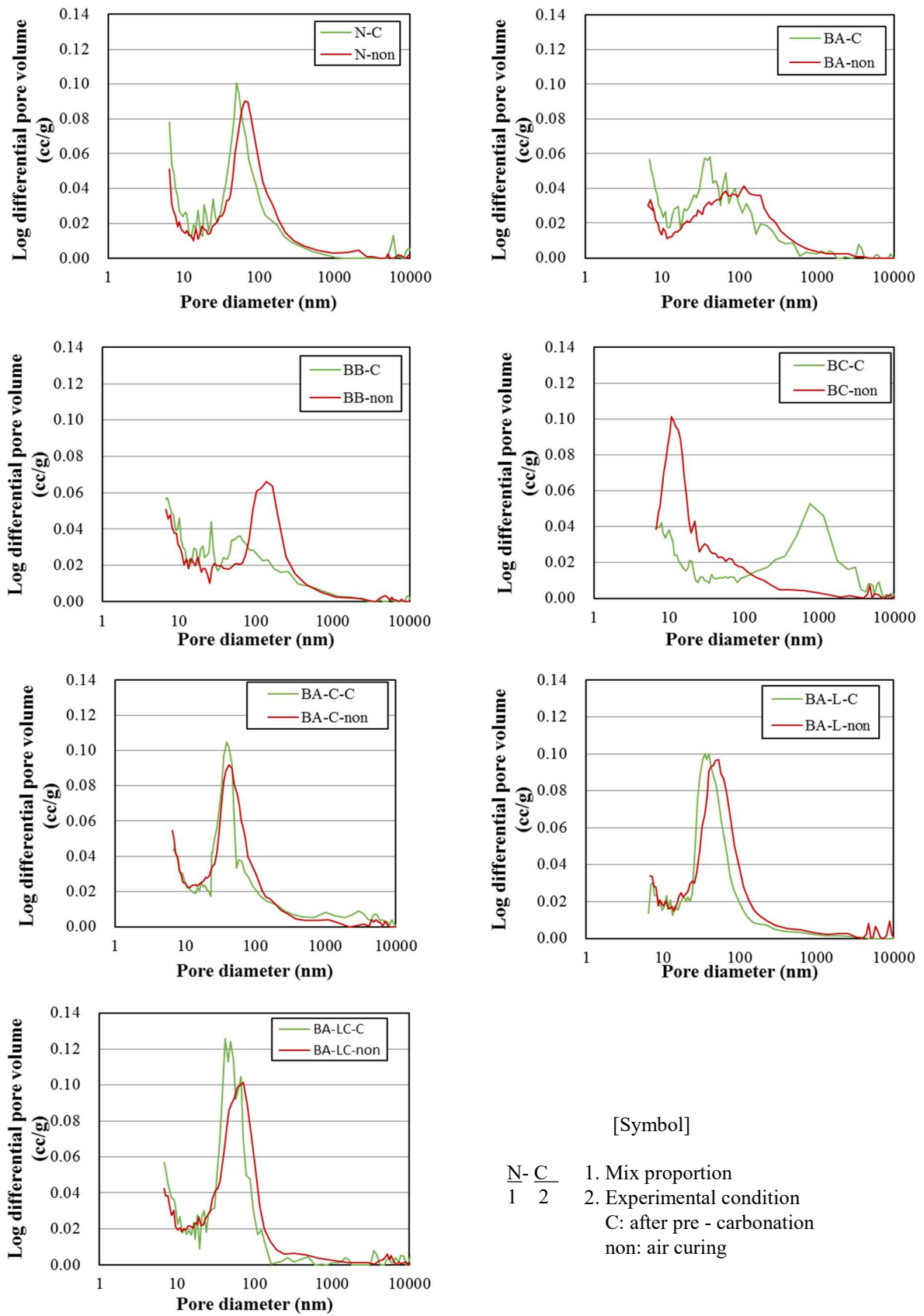


Fig. 4.13 Pore size distribution comparison of mortar after air curing and pre-carbonation.

The pore size distribution measured by the MIP method is presented in Fig. 4.13. It can be observed that the peak of the pore value shifts toward smaller pores after carbonation and that the pore volume of the small pores (diameters of approximately 80 nm) increases as the pre-carbonation progresses, indicating that the pore structure undergoes densification. Therefore, the densified surface of mortar could resist to the deterioration during freeze-thaw process and the scaling mass loss of mortar after pre-carbonation during freezing and thawing tends to decrease compared with the non-carbonated specimens. These experimental results presented are useful in providing a good perspective for concrete durability design and assessment.

The authors' research group is conducting another experimental study on the combined deterioration property of concrete with BFS replacement ratio from 0% to 65%. The result of the present study show the effects of pre-carbonation on mass loss during freeze-thaw process. Furthermore, the influence of pre-carbonation on the scaling mass for the CIF test and the ASTM process will be further investigated and the outcomes will be reported in separate papers.

4.5 Conclusions

The current study examined the strength enhancement properties of mortar and the durability of BFS cement mortar incorporating different BFS replacement ratios and a small amount of mineral admixture (CS and LSP). The dual effect of freeze-thaw resistance and carbonation progress as a combined deterioration mechanism in mortar was investigated in this research. The primary findings of the study can be summarized as follows:

- (1) The compressive strength tends to decrease as the BFS replacement ratio increase from 0 to 45%. Moreover, it is found that the addition of the mineral admixture (CS and LSP) could enhance the strength of BFS mortar. To achieve the same strength as ordinary Portland cement, the additions of 2% CS and 4% LSP are required.
- (2) In the case of single deterioration, the frost resistance and carbonation resistance both decreased as the

BFS replacement ratio increases from 0 to 45%. It is likely that the increasing cumulative pore volume leads to the decrease in frost resistance. In the case of BFS cement carbonation, the alkali content decreases and a large amount of $\text{Ca}(\text{OH})_2$ is consumed with the additional hydration process of BFS; hence, the carbonation process accelerates and the carbonation resistance of BFS cementitious composite decreases.

- (3) When CS and LSP are added to BFS cement, the results show that CS has a positive effect on the durability, but the frost resistance and carbonation resistance are reduced by the use of the LSP admixture. It is illustrated that the addition of LSP increases the coarse capillary pores and the total porosity of the BFS mortar, which is detrimental to improving the performance of frost and carbonation resistance.
- (4) With respect to the effect of the degree of frost damage on the carbonation resistance, the relative dynamic modulus of elasticity of the mortar is mainly in the range of 75% to 90% as the specimens experience to 12, 30, and 60 freeze-thaw cycles. The result shows that the carbonation resistance decreases as the freezing and thawing progresses. It is considered that the inkbottle pore volume for pores with diameter above 50 nm plays an important role in the carbonation behavior. The pore volume of inkbottle pores that can retain water decreases, the continuity of the pores increases, and CO_2 could permeate the transfer path of the mortar samples, allowing the carbonation to accelerate.
- (5) With respect to the influence of pre-carbonation deterioration on the frost resistance, it is remarkable that the scaling mass loss of mortar after pre-carbonation deterioration is less than that of the non-carbonated specimens, a phenomenon primarily dominated by the pore structure densification caused by the pre-carbonation. The experimental results in this study provide a good perspective for the design and assessment of concrete durability.

References:

- ACI 213R, Guide for Structural Lightweight-aggregate Concrete, American Concrete Institute, Farmington Hills, MI, USA, 38, 2003
- Ahmed, MD., Abd, E., Ayman, AA., Long term study of mechanical properties, durability and environmental impact of limestone cement concrete, *Alexandria Engineering Journal*, 55, 2016, pp. 1465–1482
- Ahmet Ç., Investigation of freeze–thaw effects on mechanical properties of fiber reinforced cement mortars, *Composites B*, 58, 2014, pp. 463–472
- Aprianti, E., Shafigh, P., Bahri, S., Farahani, JN., Supplementary cementitious materials origin from agricultural wastes – a review, *Constr Build Mater*, 74, 2015, pp. 176–187
- Chao, J. and Gu, XL., Discussion of “Assessing concrete carbonation resistance through air permeability measurements” by R. Neves et al. [*Construction and Building Materials* 82(2015): 304–309], *Constr Build Mater*, 102, 2016, pp. 913–915
- Chung, CW., Shon, CS., Kim, YS., Chloride ion diffusivity of fly ash and silica fume concretes exposed to freeze–thaw cycles, *Constr Build Mater*, 24, 2010, pp. 1739–1745
- Cizer, O., Navarro, CR., Agudo, ER., Elsen, J. et al., Phase and morphology evolution of calcium carbonate precipitated by carbonation of hydrated lime, *J Mater Sci*, 47, 2012, pp. 6151–6165
- Cyr, M., Lawrence, P., Ringot, E., Efficiency of mineral admixtures in mortars: quantification of the physical and chemical effects of fine admixtures in relation with compressive strength, *Cem Concr Res*, 36, 2006, pp. 264–277
- Dhir, RK., Limbachiya, MC., Mc, Carthy, MJ., Chaipanich, A., Evaluation of Portland limestone cements for use in concrete construction, *Mater Struct*, 40, 2007, pp. 459–473
- Gerard, B. and Marchland, J., Influence of cracking on the diffusion properties of cement-based materials: Part I: influence of continuous cracks on the steady-state regime, *Cem Concr Res*, 30, 2000, pp. 37–43

Guemmedi, Z., Resheidat, M., Chabil, H., Toumi, B., Modeling the influence of limestone filler on concrete: a novel approach for strength and cost, *Jordan J. Civil Eng*, 3, 2009, pp. 158–171

Harada, H., A study on the formation mechanism of various properties of concrete from the pore void structure, Shimizu Corporation research report, 63, 1996, pp. 1–10

Hesami, S., Modarres, A., Soltaninejad, M., Madani, H., Mechanical properties of roller compacted concrete pavement containing coal waste and limestone powder as partial replacements of cement, *Constr Build Mater*, 111, 2016, pp. 625–636

Jawed, I. and Skalny, J., Alkalies in cement: a review: II. Effects of alkalies on hydration and performance of Portland cement, *Cem Concr Res*, 8, 1978, pp. 37–51

JIS A 1148, Method of test for resistance of concrete to freezing and thawing, Japan Industrial Standards Committee, 2010 (in Japanese).

JIS A 1153, Method of accelerated carbonation test for concrete, Japan Industrial Standards Committee, 2013 (in Japanese)

Kamada, E., Frost damage and pore structure of concrete, *Proceeding of the Japan Concrete Institute*, 10, 1988, pp. 51–60 (in Japanese)

Kaufmann, J., Loser, R., Leemann, A., Analysis of cement-bonded materials by multi-cycle mercury intrusion and nitrogen sorption, *J Colloid Interface Sci*, 336, 2009, pp. 730–737

Kayyali, O., Mercury intrusion porosimetry of concrete aggregate, *Mater Struct*, 18, 1985, pp. 259–262

Kumar, P. and Paulo, J., *Concrete microstructure properties and materials*, 2006

Lee, ST., Hooton, RD., Jung, HS., Park, DH., Choi, CS., Effect of limestone filler on the deterioration of mortars and pastes exposed to sulfate solutions at ambient temperature, *Cem Concr Res*, 38, 2008, pp. 68–76

Leemann, A., Moro, F., Carbonation of concrete: the role of CO₂ concentration, relative humidity and CO₂ buffer capacity, *Materials and Structures*. DOI 10.1617/s11527-016-0917-2, 2017

Lim, S. and Mondal, P., Effects of incorporating nanosilica on carbonation of cement paste, *J Mater Sci*, 50, 2015, pp. 3531–3540.

Liu, W., Cui, HZ., Dong, ZJ. et al., Carbonation of concrete made with dredged marine sand and its effect chloride binding, *Constr Build Mater*, 120, 2016, pp. 1–9

Moon, HY., Jung, HS., Kim, JP., Diffusion of chloride ions in limestone powder concrete, *J. Korea Concr. Inst*, 161, 2004, pp. 859–865

Moro, F. and Bohni, H., Ink-Bottle Effect in Mercury Intrusion Porosimetry of Cement-Based Materials, *J Colloid and Interface Sci*, 246, 2002, pp. 135–149

Moura, WA., Goncalves, JP., Lime, Copper slag waste as a supplementary cementing material to concrete, *J Mater Sci*, 42, 2007, pp. 2226–2230

Na, SH., Hama, Y., Taniguchi, M., Katsura, O., Sagawa, T., Zakaria, M., Experimental investigation on reaction rate and self-healing ability in fly ash blended cement mixtures, *J Adv Concr Technol*, 10, 2012, pp. 240–253

Nam, J., Kim, G., Lee, B., Hasegawa, R., Hama, Y., Frost resistance of polyvinyl alcohol fiber and polypropylene fiber reinforced cementitious composites under freeze thaw cycling, *Composites Part B*, 90, 2016, pp. 241–290

Neves, R., Sena, B., Branco, F., De, Brito, J., Castela, A., Montemor, MF., Assessing concrete carbonation resistance through air permeability measurements, *Constr Build Mater*, 82, 2015, pp. 304–309

Özbay, E., Karahan, O., Lachemi, M., Hossain, K., Atis, CD., Dual effectiveness of freezing–thawing and sulfate attack on high-volume slag-incorporated ECC, *Composites B*, 45, 2012, pp. 1384–1390

Pang, B., Zhou, Z.H., Cheng, X. et al., ITZ properties of concrete with carbonated steel slag aggregate in salty freeze-thaw environment, *Constr Build Mater*, 114, 2016, pp. 162–171

Park, H., Jeong, Y., Jun, Y., Strength enhancement and pore-size refinement in clinker-free CaO activated GGBFS systems through substitution with gypsum, *Cem Concr Compos*, 68, 2016, pp. 57–65

Parrott, LJ., Some effects of cement and curing upon carbonation and reinforcement corrosion in concrete, *Mater Struct*, 29, 1996, pp. 164–173

Pipilikaki, P., Katsioti, M., Gallias, JL., Performance of limestone cement mortars in a high sulfates

environment, *Constr Build Mater*, 23, 2009, pp. 1042–1049

Ramezaniapour, A.A. et al., Influence of various amounts of limestone powder on performance of Portland limestone cement concretes, *Cem Concr Compos*, 31, 2009, pp. 715–720

Sagawa, T., Hama, Y., Tsukamoto, Y., Effect of anhydrite and limestone powder on the strength development and hydration of blast-furnace slag cement type A, *Cem Sci and Concr Tech*, 68, 2015, pp. 239–245 (in Japanese)

Shirota, T.K. and Murakami, K., Application study of a small amount mixed material to the blast furnace cement A species for the purpose of improving durability and reducing environmental impact, *Concrete Engineering Proceedings*, 2, 2014, pp. 125–134

Sun, W., Mu, R., Luo, X., Miao, CW., Effect of chloride salt, freeze–thaw cycling and externally applied load on the performance of the concrete, *Cem Concr Res*, 32, 2002, pp. 1859–1864

Thomas, MDA., Shehata, MH., Shashiprakash, SG., Hopkins, DS., Cail, K., Use of ternary cementitious systems containing silica fume and fly ash in concrete, *Cem Concr Res*, 29, 1999, pp. 1207–1214

Tsakiroglou, CD. and Payatakes, AC., A new simulator of mercury porosimetry for the characterization of porous materials, *J. Colloid Interface Sci*, 137, 1990, pp. 315–339

Vocĭka, R., GalleÂ, C., Dubois, M., Lovera, P., Mercury intrusion porosimetry and hierarchical structure of cement pastes theory and experiment, *Cem Concr Res*, 30, 2000, pp. 521–527

Wachi, MH., Ryo, KN., TsujiMasaru, JR., A study on the fundamental properties of concrete using ground granulated blast furnace slag-rich cement, *Takenaka technology research report*, 67, 2011, pp. 1–6

Zhang, P., Zhao, T., Jin, Z., Influence of freezing and thawing on carbonation of concrete materials, *Sichuan Building Science*, 34, 2008, pp. 66–68 (in Chinese)

Zhang, W.Y., Zakaria, M., Hama, Y., Influence of Aggregate Materials Characteristics on the Drying Shrinkage Properties of Mortar and Concrete, *Constr Build Mater*, 49, 2013, pp. 500–510

Zhang, WY., Hama, Y., Na, SH., Drying shrinkage and microstructure characteristics of mortar incorporating ground granulated blast furnace slag and shrinkage reducing admixture, *Constr Build Mater*, 93, 2015, pp.

267–277

Zhang, Y., and Ye, G., Effect of limestone powder on microstructure of ternary cementitious system, American Society of Civil Engineers, 2012, pp. 224–233

Zhao, J., Cai, GC., Gao, DY., Study on bonding characteristic of mixed-type chloride ion in sulphoaluminate cement, Key Eng Mater, 2011, pp. 698–702

Zhao, J., Cai, GC., Zhao, S., Influences of freeze–thaw cycle and curing time on chloride ion penetration resistance of Sulphoaluminate cement concrete, Constr Build Mater, 53, 2014, pp. 305–311

Zomerén, AV., Changes in mineralogical and leaching properties of converter steel slag resulting from accelerated carbonation at low CO₂ pressure, Waste Manag, 31, 2011, pp. 2236–2244

CHAPTER 5

CURING AGE AND CARBONATION CHARACTERISTICS INCORPORATING BFS

5.1 Overview

The Ca/Si of C-S-H had an effect on the properties of cement, and the blended BFS had decreasing Ca/Si ratio of C-S-H in the cement composite. Many studies have tried to resolve the characteristics of the Ca/Si ratio of C-S-H. Tanaka et al. (2009) reported that the density of C-S-H was proportional to the Ca/Si ratio, and it has no relationship with the environment of C-S-H hydration. Ishida et al. (2013) found that the Ca/Si ratio had no effect on the carbonation speed. Suda et al. (2010) indicated that the low Ca/Si ratio specimen had high specific surface area compared with other specimens. Hargis et al. (2014) found that the vaterite and calcite reacted with monosulfoaluminate.

Many researchers have studied the effect on compressive strength and durability due to carbonation of cement. A lot of research (Ishida et al., 2011; Saeki et al., 1990; Ishida et al., 2012; Li et al., 2009) has drawn attention to carbonation in concrete, with particular focus on pore structure change after carbonation. Phung et al. (2015) evaluated how carbonation induced change in the microstructure and decreased the water permeability. Borges et al. (2010) observed that durability increased with increased curing temperature; post carbonation saw reduced porosity and increasing density of the cement paste. Rostami et al. (2012) noted that carbonation increased strength and durability.

Therefore, in this chapter, in order to obtain the applicable pore structure involved in the carbonation of BFS blended cementitious composite, the effects of pore structure on the carbonation of paste samples was further analyzed by statistical investigation method for MIP, XRD analysis, and thermal analysis. Moreover, the analysis of MIP was applied to identify the pore structure change, and the analysis of the XRD was investigated to identify the chemical composition of cement paste, and thermal analysis indicated the amount of calcium hydroxide and calcium carbonate. The experimental program in this study is designed to investigate the carbonation effect in various BFS blended pastes. Through the investigations, the obtained results from this study provide valuable information regarding cement durability, offering a better understanding of the carbonation performance of BFS cementitious composites.

5.2 Experimental program

5.2.1 Experimental materials and sample preparation

The cement used in this experiment was a kind of ordinary Portland cement (OPC). The cement was denoted as N, with a density of 3.16 g/cm³. In addition, BFS with a fineness of 4000 cm²/g (density of 2.91 g/cm³) was used to replace cement at 15%, 45%, and 65% by weight of cement. All paste specimens were cast into ϕ 50×100mm plastic molds with a water-to-binder ratio (W/B) of 0.65 without any chemical admixture. The mixture proportions of paste and the dosage of mineral admixtures are shown in Table 5.1. The mixture was cured after seven hours. Sealed curing was utilized with this sample for three kinds of curing conditions (water curing, air curing, and accelerate carbonation) at 20°C.

Table 5.1 mixture design of paste samples

	W/C	Replacement ratio (%)	
		OPC	BFS
N	0.65	100	-
BA		85	15
BB		55	45
BC		35	65

5.2.2 Experimental method

5.2.2.1 Mercury intrusion porosimetry

The pore size distribution was determined by the mercury intrusion porosimetry (MIP) method, which is a method commonly used to measure the pore size distribution in cement-based materials (Kayyali, 1985; Zhang et al., 2013; Zhang et al., 2015). The surface tension of the mercury and the mercury density were 0.480 N/m and 13.546 g/ml, respectively, assuming a contact angle of 140°. The samples for measurements were taken from carbonated areas of the mortar bars after exposure at 5% CO₂ in the control chamber. The MIP technique requires that hardened cement-based materials should be thoroughly treated to remove water and then be

evacuated prior to testing. After the specified curing time, the mortar prisms were cut into 5mm cubic samples. The samples were subsequently dried to stop the cement hydration reaction with acetone, followed by a D-drying pretreatment. The pore size of the samples was measured using the Autopore Master33 porosimeter in which a hydraulic pump was used to generate the pressure, and a contact sensor was used to measure the mercury volume. It has been sufficiently demonstrated that the effect of the sample mass and size on the pore result is relatively small from the reference (Karen et al., 2015). Moreover, the MIP procedure measurement highly depends on the equipment. Based on the manufacturer of the Autopore Master33 porosimeter equipment, the accuracy of this equipment is in the range of 0–1500MPa, and is $\pm 0.11\%$ fso (full scale output) and the linearity in the range from 0 to maximum pressure is $\pm 0.05\%$ fso, which also reveals that the measurement result in this study is reliable.

5.2.2.2 X-ray diffraction

An analysis of the hydration was conducted using the XRD method. To assess various cement hydration products, the XRD and ignition loss characteristics were measured for samples which were 5mm³ in size. For each aging condition, acetone replacement was carried out to stop the hydration reaction, and the samples were dried before the measurements.

The drying condition involved drying for 24 hours at D-dry before the samples were measured. Powder was used for the XRD and ignition loss measurements, and the samples were made into powder form using a vibration mill. Then, the sample underwent XRD measurement. For the XRD measurement, a semiconductor-type high-speed detector was used with CuK α as a target, a tube voltage of 45kV, a tube current of 40mA, a 2θ scan range of 5–70deg, and a step width of 0.02 degrees.

5.2.2.3 Thermal analysis

These samples were using a powder type paste; heating rate was 30°C–1000°C (20°C/min) under a nitrogen atmosphere. The weight loss from TG was used to investigate the amounts of calcium hydroxide (CH) and calcium carbonate (CC), respectively. It was identified that in the paste by TG measurement from calcium

hydroxide, the CO₂ loss in the carbonation range 600~750°C was converted into a calcium hydroxide loss, and the calcium hydroxide was calculated from the dihydroxylation range 400~500°C. Borges et al. (2010) suggested the amount of calcium hydroxide and calcium carbonation. The amount of carbonation from CH and C-S-H was calculated from the amounts of water curing and after carbonation by using Borges equation.

5.3 Experiment result and discussion

5.3.1 Characteristics of pore structure after carbonation

5.3.1.1 Pore volume of log differential results

Figure 5.1 shows the result for the pore size distribution of change in BFS blended paste samples at 4 weeks of water curing. Figure 5.1 (a) shows the pore change result for the N samples carbonation (13w), air curing (13w), and water curing (4w), respectively. It can be observed that the peak of the pore value shifts toward smaller pore increasing water curing age, and that the pore volume of the small pores (diameters of approximately 80nm) decreases as the air curing progresses, indicating that the pore structure undergoes change according to curing age. In addition, the post carbonation of the paste samples tends to decrease compared with the air-cured samples. It is recommended that the effect of the carbonation process should be considered in the durability of concrete. Figure 5.1 (b), (c), and (d) shows the pore change result for the BFS blended paste samples. It can be seen that the peak of the pore value is higher than N paste samples at low pore diameter, and that the pore volume of the small pores decreases as carbonation progresses, indicating the changes that the pore structure undergoes. Figure 5.2 shows the result for the pore size distribution of change in BFS blended paste samples at 2 weeks of water curing. Figure 5.2 (a) shows the pore change result for the N samples carbonation (6w), air curing (6w), and water curing (2w), respectively. In the case of the N samples at 2 weeks of water curing, it can be found that the peak of the pore value lower than N-4w samples occurs at low pore diameter, and the peak of the pore value is higher than N-4w samples at high pore diameter. Figure 5.2 (b), (c), and (d) shows the pore change result for the BFS blended paste samples. However, in the case of 2 weeks of water curing, it can be seen that the low pore diameter is lower than BFS blended paste samples at 4 week curing age. However, in the case of the carbonation samples, experimental investigation revealed that the paste

mixture with water curing at 2 weeks of age showed similar pore size distribution of change compared to water curing in the 4 week paste mixture. It is concluded that the same results for pore size distribution were also found post carbonation.

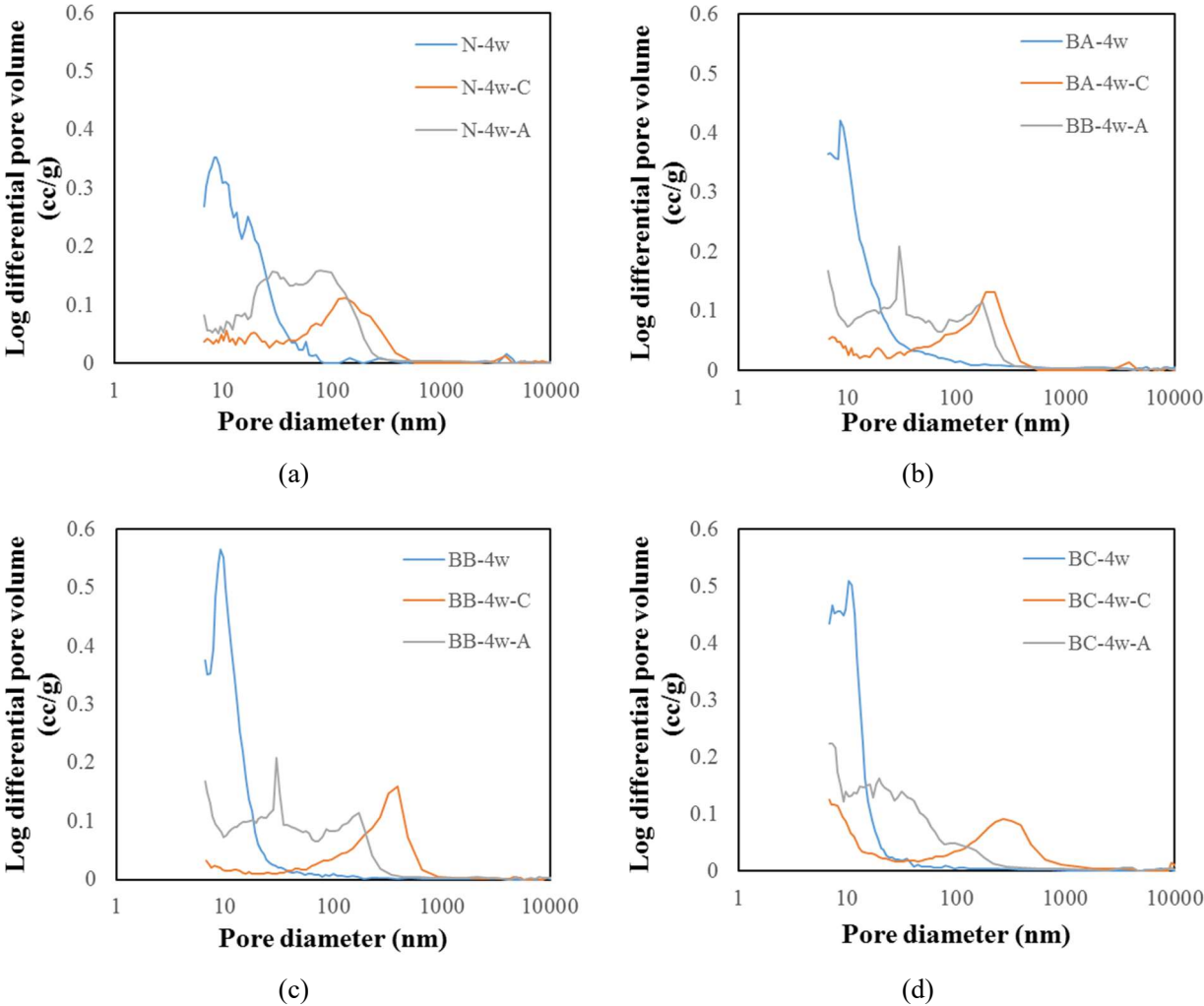
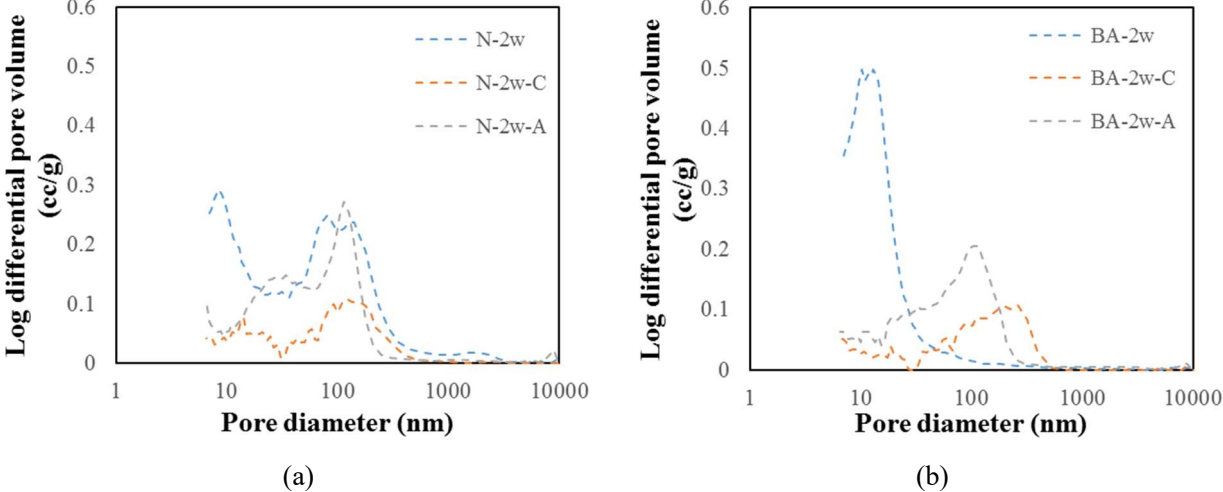
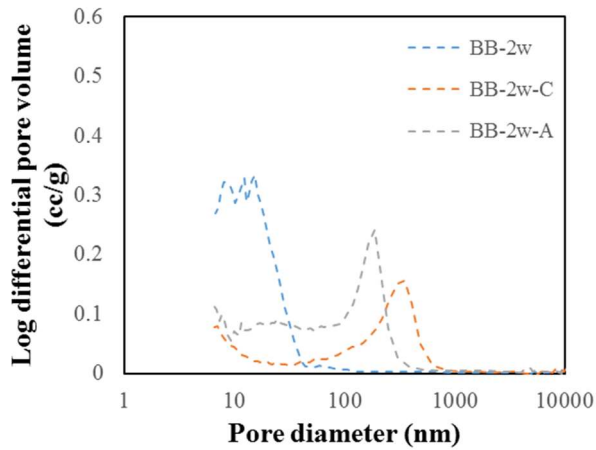
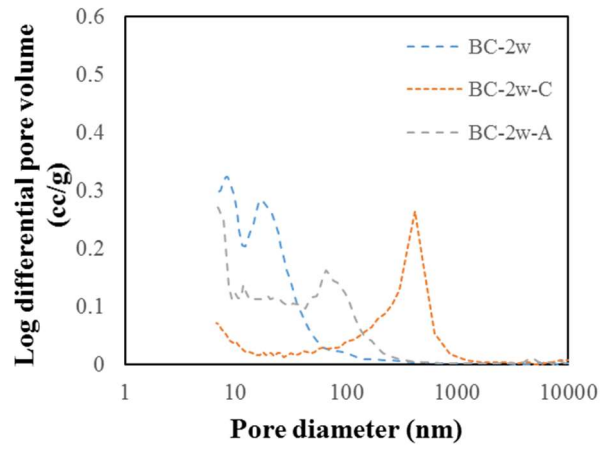


Fig. 5.1 Pore size distribution of the paste with different replacement ratio of BFS at curing ages 4 weeks.





(c)

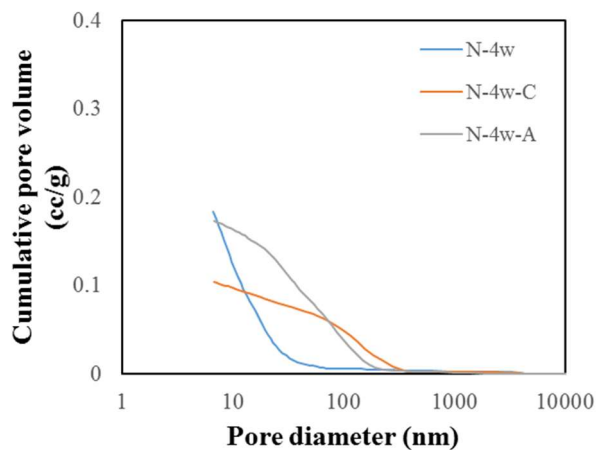


(d)

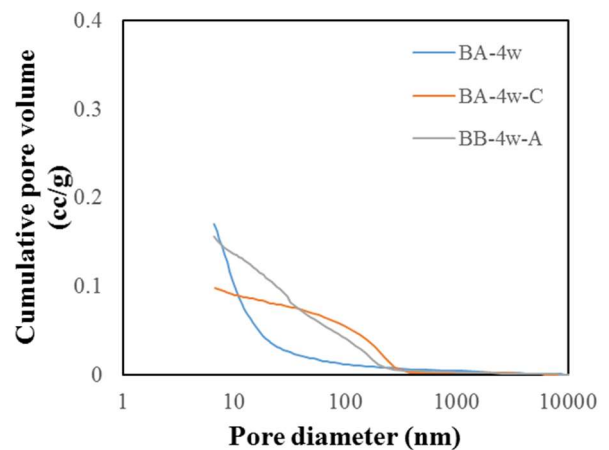
Fig. 5.2 Pore size distribution of the paste with different replacement ratio of BFS at curing ages 2 weeks.

5.3.1.2 Cumulative pore volume results

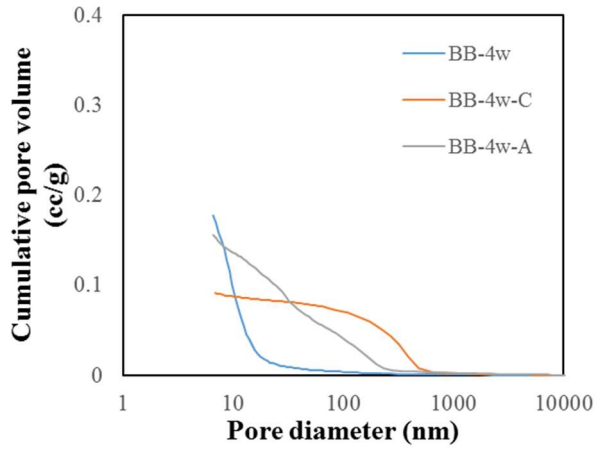
Figure 5.3 shows the result for the cumulative pore volume in the BFS blended paste samples at 4 weeks of water curing. Figure 5.3 shows the cumulative pore volume result for the samples carbonation (13w), air curing (13w), and water curing (4w), respectively. Figure 5.4 shows the result for the cumulative pore volume in BFS blended paste samples at 2 weeks of water curing, and the samples carbonation (6w), air curing (6w), and water curing (2w), respectively. In the case of the N-4w paste samples, the decreasing cumulative pore volume is lower than 2 weeks of water curing. It is well-known that the pore volume of cement-based composite depends on cement hydration. This finding is in good agreement with in the BFS blended paste samples. In fact, a decrease occurs in the pore volume after carbonation, implying a negligible effect on water curing.



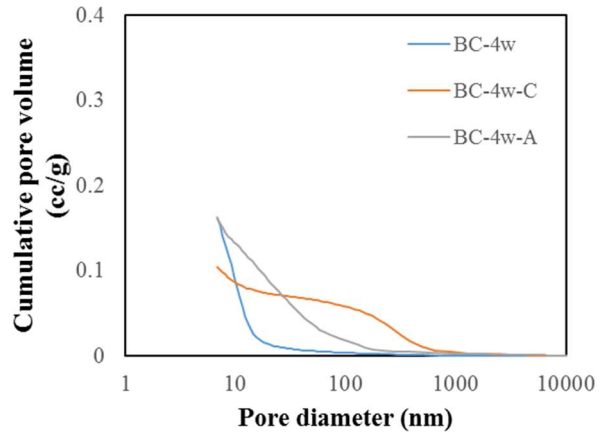
(a)



(b)

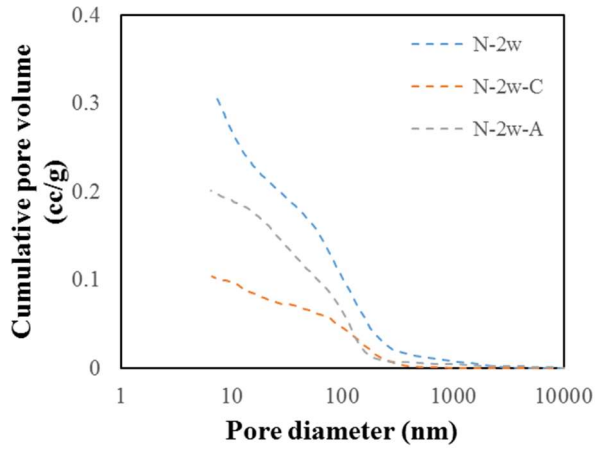


(c)

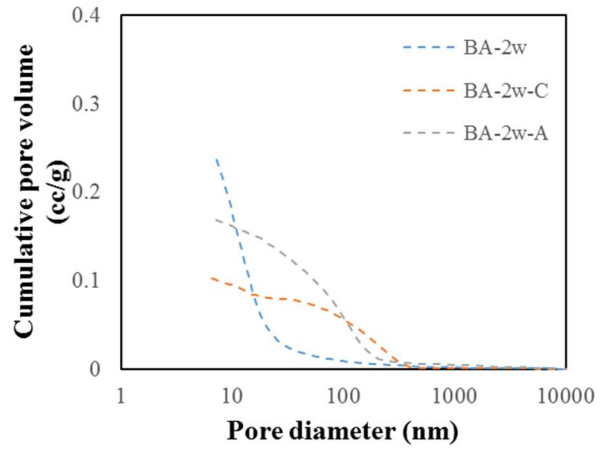


(d)

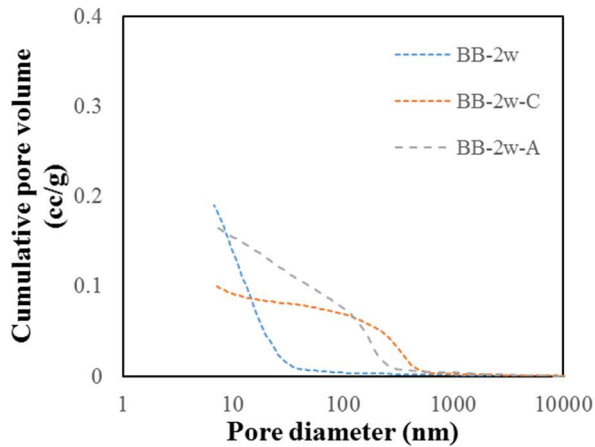
Fig. 5.3 Cumulative pore volume of the paste with different replacement ratio of BFS at curing ages 4 weeks.



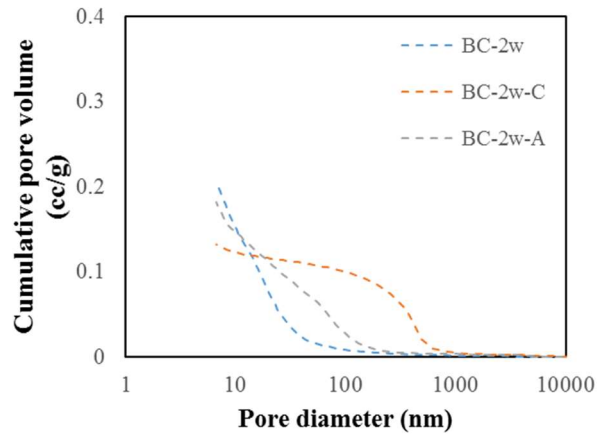
(a)



(b)



(c)



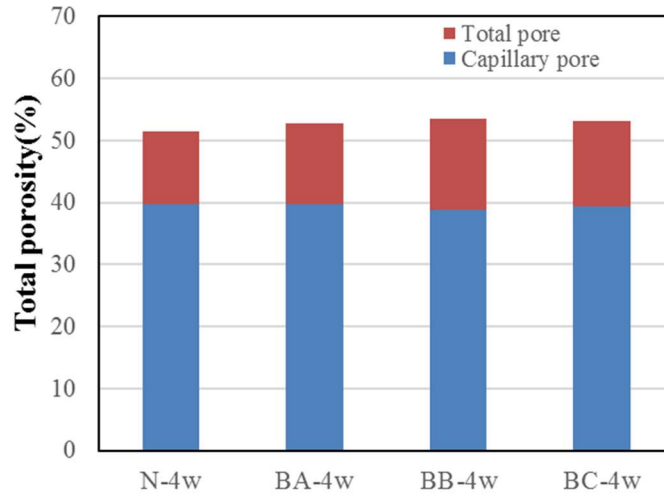
(d)

Fig. 5.4 Cumulative pore volume of the paste with different replacement ratio of BFS at curing ages 2 weeks.

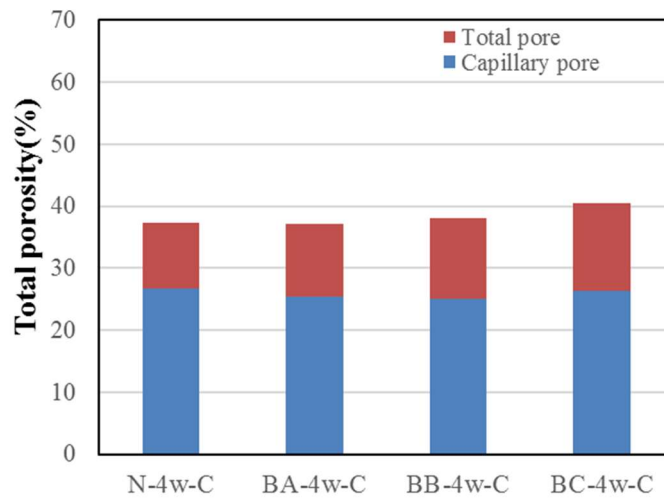
5.3.1.3 Total porosity results

Figure 5.5 shows the result for the total porosity in BFS blended paste samples at 4 weeks of water curing. Figure 5.5 shows the total porosity result for the samples carbonation (13w), air curing (13w), and water curing (4w), respectively. Figure 5.5 (a) shows the total porosity result with respect to the different BFS replacement ratios after 4 weeks of water curing. It can be revealed that the total porosity of the paste samples tends to increase with the increasing BFS replacement ratio due to the fact that the proportion of cement content decreases and the reaction rate of BFS is delayed (Çetin et al., 2016; Barnett et al., 2006; Boukendakdji et al., 2012; Miyazawa et al., 2014; Özbay et al., 2016; Jaya Prithika & Sekar, 2016). Moreover, in the case of the paste samples after

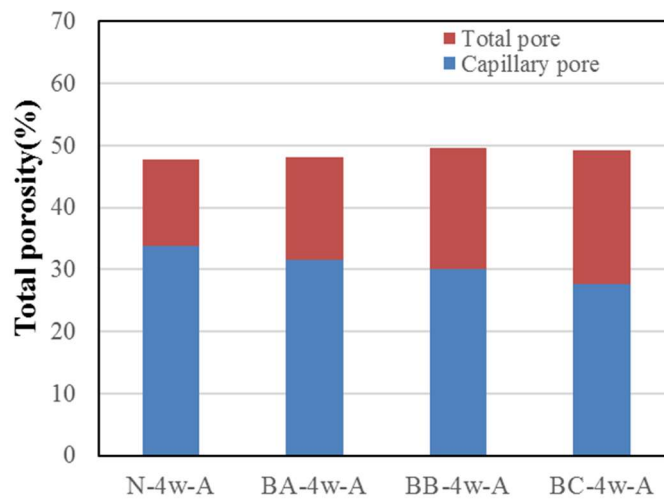
carbonation, as shown in Fig. 5.5 (b), the total porosity was reduced as the carbonation, which shows the same tendency as the BFS cement paste. It is the same results of cumulative pore volume. Figure 5.5 (c) shows the total porosity result after air curing. The capillary pore decreased with increasing BFS replacement ratio. This is for the same reason as the water curing result. Figure 5.6 shows the result for the total porosity in the BFS blended paste samples at two weeks of water curing. Figure 5.6 shows the total porosity result for the samples carbonation (6w), air curing (6w), and water curing (2w), respectively. Figure 5.6 (a) shows the total porosity result with respect to the different BFS replacement ratios after water curing for 2 weeks. It can be seen that the amount of total porosity increased as BFS replacement ratio increased. Figure 5.6 (b) shows the total pore result of the after carbonation paste samples, it was observed that the total porosity was similar to that of Fig. 5.5 (b).



(a)

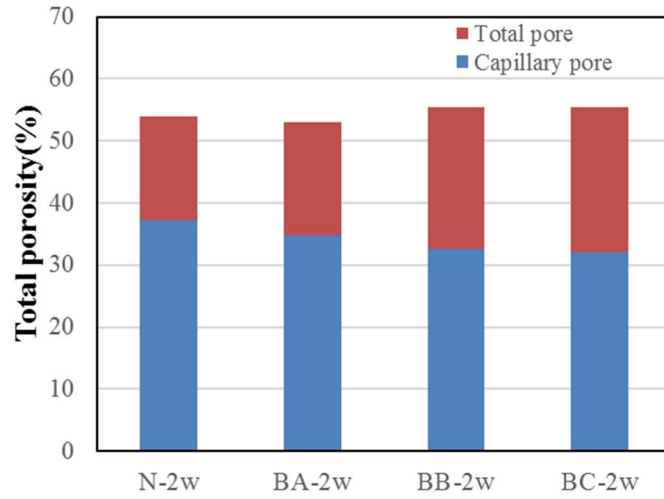


(b)

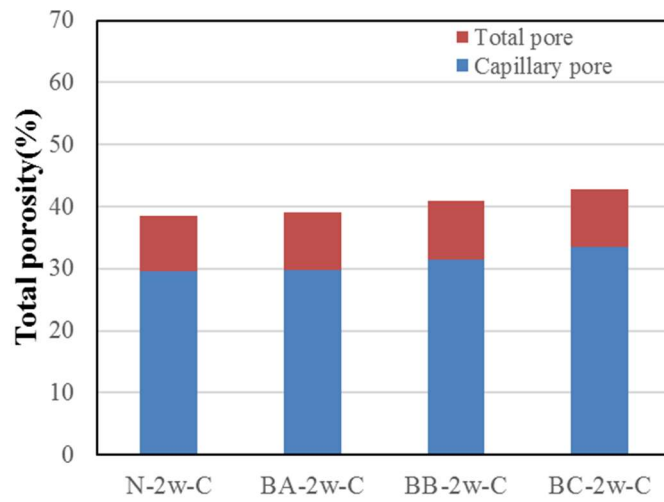


(c)

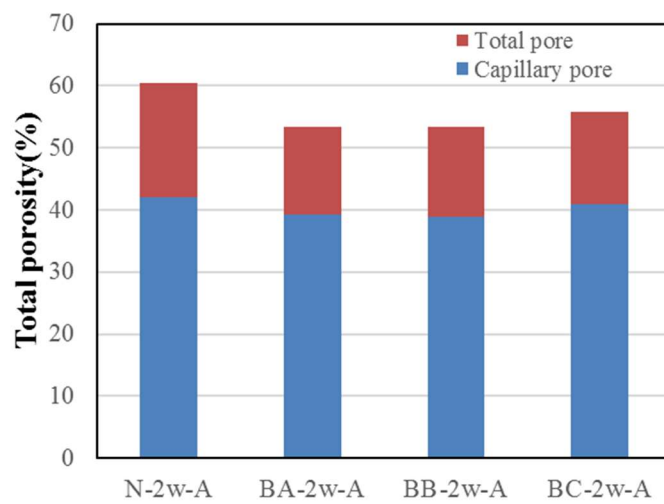
Fig. 5.5 Total porosity of the paste with different replacement ratio of BFS at curing ages 4 weeks.



(a)



(b)



(c)

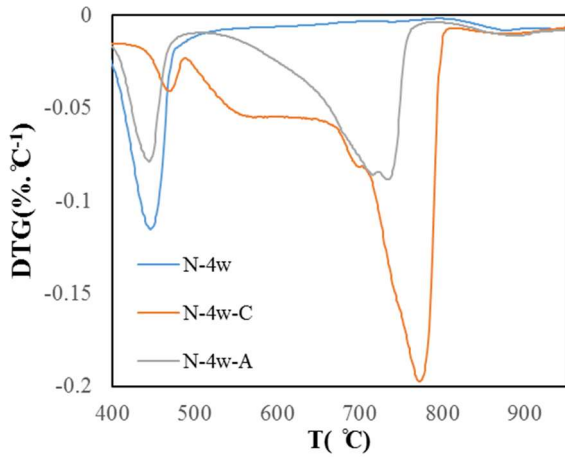
Fig. 5.6 Total porosity of the paste with different replacement ratio of BFS at curing ages 2 weeks.

The tendency of pore structure of each compound was obtained by MIP and total porosity results. It can be summarized as follows: the pore value could shift toward larger pores by the carbonation, and the total porosity of the carbonated samples is found to decrease.

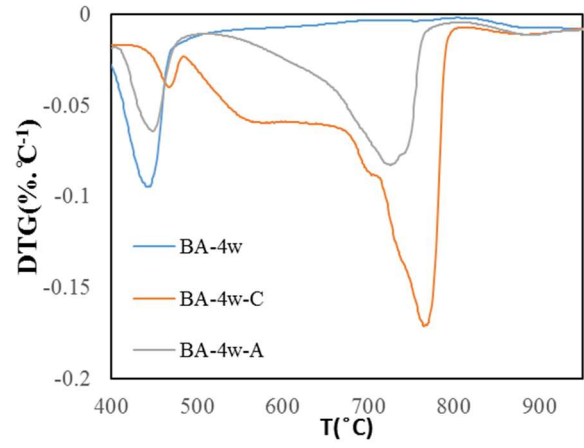
5.3.2 Characteristics of amount of calcium hydroxide and calcium carbonate after carbonation

5.3.2.1 DTG curve of calcium hydroxide and calcium carbonate results

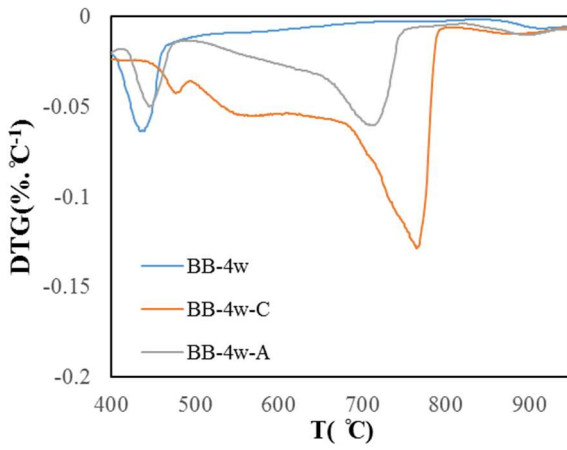
Figure 5.7 shows the DTG result for the thermal analysis in BFS blended paste samples at 4 weeks of water curing. Figure 5.7 shows the DTG result for the thermal analysis at the curing age of 2 weeks. The peaks shown from the DTG curve, for the investigation of carbonation and calcium hydroxide. It could be found that the calcium hydroxide shows decreased peaks between 400°C~500°C. It was also found that the carbonation from 600°C~800°C resulted in decreased peaks in this study. In the case of the 4 week water curing samples (4w), it can be seen that the peaks of calcium hydroxide tend to decrease with increasing BFS replacement ratio. It is known that the BFS blended samples showed slow hydration of cement. Moreover, the peaks of calcium hydroxide decreased with increased BFS replacement ratio. This decrease affected the peaks of the calcium carbonate result. In the case of the after carbonation paste samples (4w-C), the results of the peaks of calcium carbonate show an increase with the decrease of calcium hydroxide. This is because the products of calcium carbonate depended on the amount of calcium hydroxide. Figure 5.8 shows the DTG result for the thermal analysis in the BFS blended paste samples at 2 weeks of water curing. It can be seen that regardless of the types of paste samples, the relationship between the peaks of calcium hydroxide and calcium carbonate is similar to the peak values, and these values were almost the same compared to the 4 week water-cured samples.



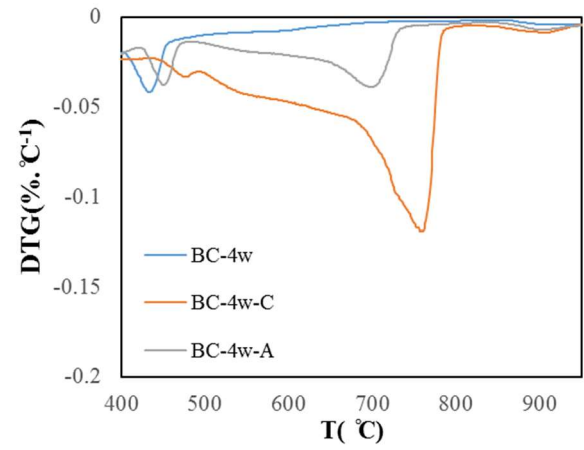
(a)



(b)

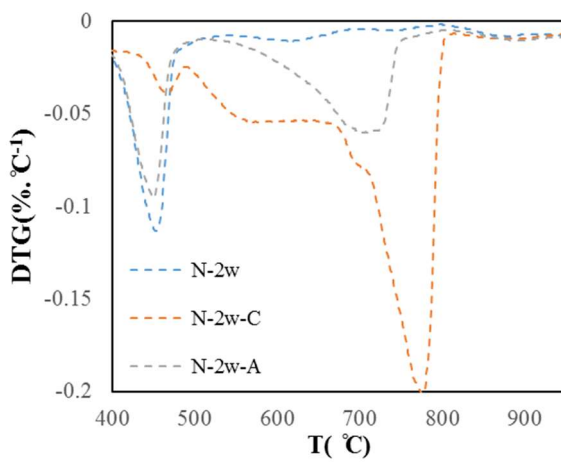


(c)

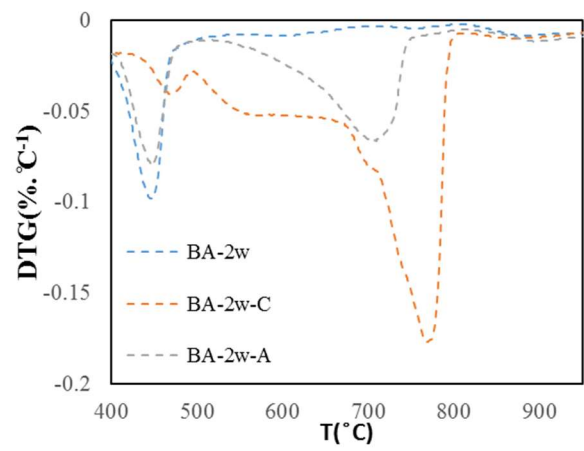


(d)

Fig. 5.7 DTG curve of the paste with different replacement ratio of BFS at curing ages 4 weeks.



(a)



(b)

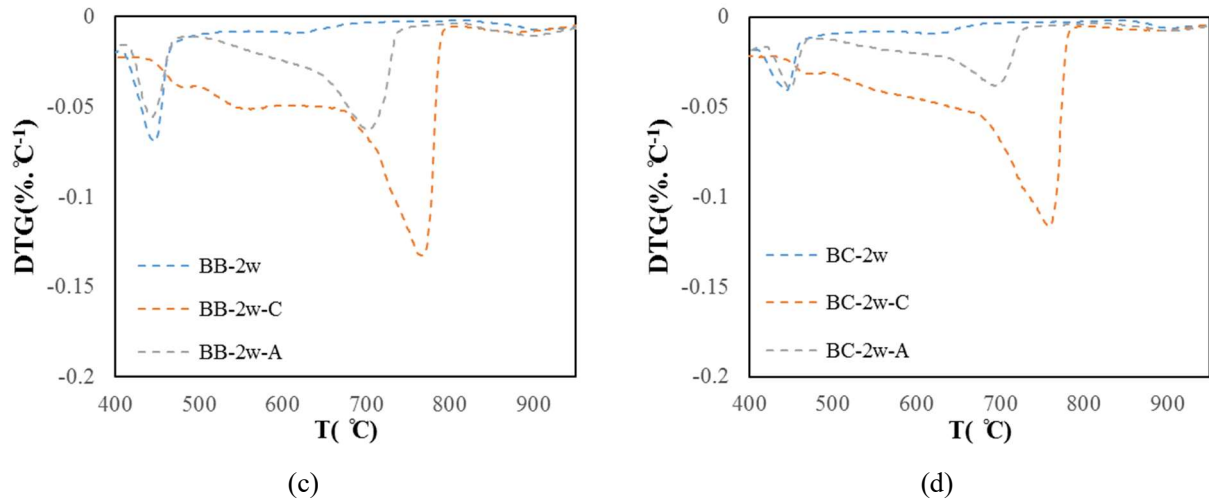
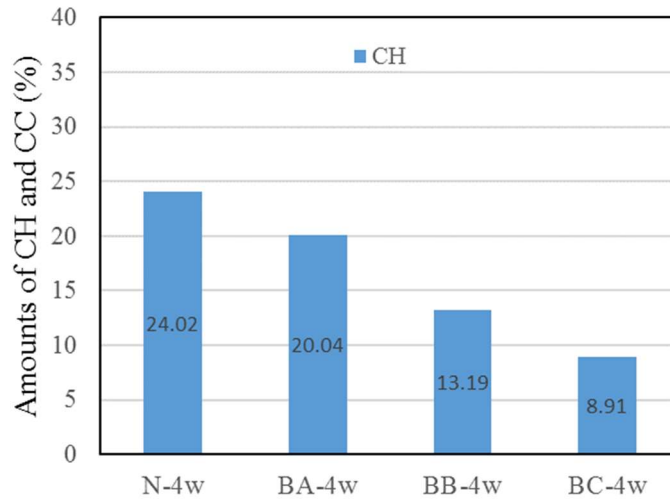


Fig. 5.8 DTG curve of the paste with different replacement ratio of BFS at curing ages 2 weeks.

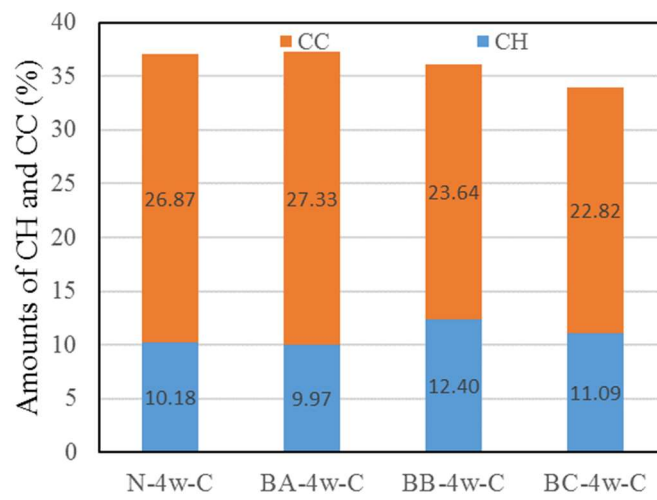
5.3.2.2 Amount of calcium hydroxide and calcium carbonate

Figure 5.9 shows the results of the amount of calcium hydroxide (CH) and calcium carbonate (CC) for the thermal analysis in the BFS blended paste samples at 4 weeks of water curing. Figure 5.9 (a) shows the results of the amount of CH and CC after water curing, and for BFS blended cement paste samples with replacement ratios varying at 15%, 45%, and 65% by weight of cement. It can be revealed that the CH amount of the paste samples tends to decrease with increased BFS replacement ratios due to the fact that the proportion of the reaction rate of BFS was slow and the cement content decreases. Figure 5.9 (b) shows the result of after carbonation. In the case of the BFS blended samples, the CH amount was similar with the N samples in this study. Figure 5.9 (c) shows the result of 13 weeks of air curing in order to investigate the relationship between the curing age and

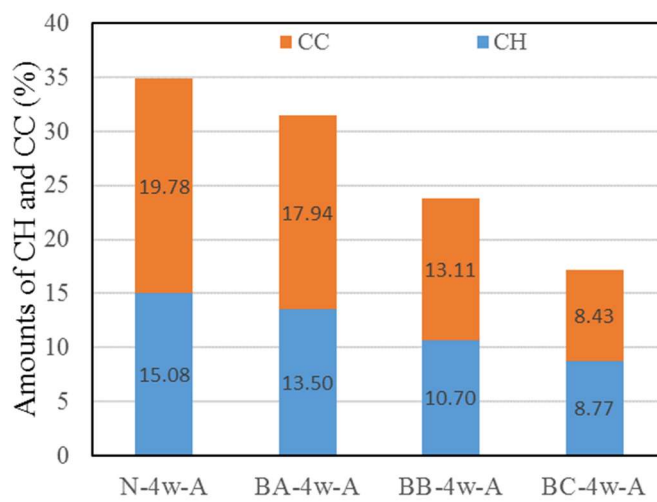
carbonation. In the results, the ratio amount of CH and CC changes depending on curing age. In addition, there is a similar trend with the total amount of CH and CC with water curing samples. Figure 4.10 shows the results of the amount of CH and CC for the thermal analysis in the BFS blended paste samples at two weeks of water curing. It shows a trend similar to the four week curing age samples.



(a)

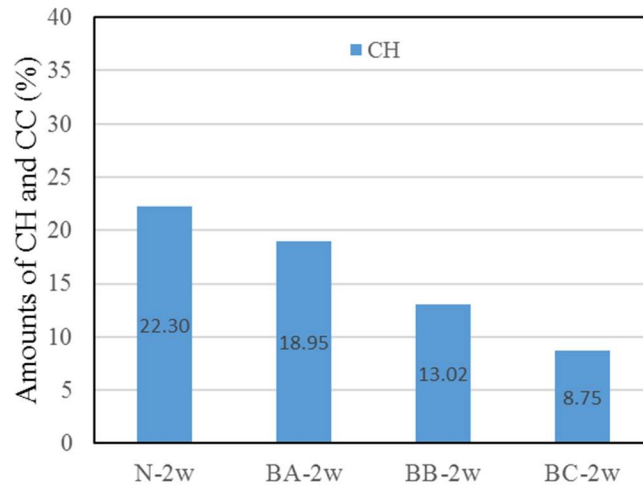


(b)

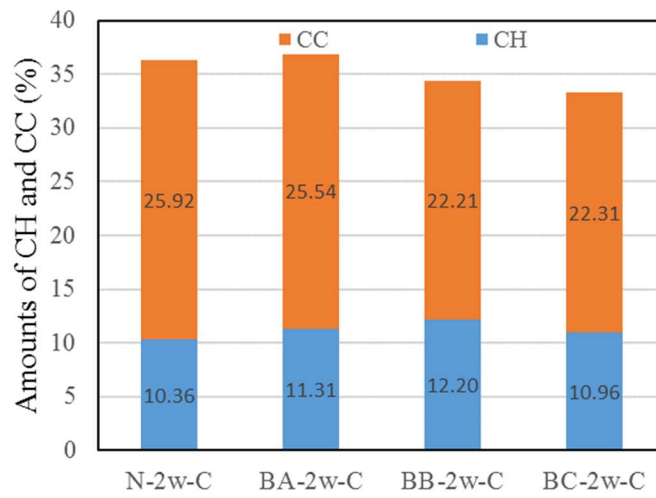


(c)

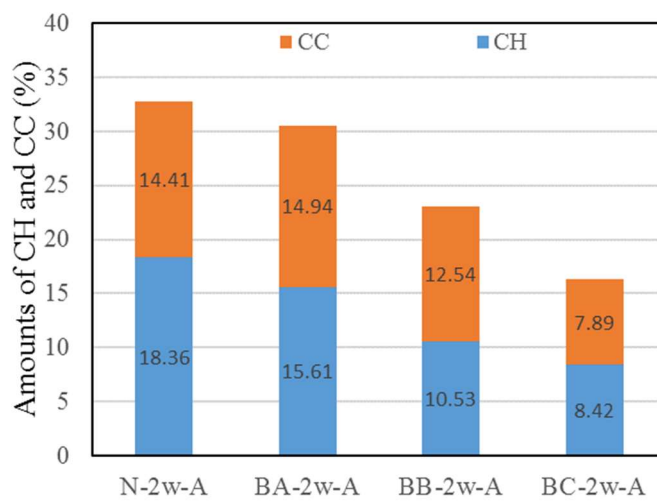
Fig. 5.9 Amount of CH and CC of the paste with different replacement ratio of BFS at curing ages 4 weeks.



(a)



(b)

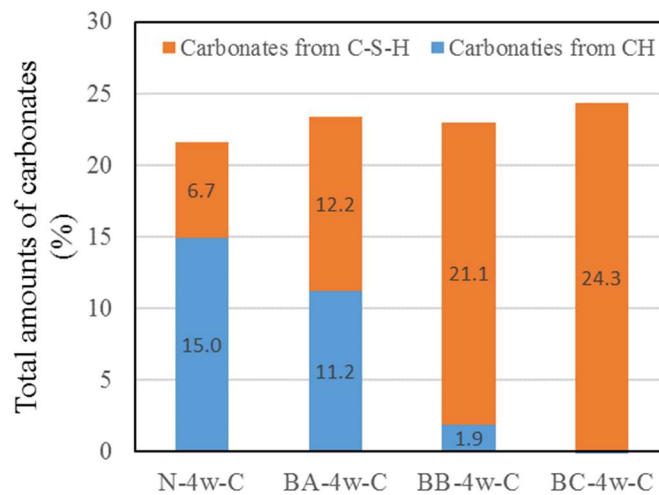


(c)

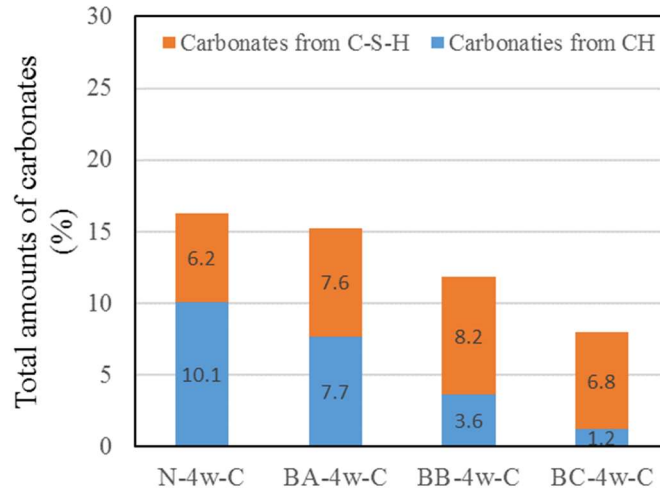
Fig. 5.10 Amount of CH and CC of the paste with different replacement ratio of BFS at curing ages 2 weeks.

5.3.2.3 Carbonation of CH and C-S-H

Figures 5.11 and 5.12 show the carbonation of CH and C-S-H result in BFS blended paste samples at 4 weeks and 2 weeks of water curing. These figures show the extent of carbonation of CH and C-S-H in air curing and after carbonation paste samples, respectively. Figures 5.11 (a) and 5.12 (a) show the calculated results between water curing and after carbonation paste samples. The CH did not carbonate significantly in the BC samples, probably due to the higher amount of CH present in the N samples. It shows a similar trend to the 2 week water-cured samples in Fig 5.12 (a). In addition, the amount of carbonates from C-S-H increases with BFS blended rate increase. Most of the carbonates formed in these samples were from the C-S-H in the BC-4w-C and the BC-2w-C paste samples. In the BB, the BC of after carbonation samples, the CH amount was extremely low due to additional hydration, and the total carbonation was lower, due to the lower total porosity. The obtained results agree with those in previous studies reported in the literature (Borges et al., 2010).



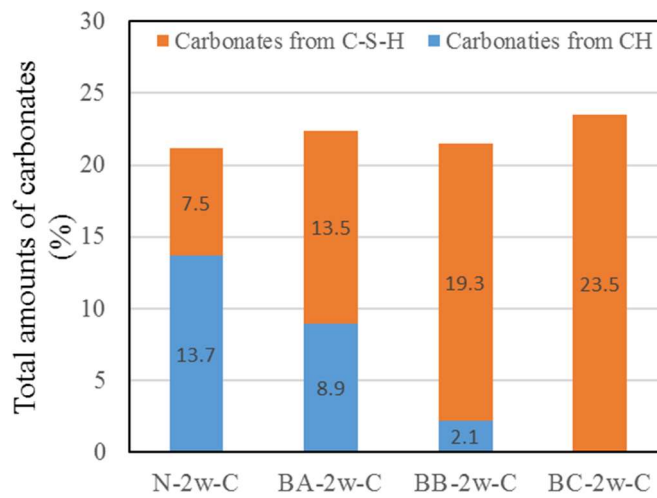
(a)



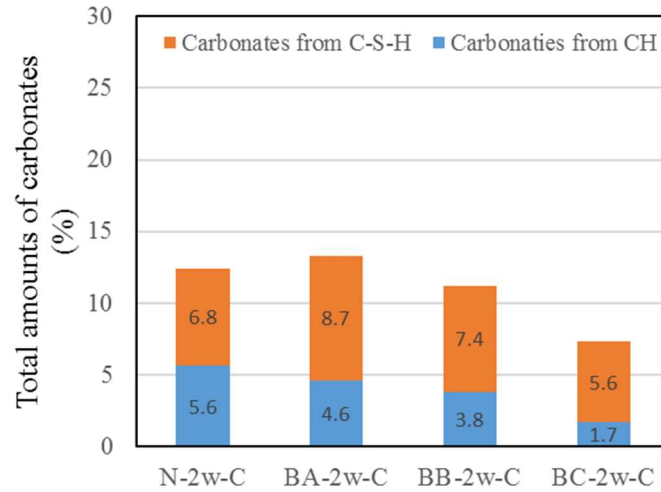
(b)

Fig. 5.11 Carbonation of CH and C-S-H of the paste with different replacement ratio of BFS at curing ages 4 weeks.

Figures 5.11 (b) and 5.12 (b) show the calculated results of the amount of carbonation from CH and C-S-H between the water-cured and air-cured paste samples. It can be seen that the total carbonation amount of the paste samples tends to decrease with increasing BFS replacement ratio. In the carbonation amount of C-S-H, there is little difference. However, when the replacement rate of BFS was increased, the carbonation amount from CH decreased.



(a)



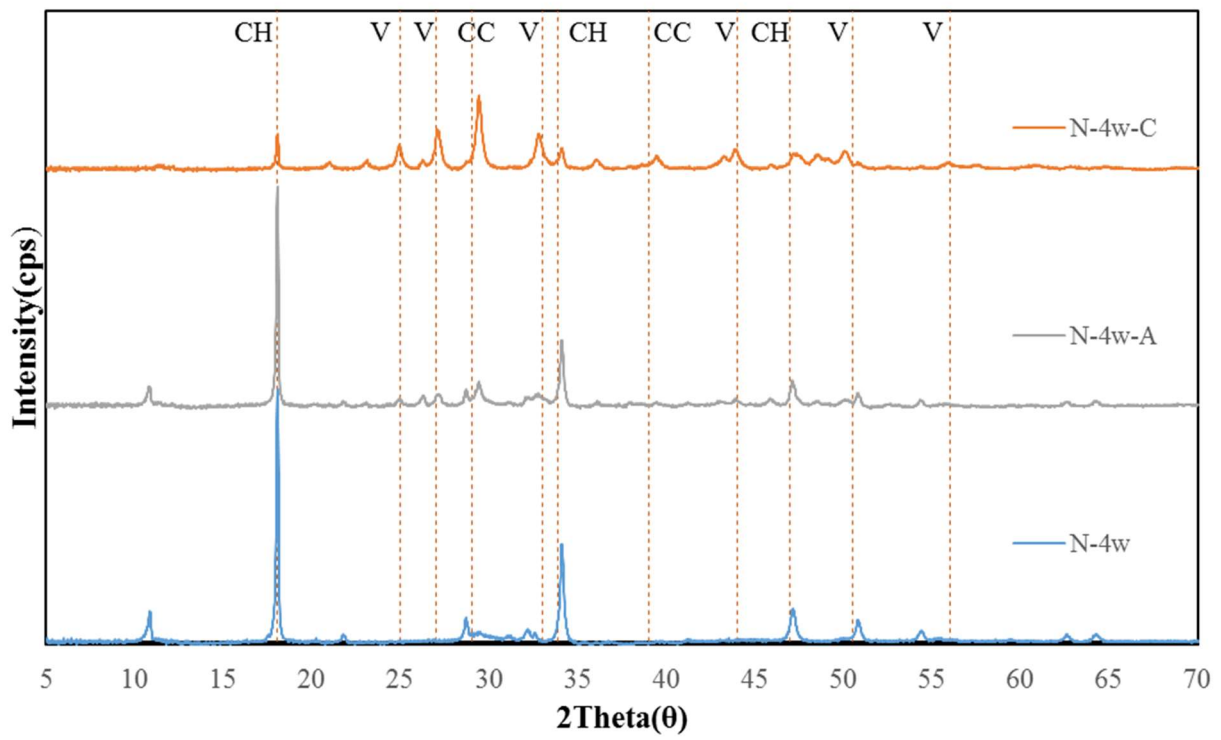
(b)

Fig. 5.12 Carbonation of CH and C-S-H of the paste with different replacement ratio of BFS at curing ages 2 weeks.

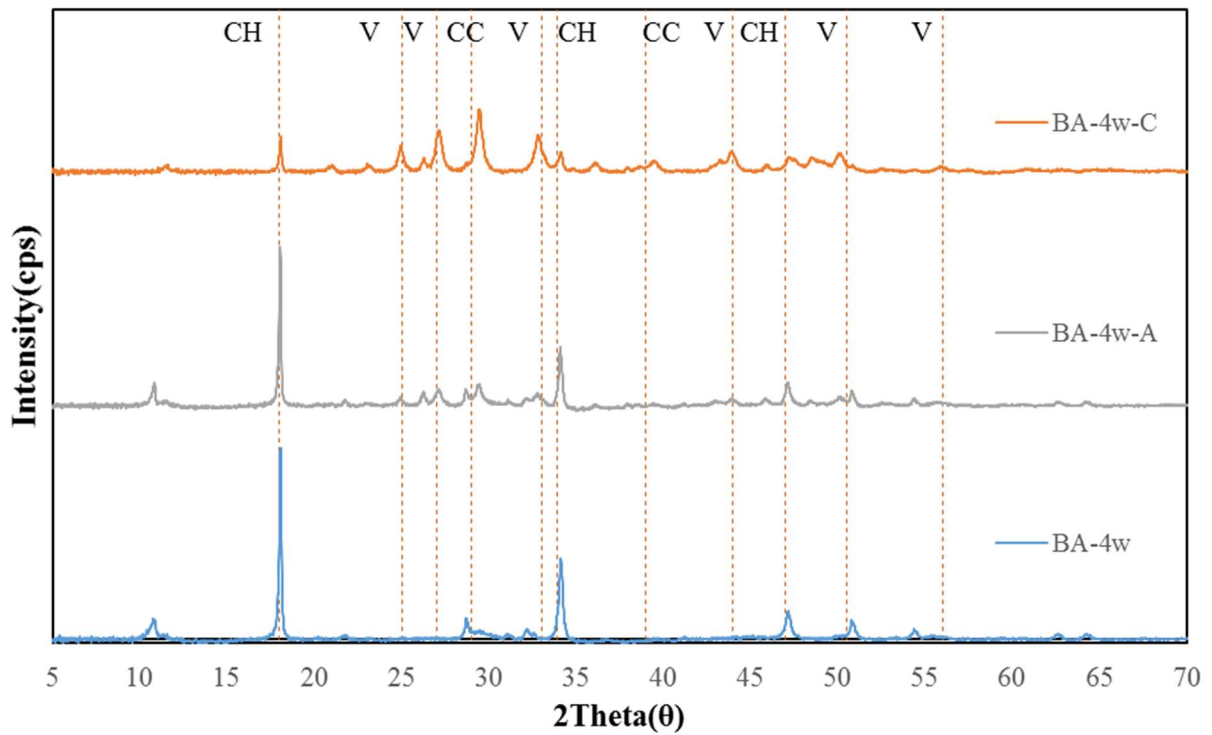
5.3.3 Characteristics of chemical properties according to carbonation

5.3.3.1 X-ray diffraction result

Figures 5.13 and 5.14 show the results of the effects of the crystalline phases in hardened cement paste of BFS replacement ratios 15%, 45%, and 65% for various cements. The XRD data for the paste samples were collected for water curing, air curing, and after carbonation. A calcium hydroxide ($\text{Ca}(\text{OH})_2$; CH, peaks of $2\theta=18, 33.9, 47$) peak is found in all cement paste samples. However, with the blended BFS samples, the peaks of CH phase decreased compared to the N samples. In addition, it can be seen that the intensity of the CH phase peaks tends to decrease with an increase of BFS replacement ratio. The CH was still present in the after carbonation samples. The vaterite (V, peaks of $2\theta=25, 27, 33, 44, 50.5, 56$) and calcite (C, peaks of $2\theta=29, 39$) were the main phase of calcium carbonate, and only vaterite and calcite were formed as carbonated products. The vaterite phase peaks tend to increase with BFS replacement ratio increase. It has been indicated that the product of vaterite phase peaks increased when BFS was used. The intensity of vaterite phase peaks is dependent on the BFS replacement ratio.



(a)



(b)

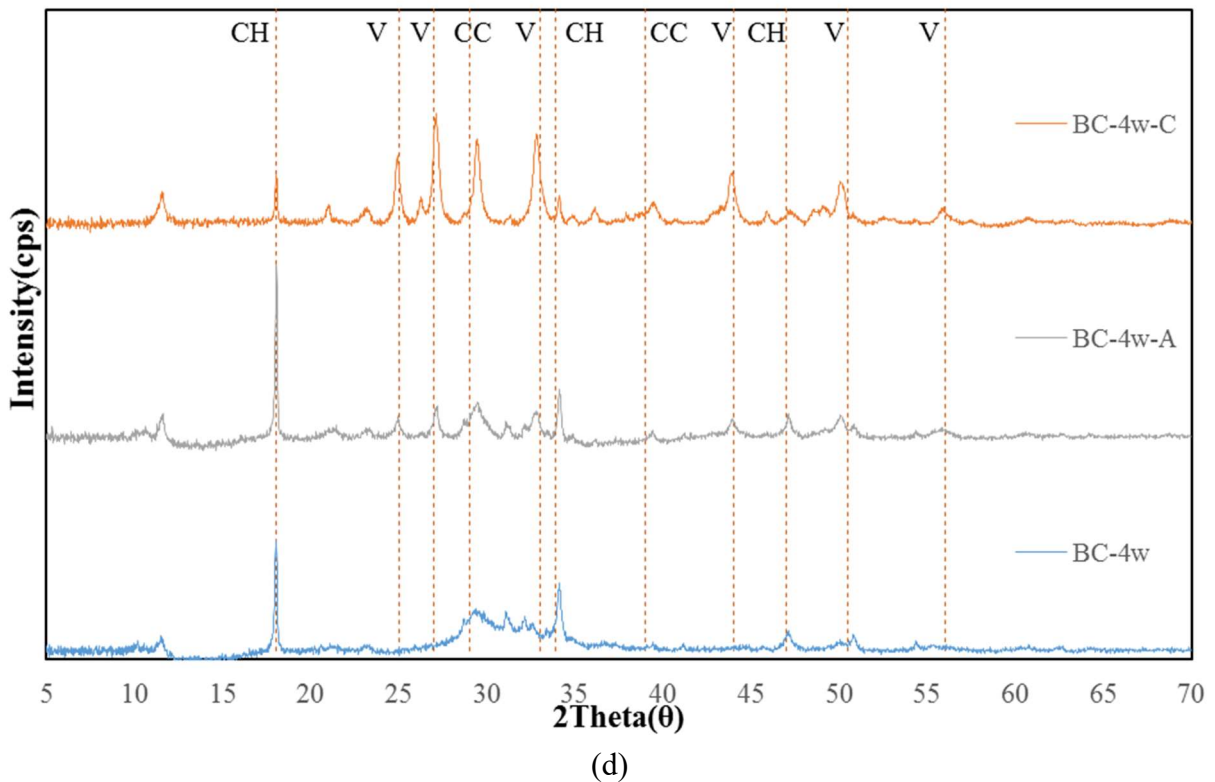
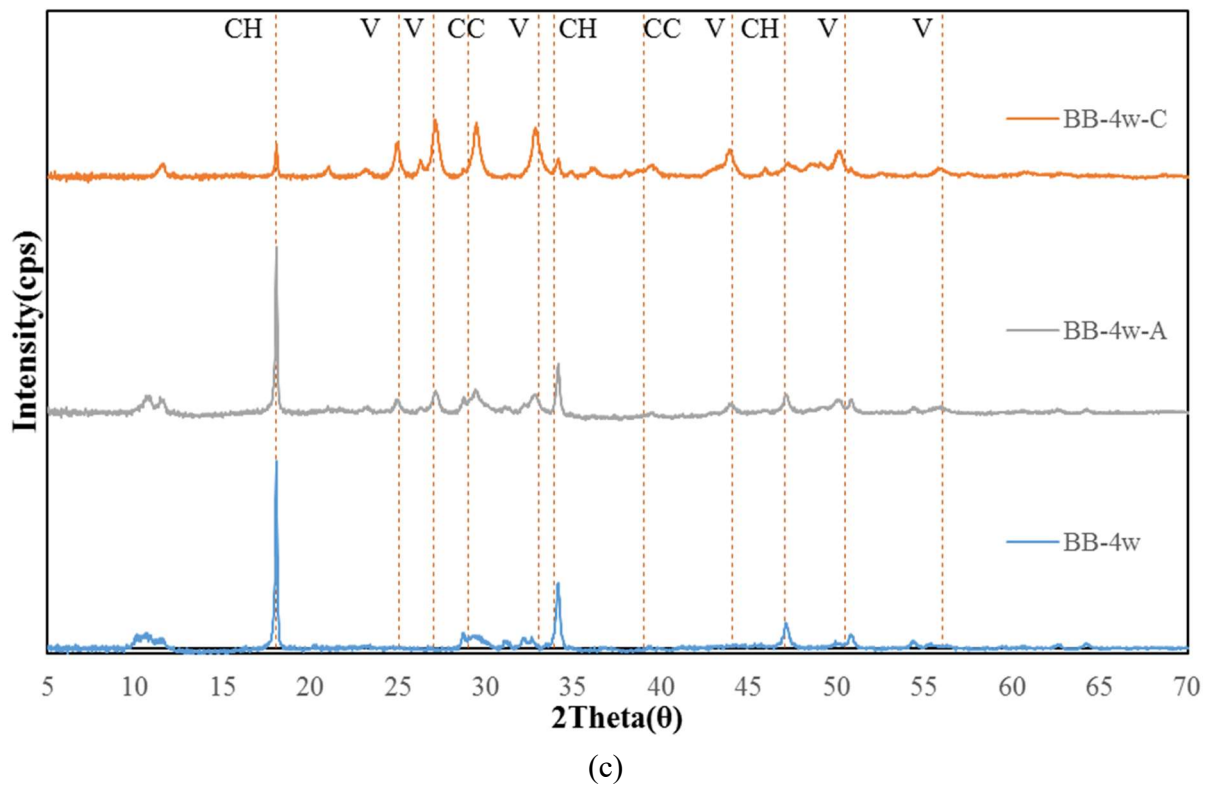
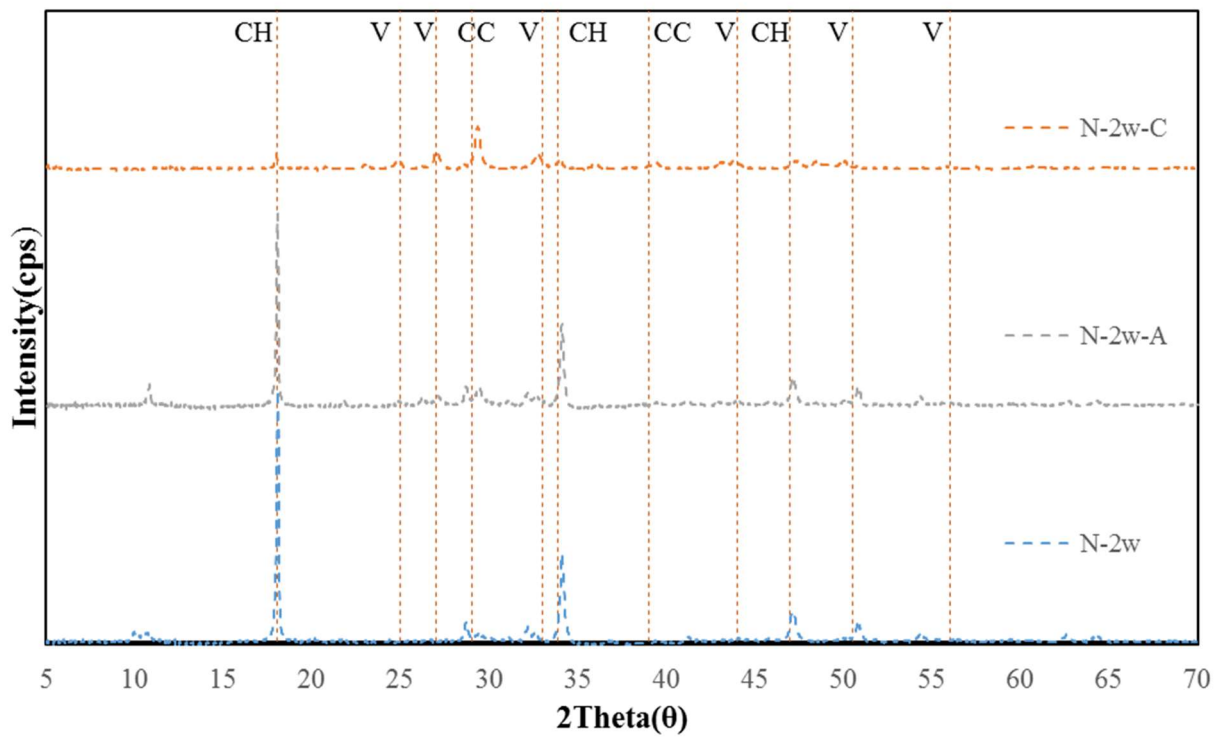
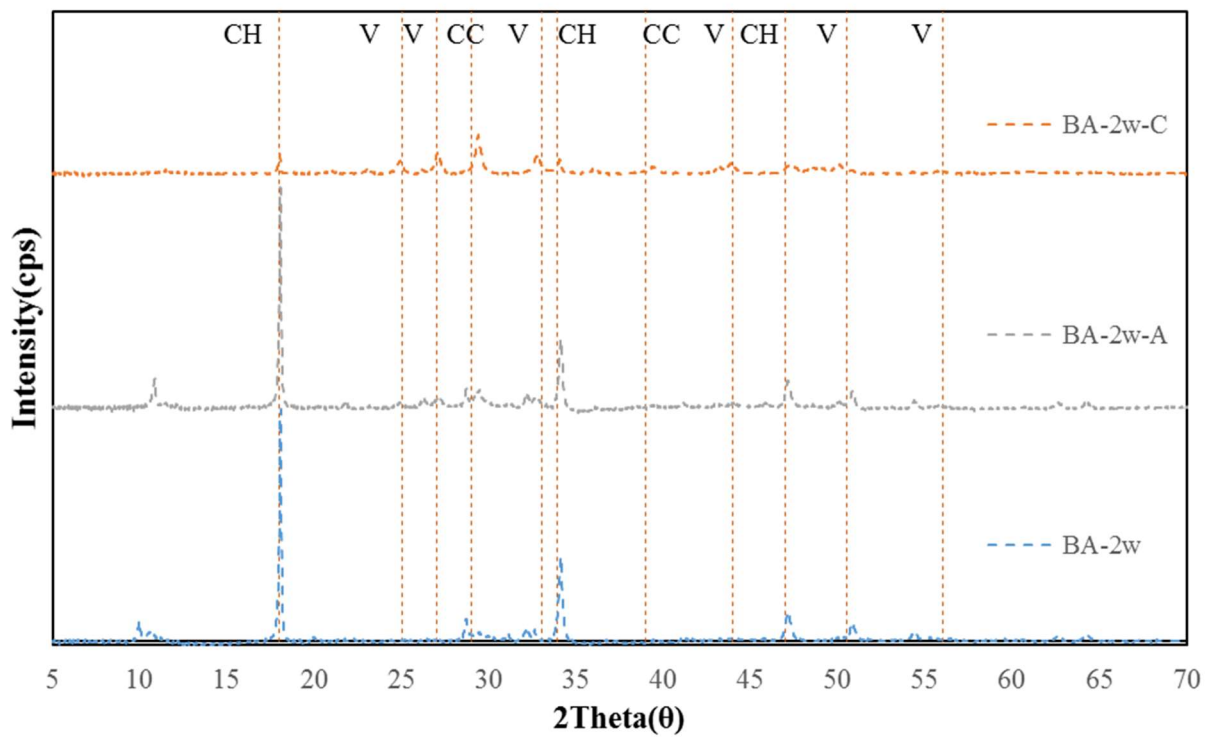


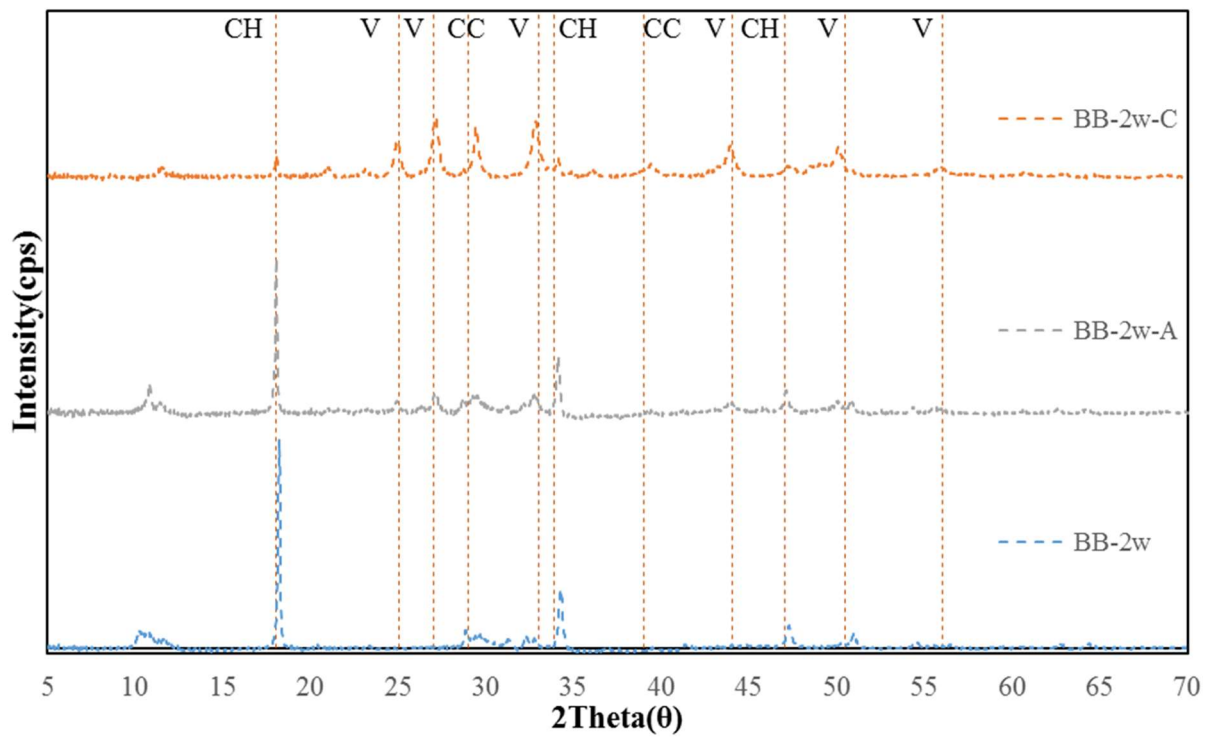
Fig. 5.13 X-ray diffraction pattern of the paste with different replacement ratio of BFS at curing ages 4 weeks.



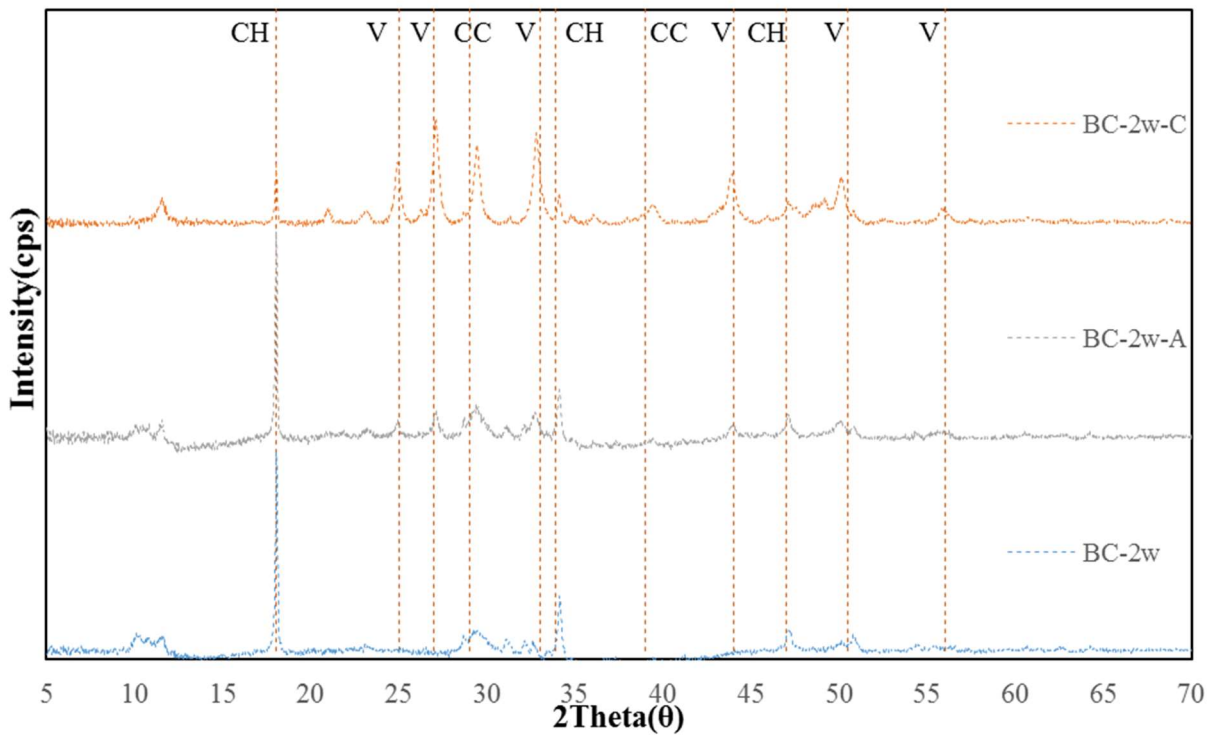
(a)



(b)



(c)



(d)

Fig. 5.14 X-ray diffraction pattern of the paste with different replacement ratio of BFS at curing ages 2 weeks.

5.4 Conclusion

In this chapter, the current study examined the carbonation effect on the properties of pore structure change and the chemical composite properties of BFS cement paste incorporating different BFS replacement ratios. The measurement of MIP, thermal analysis, and XRD analysis as a carbonation deterioration in paste was investigated in this research. The primary findings of the study can be summarized as follows:

- (1) Small pore distribution tends to increase as BFS replacement ratio increases. Moreover, it is found that the carbonation of the cementitious composite could enhance the densification of the paste samples. The after carbonation significantly causes the shift toward larger pore distribution.
- (2) In the case of total porosity, the total porosity at water curing increased as the BFS replacement ratio increased. The after carbonation significantly causes reduced capillary pore decrease compared with air curing. This is thought to be due to the dependency of carbonation affecting the pore structure of the paste samples.
- (3) With respect to the influence of the DTG curve on each curing environment, it is notable that the CH peaks of the paste samples are found after carbonation.
- (4) With respect to the effect of the amount of CH and C-S-H on the carbonation, the thermal analysis of the carbonation amount from C-S-H increased mainly with the BFS replacement ratio of 45% and 65% in the specimens after carbonation. The result shows that the carbonation amount from CH decreases as the BFS replacement progresses. This is relative to the CH amount of water curing before carbonation behavior. The lower the amount of CH, the more easily the C-S-H of carbonation progresses.
- (5) With respect to the influence of cement mineral composite measurement on the

carbonated samples, it is notable that the vaterite of the BFS blended paste samples is larger than that of the N specimens, a phenomenon primarily dominated by the low C/S of the C-S-H phase caused by BFS replacement.

References:

- Borges, H.R. P., Costa, O. J., Milestone, B. N., Lynsdale, J. C., Streatfield, E. R., (2010). "Carbonation of CH and C-S-H in composite cement pastes containing high amounts." *Cement and Concrete Research*, 40, 284-292.
- Escalante-Garcia, J.I., Mendoza, G., Sharp, J.H., (1999). "Indirect determination of the Ca/Si ratio of the C-S-H gel in Portland cements." *Cement and Concrete Research*, 29, 1999-2003.
- Hargis, C.W., Telesca, A., Monteiro P.J.M., (2014). "Calcium sulfoaluminate (Ye`elimitite) hydration in the presence of gypsum, calcite, and vaterite." *Cement and Concrete Research*, 65, 15-20.
- Ishida, S., Igarashi. S., (2012). "Influence of progress of neutralization on the capillary void structure of cement paste." *Concrete Research and Technology*, 34(1), 622-627.
- Ishida, S., Igarashi. S., Koike, Y., (2011). "Effects of early-age carbonation on mechanical and electrical properties of cement pastes and concretes." *Japan Cement Association*, 65(1), 282-289.
- Ishida, T., Ito, Y., Kawai, K., (2013). "Carbonation characteristics of the C-S-H with various Ca/Si ratios." *Japan Cement Association*, 67(1), 487-494.
- Kakali, G., Tsivilis, S., Aggeli, E., Bati, M., (2000). "Hydration products of C₃A, C₃S and Portland cement in the presence of CaCO₃." *Cement and Concrete Research*, 30, 1073-1077.
- Karen S., Ruben S., Barbara L. (2015). "A Practical Guide to Microstructural Analysis of Cementitious Materials." Taylor and Francis Group, Boca Raton.
- Kayyali O. (1985). "Mercury intrusion porosimetry of concrete aggregate." *Mater Struct* 18, 259-262.

Li, C., Nakarai, K., Ishii, Y., Yokozuka, K., (2009). "Experimental study on effect of carbonation of early aged cement paste on micro-pore structure and effective diffusion coefficient of oxygen." *Cement Science and Concrete Technology*, 63, 99-106.

Ngala, V.T., Page, C.L., (1997). "Effects of carbonation on pore structure and diffusional properties of hydrated cement pastes." *Cement and Concrete Research*, 27, 995-1007.

Phung, Q.T., Maes, N., Jacques, D., Bruneel, E., Driessche, I. V., Ye, G., Schutter, G.D., (2015). "Effect of limestone fillers on microstructure and permeability due to carbonation of cement pastes under controlled CO₂ pressure conditions." *Construction and Building Materials*, 82, 376-390.

Rostami, V., Shao, Y., Boyd, A. J., He, Z., (2012). "Microstructure of cement paste subject to early carbonation curing." *Cement and Concrete Research*, 42, 186-193.

Saeki, T., Ohga, H., Nagataki, S., (1990). "Change in micro-structure of concrete due to carbonation." *Journal of Japan Society of Civil Engineers*, 420, 33-42.

Suda, Y., Tanaka, Y., Saeki, T., (2010). "Fundamental study on chemical composition and physical properties." *Japan Society of Civil Engineers*, 66(4), 528-544.

Tanaka, Y., Saeki, T., Sasaki, K., Suda, Y. (2009). "Fundamental study on density of C-S-H." *Japan Cement Association*, 63(1), 70-76.

Thiery, M., Villain, G., Dangla, P., Platret, G., (2007). "Investigation of the carbonation front shape on cementitious materials: Effects of the chemical kinetics." *Cement and Concrete Research*, 37, 1047-1058.

Zhang W.Y., Zakaria M., Hama Y. (2013). "Influence of aggregate materials characteristics on the drying shrinkage properties of mortar and concrete." *Constr Build Mater* 49, 500-510.

Zhang W.Y., Hama Y., Na S.H. (2015). "Drying shrinkage and microstructure characteristics of mortar incorporating ground granulated blast furnace slag and shrinkage reducing admixture." *Constr Build Mater* 93, 267-277.

CHAPTER 6
CONCLUSIONS

6.1 Introduction

The present research investigated the influence of BFS on the compressive strength development, and also focused on the frost damage behavior caused by carbonation by various BFS replacement ratios, such as C-S-H accelerator, little admixture amount, and combined deterioration with carbonation properties, and freeze–thaw resistance due to BFS was also investigated.

6.2 Effect of C-S-H type accelerator on the compressive strength at early curing age as blended BFS (Chapter 2)

This chapter presents an experimental study to clarify the effect of C-S-H type accelerator characteristics on the BFS blended mortar and concrete samples. The early curing ages and strength development properties were investigated by XRD and TG.

For compressive strength results in a low-temperature environment, in the case of ordinary Portland cement (OPC), the addition of a C-S-H type accelerator exerted performance even at a low-temperature environment. However, in the case of the BFS blended cement, the low effect occurred at both the normal temperature and low temperature because the C-S-H type accelerator reacted with C_3S in the cement composite, of which the C_3S amount of BFS blended cement was lower than OPC. This effect can be observed in measurement setting time. Setting time was short with adding C-S-H type accelerator.

For the compressive strength result of various types of cement, it was observed that various types of cement had varied C_3S amounts. A higher amount of C_3S cement showed higher strength development than low C_3S cement. Moreover, characteristics of C-S-H type accelerator on the XRD and heat production result, when the heat flow increased with increased amount of C-S-H type accelerator.

Therefore, in the case of OPC, the C-S-H type accelerator can be affected by the low-temperature environment.

However, in the case of BFS blended cement, there was no effect of compressive strength development in this study. The literature observed the influence of the water binder ratio effect in BFS blended cement. Finally, as a result of the experiment of various types of cement for the effect on compressive strength development, it was concluded that the amount of C-S-H type accelerator was affected by the amount of C_3S .

6.3 Effect of limestone powder and gypsum on the compressive strength mixture design of blended BFS (Chapter 3)

This chapter presents an experimental study to investigate the combined effects of limestone powder and gypsum on BFS blended cement mortar. In addition, for the investigation of cement composite by XRD/Rietveld method, the calculation of volume of cement composite by power equation was made. Finally, the tendency compared pore volume and compressive strength.

A mortar with BFS replacement exhibited a low early age strength, which is thought to be due to the dependency of the initial strength of the BFS cement on the OPC amount. For long-term aging, the strength obtained was high, in agreement with the literature. When using CS as a replacement, the initial strength at a curing age of 1 day was equal to that of OPC. When CS was used as a replacement, significant heat was observed initially; this was determined to be an effect of the addition of calcium. When using LSP as a replacement, the strength increased at replacement ratios of 20 and 25 wt%. However, at a BFS replacement ratio of 15 wt%, the strength decreased slightly. This result was thought to be due to the effect of LSP on the strength enhancement for BFS replacement ratios above a certain value. No consistent trends were observed for the results of LSP and CS replacement. However, the initial strength at a curing age of 1 day was equal to that of OPC. The mixture that exhibited a compressive strength similar to that of OPC was BFS 35 wt% + LSP 3 wt% + CS 2 wt% (base cement HPC).

From the results for the measured cement mineral reaction rate, the C_3S reaction amount increased for the

case of CS replacement. This increase was thought to have affected the strength enhancement of the CS replacement mixture. From the results for the measured hydration product, AFt was not converted to AFm as a result of LSP replacement. This is thought to be due to the contribution of AFt to the initial production of MC or HC in the LSP replacement case. With regard to the relationship between porosity and strength, while the amount of capillary pores decreased with additional aging, the strength increased. Therefore, it was determined that, as the degree of hydration increased, the amounts of capillary pores decreased with aging and the strength increased accordingly.

6.4 Evaluation of the combined deterioration by freeze-thaw and carbonation of mortar incorporating BFS (Chapter 4)

The experimental program in this study is designed to assess the interaction between accelerated carbonation and freeze–thaw resistance in BFS mortar with limestone powder (LSP) and calcium sulfate (CS). First, the influence of mineral admixtures as cement replacement on the mechanical properties, carbon resistance, and freeze–thaw resistance of mortar is determined. Furthermore, the combined deterioration under the combined effects of carbonation and frost damage is investigated. Mortar subjected to different degrees of frost damage is examined to assess the influence of frost damage on carbonation resistance and the pore structure change in BFS cement mortar. Then, the influence of pre-carbonation on the frost resistance is investigated, and the pore structure change with the accelerated carbonation progress is also measured. Through the above investigations, the obtained results from this study provide invaluable information regarding concrete durability, offering a better understanding of the durability performance of cementitious composites.

In the case of single deterioration, the frost resistance and carbonation resistance both decrease as the BFS replacement ratio increases from 0 to 45%. It is likely that the increasing cumulative pore volume leads to the decrease in frost resistance. In the case of BFS cement carbonation, the alkali content decreases, and a large amount of $\text{Ca}(\text{OH})_2$ is consumed with the additional hydration process of BFS; hence, the carbonation process

accelerates, and the carbonation resistance of BFS cementitious composite decreases. When CS and LSP are added to BFS cement, the results show that CS has a positive effect on the durability, but the frost resistance and carbonation resistance are reduced by the use of the LSP admixture. It is illustrated that the addition of LSP increases the coarse capillary pores and the total porosity of the BFS mortar, which is detrimental to improving the performance of frost and carbonation resistance.

With respect to the effect of the degree of frost damage on the carbonation resistance, the relative dynamic modulus of elasticity of the mortar is mainly in the range of 75%–90% as the specimens experience to 12, 30, and 60 freeze–thaw cycles. The result shows that the carbonation resistance decreases as the freezing and thawing progresses. It is considered that the inkbottle pore volume for pores with a diameter above 50nm plays an important role in the carbonation behavior. As the pore volume of inkbottle pores that can retain water decreases, the continuity of the pores increases, and CO₂ could permeate the transfer path of the mortar samples, allowing the carbonation to accelerate.

With respect to the influence of pre-carbonation deterioration on the frost resistance, it is remarkable that the scaling mass loss of mortar after pre-carbonation deterioration is less than that of the non-carbonated specimens, a phenomenon primarily dominated by the pore structure densification caused by the pre-carbonation. The experimental results in this study provide a good perspective for the design and assessment of concrete durability.

6.5 Curing age and carbonation characteristics incorporating BFS (Chapter 5)

Therefore, in this chapter, in order to obtain the applicable pore structure involved in the carbonation of BFS blended cementitious composite, the effects of pore structure on the carbonation of paste samples were further discussed by statistical investigation method for mercury intrusion porosimetry (MIP), XRD analysis and thermal analysis. Moreover, the analysis of MIP was applied to identify the pore structure change, the analysis

of XRD was to identify the chemical composition of cement paste, and thermal analysis indicated the amount of calcium hydroxide and calcium carbonate. The experimental program in this study was designed to investigate the carbonation effect in various BFS blended pastes. Through the above investigations, the obtained results from this study provide valuable information regarding cement durability, offering a better understanding of the carbonation performance of BFS cementitious composite.

The small pore distribution tends to increase as the BFS replacement ratio increases. Moreover, it is found that the carbonation could enhance the densification of the paste samples. Post carbonation significantly causes the shift toward large pore distribution. In the case of total porosity, the total porosity at water curing increased as the BFS replacement ratio increased. Carbonation significantly causes the reduction of capillary pore decrease compared with air curing. This is thought to be due to the dependency of carbonation affecting the pore structure of the paste samples.

With respect to the influence of the DTG curve on each curing environment, it is notable that the CH peaks of the paste samples are found after carbonation. With respect to the effect of the amount of CH and C-S-H on the carbonation, the thermal analysis of the carbonation amount from C-S-H increased mainly due to the BFS replacement ratios of 45% and 65% in the specimens after carbonation. The result shows that the carbonation amount from CH decreases as the BFS replacement progresses. This is relative to the CH amount of water curing as before carbonation behavior. The lower the amount of CH, the more easily the C-S-H of carbonation progresses.

With respect to the influence of cement mineral composite measurement on the carbonated samples, it is remarkable that the vaterite of the BFS blended paste samples is larger than that of the N specimens, a phenomenon primarily dominated by the low C/S of C-S-H phase caused by BFS replacement.

6.6 Summary and future work

This thesis investigated increasing the usability of BFS for reduced CO₂ emission. We investigated the two ways – the compressive strength development method and the combined deterioration of carbonation and frost damage, evaluated from using XRD, thermal analysis, and mercury intrusion porosimetry, respectively. The obtained results in this study are valuable information for BFS blended cement and concrete development.

In this research, the mixture that exhibited compressive strength similar to that of ordinary Portland cement was BFS 35 wt% + LSP 3 wt% + CS 2 wt% (base cement HPC). However, in the case of compressive strength development by C-S-H type accelerator, it is not completely clear that the development mechanism is due to incorporating BFS cement. Hence, it is necessary to research the C-S-H type accelerator for further investigating the mechanism of compressive strength development. In addition, quantifying the relationships between pore structure and frost damage resistance by BFS blended cement is not clear. This is a problem which we should address in future work.

Thus, in order to enhance the BFS blended concrete performance, it is necessary to add an accelerator and/or mineral admixture of compressive strength development and increase the durability. Also, the effect on concrete structure performance should be considered based on the balance caused by cementitious composite mechanical properties and durability restraining effect.

ACKNOWLEDGEMENTS

The completion of my doctoral dissertation would not have been possible without the help and support of the kind people around me, to some of whom I would like to express my sincere gratitude here.

I would like to thank my supervisor, Professor Hama Yukio for giving me the opportunity to conduct this work, and for his continuous advice and guidance. Without his guidance persistent help this dissertation would not have been possible.

I would like to thank my vice supervisors, Professor Mizoguchi and Professor Sugata, who offered important opinions for the revision of my doctoral dissertation and the doctoral dissertation presentation.

Further, I also wish to express my appreciation to Assistant Professor Hyeonggil Choi. He always provided encouragement and kind advice for my research.

Special thanks go to my external supervisor, Professor Cheongoo Han, and Associate Professor Mincheol Han, my supervisor during the master's course. When studying abroad, unconditional support encouraged me to overcome some challenges and continue my study.

I would like to thank Dr. SeungHyun Na and Dr. Wenyan Zhang. Their advice and counsel were really helpful, and they became a most reliable source of help for me. My research would not have been possible without their help.

I would like to thank rotary scholarship members. They were really helpful for my life in Japan. And they gave me due to enjoy life in Japan.

I would like to thank NIPPON STEEL & SUMIKIN cement members. They gave a lot of help with my research to measurement, especially allowed us to use their equipment. I'm very much obliged to them.

I would also like to express my deep appreciation to my postgraduate peers and my friends, Messrs. Hasegawa, Quy, Van, Kishimoto, Miwa, Kawamura, Shimakage, and Matsumoto, among others. Their friendship, their kindness, their conversation, and their encouragement helped me to make my life of studying abroad happier and make my doctoral study journey colorful and unforgettable.

Finally, I would like to express my gratitude and appreciation to my parents and sister. They always help

me in my life. They are always strong supporters of my decisions. Sincere gratitude goes to my love, Wang Ni. She always encourages me to overcome all encountered difficulties and make me heal. Her support and encouragement has enabled me to complete the doctoral study.

LIST OF PAPERS

Publications:

Junho Kim, Seunhyun Na, Wenyan Zhang, Takahiro Sagawa, Yukio Hama, “Effect of Limestone Powder and Gypsum on the Compressive Strength Mixture Design of Blast Furnace Slag Blended Cement Mortar”, Journal of Advanced Concrete Technology, Vol. 15, pp.67-80, 2017, 02

Wenyan Zhang, Seunghyun Na, Junho Kim, Hyeonggil Choi, Yukio Hama, “Evaluation of the combined deterioration by freeze-thaw and carbonation of mortar incorporating BFS, limestone powder and calcium sulfate”, Materials and Structures, 50:171, 2017

三輪 真也, 金 準鎬, 崔 亨吉, 濱 幸雄, “高炉スラグ微粉末を用いたコンクリートの中性化による細孔構造と耐凍害性の変化”, コンクリート工学年次論文集, Vol. 39, 2017, 07

Presentations:

Junho KIM, Wenyan ZHANG, Mohamed ZAKARIA, Hyeonggil CHOI, Yukio HAMA, “Influence of combined deterioration between freezing-thawing and carbonation on mineral admixture mortar”, International Symposium between China, Japan & Korea on Performance Improvement of Concrete for Long Life Span Structure, 9th, 2015.07

Junho KIM, Wenyan ZHANG, Yasuyoshi TSUKAMOTO, Hyeonggil CHOI, Yukio HAMA, “Mixture design of blast furnace slag concrete based on high early strength cement using the limestone powder and CaSO₄”, International Symposium between China, Japan & Korea on Performance Improvement of Concrete for Long Life Span Structure, 10th, 2016.07

Naoya MIWA, Junho KIM, Yasuyoshi TSUKAMOTO, Wenyan Zhang, Hyeonggil CHOI, Yukio HAMA, “Influence of pore structure change due to carbonation on frost resistance of bfs cement mortar”, International Symposium between China, Japan & Korea on Performance Improvement of Concrete for Long Life Span Structure, 10th, 2016.07

Wenyan Zhang, Junho Kim, Hyeonggil Choi, Yukio Hama, “Combined deterioration by freezing-thawing and carbonation of bfs cement mortar with mineral materials”, International Symposium between China, Japan & Korea on Performance Improvement of Concrete for Long Life Span Structure, 10th, 2016.07

Junho KIM, Naoya MIWA, Wenyan ZHANG, Hyeonggil CHOI and Yukio HAMA, “Influence of pore structure change due to carbonation on frost resistance of BFS cement mortar”, Korean Recycled Construction Resource Institute International Conference, 2016. 10